Doctoral Thesis

Controlling Morphologies of Self-Assembled Structures of Block Copolymers by Molecular Designs and External Stimuli

Moon Gon Jeong

Department of Chemistry

Graduate School of UNIST

2019

Controlling Morphologies of Self-Assembled Structures of Block Copolymers by Molecular Designs and External Stimuli

Moon Gon Jeong

Department of Chemistry

Graduate School of UNIST

Controlling Morphologies of Self-Assembled Structures of Block Copolymers by Molecular Designs and External Stimuli

A thesis/dissertation
submitted to the Graduate School of UNIST
in partial fulfillment of the
requirements for the degree of
Doctor of Philosophy

Moon Gon Jeong

11/28/2018 of submission
Approved by

Advisor
Ja-Hyoung Ryu

Controlling Morphologies of Self-Assembled Structures of Block Copolymers by Molecular Designs and External Stimuli

Moon Gon Jeong

This certifies that the thesis/dissertation of Moon Gon Jeong is approved.

11/28/2018 of submission

_____

Advisor: Prof. Ja-Hyoung Ryu

_____

Kyoung Taek Kim: Thesis Committee Member #1

_____

Sung You Hong: Thesis Committee Member #2

_____

Bongsoo Kim: Thesis Committee Member #3

_____

Min Sang Kwon: Thesis Committee Member #4

Abstract

Self-assembly of amphiphilic block copolymers (BCPs) in solution has received attention from polymer chemists due to their potential applications such as drug delivery system and nanoreactors for two decades. Because sorts of morphologies formed by self-assembly were so diverse, predicting and designing the desired morphologies were considered as one of the goals. The morphologies were classically controlled by modifying a block ratio of BCPs. Herein, however, I demonstrated that morphologies of self-assembled structures of BCPs can be controlled by molecular designs and external stimuli with a fixed block ratio.

In this dissertation, dendritic-linear poly(ethylene glycol)-*block*-polystyrene (PEG-*b*-PS) BCPs were synthesized and their self-assembled structures were observed. Morphologies of dendritic-linear PEG-*b*-PS were toroids while morphologies of linear-linear PEG-*b*-PS with same block ratios were polymersomes. That's because the molecular area of BCPs was expanded by branched PEG chains.

To stabilize those structures, photo-cross-linkable monomers were introduced to the hydrophobic blocks. Portions of indenylstyrene that can be dimerized under UV light were copolymerized with styrene monomers by atom transfer radical polymerization (ATRP). The BCPs could be self-assembled in various morphologies and they were cross-linked under an irradiation of UV light for few hours. The enhanced stability of morphologies was demonstrated by an extreme dilution into the organic solution and the self-assembled structures survived.

Furthermore, BCPs with high molecular weights (> 200 kDa) were synthesized in order to access photonic bandgap properties of polymer cubosomes because structural periodicity of polymer cubosomes was proportion to their molecular weights. However, the polymerization of BCPs with high molecular weights through living radical polymerization has been challengeable. The problem was solved by the acceleration of propagation rates with an excess loading of CuBr catalysts but it simultaneously brought out broad distributions of molecular weights. Through a gradient column chromatography, high molecular weight BCPs with narrow distribution was achieved and blue light reflections were observed from their polymer cubosomes.

Finally, to control morphologies of the branched-linear PEG-*b*-PS BCPs by external stimuli, three pyridine groups that can be utilized as stimuli-receptors were introduced into junctions of peripheral PEG chains. As a result, self-assemblies with and without external stimuli such as low pH and metal precursors produced significantly different morphologies.

From the above experiments, I demonstrated that the morphologies can be controlled by designing molecular architectures and introducing external stimuli during self-assembly processes, and the morphologies can be stabilized efficiently by the photo-cross-linking system.

Table of Contents

List of Figures

Figure 3-1. A scheme of branched-linear block copolymers containing polystyrene hydrophobic blocks with indene pendant groups and their self-assembly toward complex inverse bicontinuous bilayers. The self-assembled structures were cross-linked by [2π + 2π]-cycloaddition of indene groups with irradiation of long-wavelength UV light (λ = 365 nm).

Figure 3-2. (A) ^{1}H NMR and (B) gel permeation chromatography (GPC) spectra showing the progress of polymerization for **P1-TMS** during the polymerization time. (C) Plots of polymerization time vs. $\ln([M]_0\ [M]_t^{-1})$ for the polymerization of **P1-TMS** and **P2-TMS**. $[M]_0$ and $[M]_t$ indicate the concentration of monomers at times 0 and t, respectively. (D) Plots of reaction conversion vs. the number-averaged molecular weight (M_n) and polydispersity index ($Đ$) for **P1-TMS** and **P2-TMS**. Filled circles and triangles indicate M_n and opened circles and triangles indicate $Đ$.

Figure 3-3. (A) A scheme for post-modification of **P2-TMS** to **P2**. (B) ^{1}H NMR spectra of **P2-TMS** and **P2**. The DP_n ratio was calculated based on the **P2-TMS** spectrum.

Figure 3-4. (A) Schematic procedures for post-modification of **P1-TMS** toward **P1** using deprotection and the Burgess reaction. (B) ^{1}H NMR spectra of **P1-TMS** and **P1** ("a" and "b" show the characteristic peak changes). (C) UV-Vis spectra of the **P1-TMS** and **P1** solutions in CH_2Cl_2

Figure 3-5. GPC spectra of (A) **P1-TMS**, **P1** and (B) **P2-TMS**, **P2**.

Figure 3-6. (A) UV-Vis spectra of **P1** in CH_2Cl_2 (0.01 mg mL^{-1}) with irradiation of long-wavelength UV light (λ = 365 nm) for different exposure times. (B) Plot of the UV exposure time against the cross-linking ratio ($1 - (A_t\ A_0^{-1})$), where A_0 and A_t are the absorbance values at 310 nm at time 0 and t, respectively. The cross-linking ratio at t = 20 min was 87.5%. (C) ^{1}H NMR spectra of **P1** in CD_2Cl_2 (1 mg mL^{-1}) with (20 min) and without UV irradiation. (D) Differential scanning calorimetry spectra of non-cross-linked and cross-linked **P1**.

Figure 3-7. (A) UV-Vis spectra of polymer film of **P1** spin-coated onto square quartz plate (2 cm x 2 cm) at irradiation of UV light (λ >300 nm, 200 W) for different exposure time. (B-D) Photographs of polymer film of **P1** spin-coated onto silicon wafer (1 cm x 1 cm) with scratch. (B) Polymer film of **P1** before and (C) after 2 h of UV light irradiation. (D) Cross-linked polymer film of **P1** after soaking in THF for 1 h.

Figure 3-8. UV-Vis spectra of cross-linked **P1** in CH_2Cl_2 at short-wavelength UV light (λ = 254 nm, 6 W) irradiation for different exposure times.

Figure 3-9. (A) Schematic procedures for preparation of a model compound 4-indenylstyrene (**Ind-St**) and its [2 + 2]-cycloaddition at long-wavelength UV light (λ = 365nm) and retro-cyclization of indene dimers at short-wavelength UV light (λ = 254 nm). (B) UV-Vis spectra of **Ind-St** in benzene (1 mg mL^{-1}) with irradiation of long-wavelength UV light (black) and short-wavelength UV light (red), sequentially, for different exposure times. (C) Plot of the UV exposure time against the dimerization ratio ($1 - (A_t A_0^{-1})$), where A_0 and A_t are the absorbance values at 337 nm at time 0 and t, respectively. The dimerization ratio at t = 150 min was 53.0% and t = 210 min was 36.2%. (D) ^{1}H NMR spectra of **Ind-St** solution after irradiation of long-wavelength UV light (black) and short-wavelength UV light (red), sequentially. "b_{1-4}" and "c_{1-4}" are caused by 4 different isomers of indene dimers.[41] The dimerization ratio calculated by the proton integration ($(\int b) (\int a + \int b)^{-1}$) was 39.0% at t = 150 min and was 16.0% at t = 210 min.

Figure 3-10. (A) Schematic procedures for random copolymerization of **1-TMS** and styrene with the PEG macro-initiator by atom-transfer radical polymerization and their post-modification by deprotection and the Burgess reaction. (B) Representative ^{1}H NMR spectra of deprotected block copolymers (BCPs) (**P5-OH**) and dehydrated BCPs (**P5**) showing their characteristic peak shifts. (C) Representative gel permeation chromatography spectra of **P5-OH** and **P5**.

Figure 3-11. (A) Dynamic light scattering (DLS) size plots of the self-assembled structures of **P3** in an aqueous solution (black) and cross-linked **P3** in a tetrahydrofuran (THF) solution (red). (B) Plots of the DLS-derived count rate (light intensity) and size of the cross-linked self-assembled structures of **P3** in THF with increasing UV irradiation times. (C, D) TEM images of (C) non-cross-linked micelles of **P3** and (D) cross-linked micelles after changing the dispersion solvent to THF.

Figure 3-12. (A) Dynamic light scattering (DLS) size plots of the self-assembled structures of **P4** in an aqueous solution (black) and cross-linked **P4** in a tetrahydrofuran (THF) solution (red). (B) Plots of the DLS-derived count rate (light intensity) and size of the cross-linked self-assembled structures of **P4** in THF with various UV irradiation times. (C, D) TEM images of (C) non-cross-linked vesicles of **P4** and (D) cross-linked vesicles after changing the dispersion solvent to THF.

Figure 3-13. Plot of f_{ind} vs. relative count rate. Critical content of indenylstyrene in the hydrophobic

block for decent cross-linking was around 30%.

Figure 3-14. (A-E) TEM images of non-cross-linked vesicles of (A) **P1S** (f_{ind} = 5.6%), (B) **P2S** (f_{ind} = 10.7%), (C) **P3S** (f_{ind} = 20.7%), (D) **P6** (f_{ind} = 35.3%) and (E) **P5** (f_{ind} = 56.4%). (F-J) TEM images of cross-linked vesicles of (F) **P1S**, (G) **P2S**, (H) **P3S**, (I) **P6** and (J) **P5** after changing the dispersion solvent to THF.

Figure 3-15. SEM and TEM images of (A, C) the self-assembled sponge phase particles of **P5** and (B, D) cross-linked sponge phase of **P5** after soaking in tetrahydrofuran.

Figure 3-16. (A, B) SEM images of the polymer cubosomes of **P6** showing (A) the spherical shape with surface pores and (B) internal structures. (C, D) TEM images of the polymer cubosomes of **P6** showing internal mesoporous channels.

Figure 3-17. (A, B) SEM images and (C, D) TEM images of the cross-linked polymer cubosomes of **P6** showing unchanged crystalline structures after replacing the dispersion solvent in tetrahydrofuran (THF) for at least three days. (E) Small-angle X-ray scattering results obtained from the dried non-cross-linked polymer cubosome of **P6** (*Pn3m* symmetry, a = 41.6 nm) and cross-linked polymer cubosome of **P6** after soaking in THF (*Pn3m* symmetry, a = 44.2 nm).

Figure 3-18. (A) Dynamic light scattering size plots of the self-assembled structures of **P4** exposed to long-wavelength UV light (λ >300 nm, 5 h) in a tetrahydrofuran (THF) solution (red) and sequentially exposed to short-wavelength UV light (λ = 254 nm, 2 h) in a THF solution (black). (B) TEM image of vesicles of **P4** exposed to short-wavelength UV light after changing the dispersion solvent to THF.

Figure 4-1. Schematic on the self-assembly of high molecular weight branched-linear BCPs into polymer cubosomes with internal double diamond structure (*Pn3m* symmetry group). N_{ps} is the degree of polymerization of a PS block of a BCP. *d* and *a* indicate the thickness of the BCP bilayer and the lattice parameter of the double diamond lattice, respectively.

Figure 4-2. (A) ^{1}H NMR spectrum of the macroinitiator PEG2000$_3$-Br, **1**. (B) MALDI-TOF-MS spectrum of the precursor of the macroinitiator, PEG2000$_3$-OH.

List of Tables

List of Schemes

Nomenclature

$[M]_0$	Concentration of monomers at time 0
$[M]_t$	Concentration of monomers at time t
2-D	Two-dimensional
3-D	Three-dimensional
a	Lattice parameter
A_0	Absorbance at time 0
A_t	Absorbance at time t
ATRP	Atom transfer radical polymerization
BCP	Block copolymer
C	Polymer cubosomes (self-assembly in solution)
C	Cylinders (self-assembly in bulk)
CDSA	Crystallization-driven self-assembly
COSY	Correlation spectroscopy
CTA	chain transfer agent
Cy	Cylindrical micelles
D	Double diamond
Đ	Polydispersity index
dioxane	1,4-Dioxane
DLS	Dynamic light scattering
DMF	Dimethylforamide
DP_n	Degree of polymerization
DSC	Differential scanning calorimetry
DTAB	Dodecyltrimethylammonium bromide
EBIB	Ethyl α-bromoisobutyrate
f_A	Volume fraction of the A block
f_{Ind}	indeneylstyrene ratio of hydrophobic block
fPEG	The ratio of the molecular weight of PEG block to that of PS block
G	Bicontinuous gyroid (self-assembly in bulk)
GOx	Glucose oxidase
GPC	Gel permeation chromatography
HCl	Hydrochloric acid
HRP	Horse radish peroxidase
Ind-St	4-Indenylstyrene
L	Lamellae (self-assembly in bulk)
LCST	Lower critical solution temperature
MALDI-TOF-MS	Matrix-assisted laser desorption ionization time-of-flight
M_n	Number-average molecular weight
Myo	Myoglobin
N	Degree of polymerization
NMP	Nitroxide-mediated polymerization
NMR	Nuclear magnetic resonace
ODT	Ordet-to-disorder transition

OOT	Order-to-order transition
OSER	Ordered smooth endoplasmic reticulum
p	Molecular packing parameter
P	Primitive cubic
PAA	Poly(acrylic acid)
PBOx	Polystyreneboroxole
PDEAEM	Poly(diethylaminoethyl methacrylate)
PDMIBM	Poly(dimethyl maleicimido butyl methacrylate)
PEG	poly(ethylene glycol)
PETTC	4-Cyano-4-(2-phenylethane sulfanylthiocarbonyl) sulfanylpentanoic acid
PFS	Polyferrocenylsilane
PGA	Poly(glutamic acid)
PGlyMA	Poly(glycidyl methacrylate)
PGMA	Poly(glycerol monomethacrylate)
PHPMA	Poly(2-hydroxypropyl methacrylate)
PI	Polyisoprene
PLys	Poly(*L*-lysine)
PMDETA	*N*,*N*,*N*',*N*'',*N*''-pentamethyldiethylene-triamine
PNIPAM	Poly(*N*-isopropylacrylamide)
PS	Polystyrene
PtBA	Poly(t-butylacrylate)
RAFT	Reversible-fragmentation chain-transfer
ROMP	Ring opening metathesis polymerization
SAXS	Small-angle X-ray scattering
SCFT	Self-consistent field theory
SDEMS	Solvent diffusion-evaporation self-assembly
SEM	Scanning electron microscopy
TBAF	Tetrabutylammonium fluoride
TEM	Transmission electron microscopy
T_g	Glass transition temperature
THF	Tetrahydrofuran
TMSCl	Chlorotrimethylsilane
TPMS	Triply periodic minimal surface
UV	Ultraviolet
UV-Vis	Ultraviolet-visible light spectroscopy
V	Vesicles
W	Watt
$Zn(OTf)_2$	Zinc triflate
λ	Wavelength
λ_{max}	Wavelength at maximum absorbance
χ	Flory-Huggins parameter

Chapter 1. Introduction

1.1 Self-assembly

An amphiphile is a small molecule with a hydrophilic head and one or more hydrophilic tails. Natural amphiphilic small molecules include phospholipids, which form the lipid bilayers of cell membranes by "self-assembly" processes. Another example in real life is soap, which forms bubbles by the self-assembly of surfactant molecules like sodium dodecyl sulfate. Because self-assembled structures have been discovered in various circumstances, theories of self-assembly as well as the properties, morphologies, and potential applications of self-assembling molecules and structures have been investigated for many decades.[1-3] Diverse morphologies have been observed in bulk and in aqueous solutions.[4-6] These morphologies include spherical micelles, cylindrical micelles, vesicles (liposomes), lamellae, and several types of bicontinuous structures. For these structural diversities, Israelachvili et al. (1976) proposed the concept of the molecular packing parameter (p).[7] With molecular packing theory[8-10], the morphological size and shape can be estimated by calculation. The packing parameter is defined as $p = v_o/al_o$, where v_o and l_o are the volume and length of the hydrophobic tail of the amphiphile and a is the molecular area of the hydrophilic head of the amphiphile. For $p < 1/3$, the self-assembled structures are spherical micelles (spheres); for $1/3 < p < 1/2$, cylindrical micelles (cylinders); for $1/2 < p < 1$, vesicles (liposomes); for $p = 1$, planar lamellae; for $p > 1$, various inverse structures, often inverse micelles, are obtained (Figure 1-1).

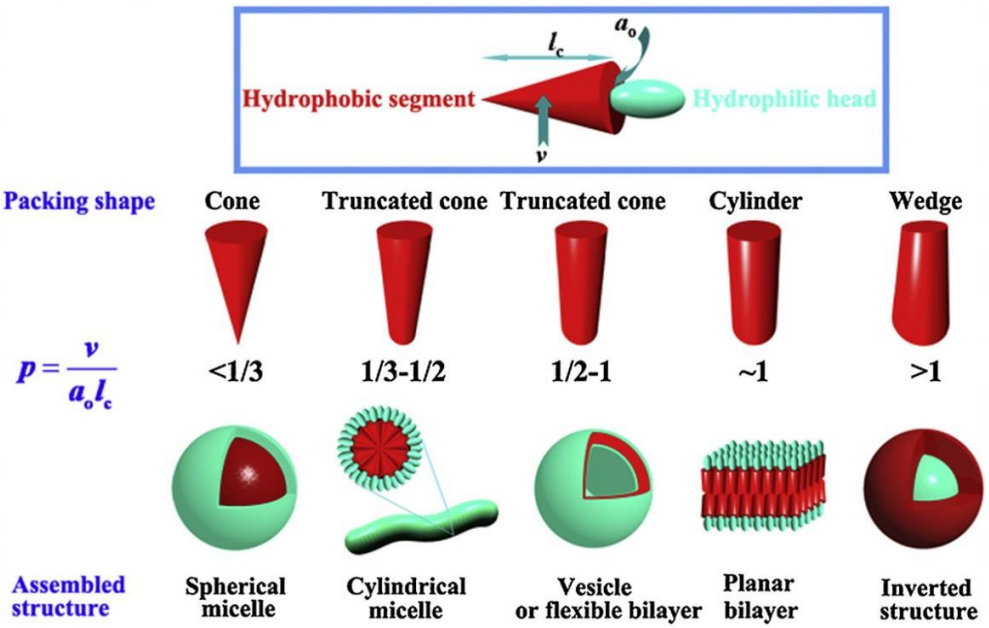

Figure 1-1. The molecular packing parameter (p) and relationships with self-assembled structures of amphiphilic small molecules.[6]

At the same time, the concept of living polymerization received attention from polymer scientists. After Szwarc (1956) discovered an anionic polymerization reaction, polymer chemists began to research the precise control of polymer molecular architecture.[11] They designed block copolymers (BCPs), graft polymers, star-like copolymers, branched polymers, and so on (Figure 1-2).[12,13] One of the desired results was BCPs with more than two blocks in a single polymer chain; this was successfully accomplished by the chain-extension property of living polymerization reactions. Among BCPs, amphiphilic BCPs with hydrophilic and hydrophobic blocks could be self-assembled like small amphiphilic molecules.[14,15] Compared to aggregates of self-assembled small molecules, polymer aggregates exhibit better stability because of their physical and mechanical properties derived from their high molecular weights.[16] Consequently, the self-assembly of BCPs was extensively investigated.[17]

In this chapter, several topics regarding self-assembling BCPs, especially diblock copolymers, are introduced, including self-assembly types in BCPs, morphologies of self-assembled structures, and techniques for morphological control.

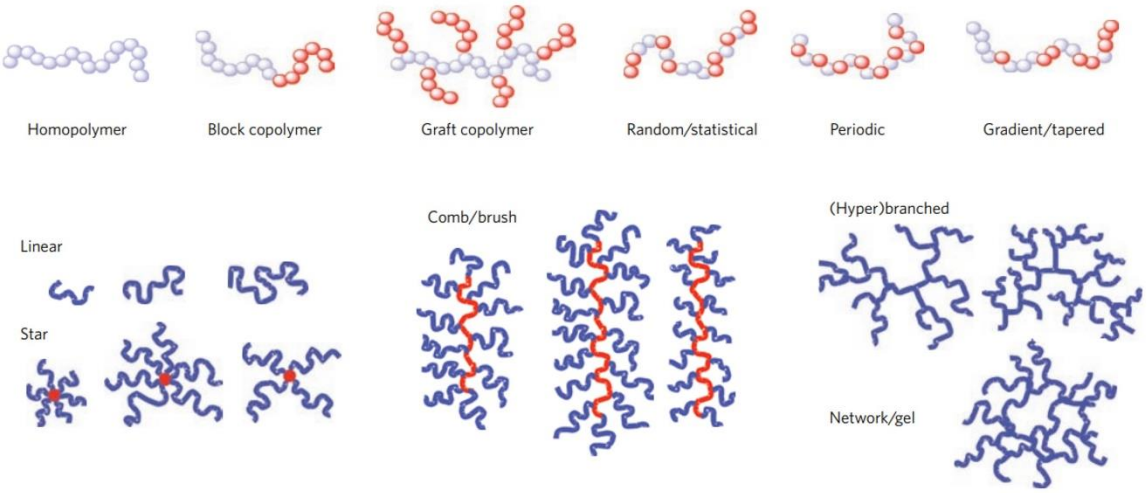

Figure 1-2. Various molecular architectures of block copolymers designed by living polymerization.[13]

1.2 Preparation of block copolymers

As mentioned previously, the concept of BCPs arose with the discovery of living polymerization. BCPs are easily synthesized by various living polymerization methods and desired properties can be introduced to each block of a BCP.[18,19] Living polymerization ideally involves no termination of the chain end and chain transfers; however, the initiation rate is much higher than the propagation rate. Because of these characteristics, the molecular weights of polymers during polymerization can be predicted precisely; polymers synthesized by living polymerization show narrow molecular weight distributions. The most important characteristic of BCPs is that chain extension can be performed because the chain end remains live after the polymerization is completed. Therefore, after the first

monomer batch is polymerized by living polymerization, another monomer can be successively polymerized as a second block by the same living polymerization method. By this process, diblock copolymers for self-assembly are acquired.

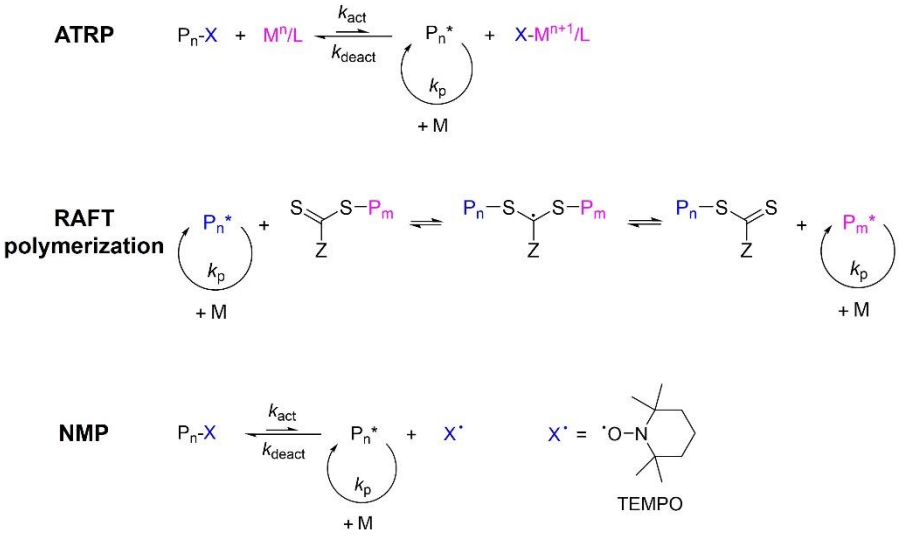

Figure 1-3. Representative living radical polymerization methods.

Living polymerization techniques are categorized by the source of reaction intermediates. They include anionic polymerization[20,21], cationic polymerization[22], radical polymerization[23], and ring-opening metathesis polymerization[24]. Among these, living radical polymerization is typically used for BCP preparation because of its versatility and convenience relative to those of other polymerization types. Living radical polymerization also includes several polymerization methods such as atom-transfer radical polymerization (ATRP)[25,26], reversible addition–fragmentation chain-transfer (RAFT) polymerization[27], and nitroxide-mediated polymerization (NMP)[28,29] (Figure 1-3). In this thesis, to achieve the desired BCPs, macro-initiators for ATRP or macro-chain transfer agents (macro-CTAs) for RAFT polymerization containing the first block, generally poly(ethylene glycol) (PEG), were synthesized in advance. The second block was introduced by living radical polymerization.

1.3 Self-assembly of block copolymers in bulk

When polymer blocks in BCPs are immiscible in the bulk state, they become separated into various morphologies including spheres, cylinders, gyroids, lamellae, *etc.* (Figure 1-4A).[30,31] This micro-phase separation process is driven by unfavorable mixing enthalpy; macro-phase separation is forbidden by the covalent bonds between the two blocks. The self-assembly of BCPs comprising A and B blocks in bulk form depends on three parameters. The first is the volume fractions of the A and B blocks (f_A and f_B; $f_A + f_B = 1$) and the second is the degree of polymerization of the entire BCP (N). The third is the Flory–Huggins parameter (χ_{AB}), which indicates the degree of incompatibility between the A and B

blocks. The combined value of N and χ_{AB} (χN) is the incompatibility degree, which determines the degree of micro-phase separation. To predict the morphologies of micro-phase separation of BCPs, Leibler established the self-consistent field theory (SCFT) and derived the phase diagram of diblock copolymers (Figure 1-4B).[32] At a fixed χN above the order-to-disorder transition (ODT) (χN > 10.5), the order-to-order transition (OOT) is observed from closed-packed spheres (CPS), body-centered-cubic spheres (S), hexagonally packed cylinders (C), and bicontinuous gyroids (G) to lamellae (L) as f_A increases from 0. These morphologies are then transformed in the inverse order with further increases in f_A.

To confirm that the SCFT works for actual systems, Bates et al. (1995) reported the self-assembly and phase diagram of bulk polyisoprene-*block*-polystyrene (PI-*b*-PS) diblock copolymer (Figure 1-4C).[33] With the self-assembly of bulk PI-*b*-PS, several morphologies were observed by electron microscopy. The phase diagram of PI-*b*-PS plotted based on these real observations was astonishingly comparable to that calculated by the SCFT because the number of variables affecting micro-phase separation was small.

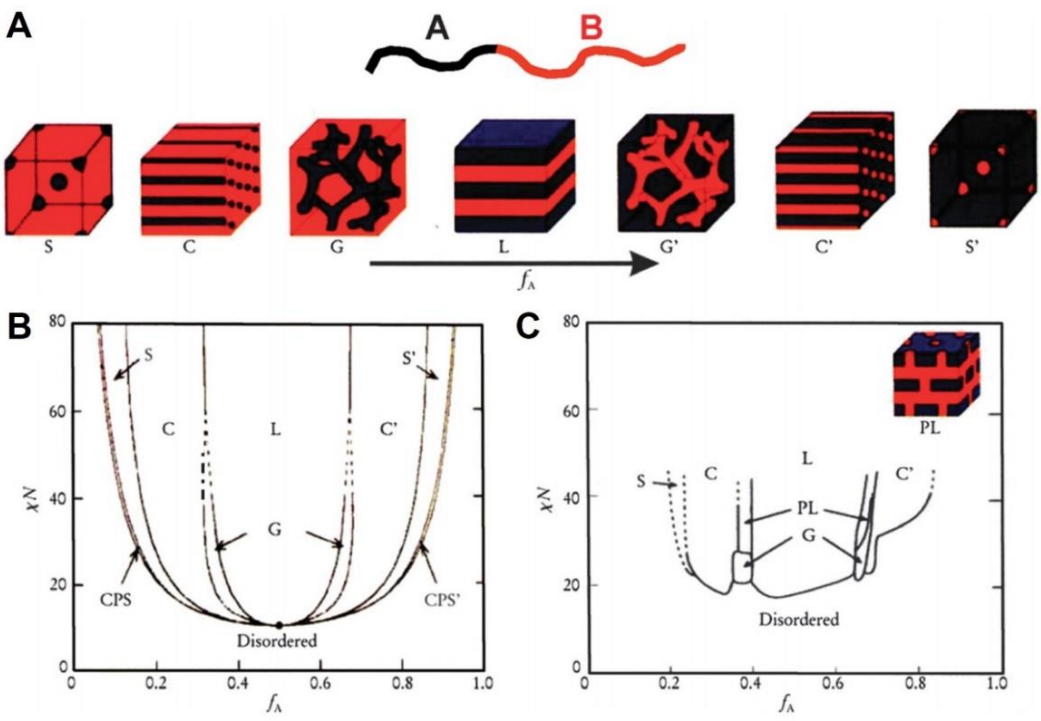

Figure 1-4. (A) Morphologies of self-assembled structures of block copolymers (BCPs) in bulk. (B) Theoretical phase diagram of diblock copolymers predicted by self-consistent field theory (SCFT). f_A = the volume fraction of A block, N = degree of polymerization of the entire BCP, χ = Flory–Huggins parameter. (C) Experimental phase diagram of self-assembly of polyisoprene-*block*-polystyrene in bulk. S and S' = body-centered-cubic spheres, C and C' = hexagonally packed cylinders, G and G' = Bicontinuous gyroids, and L = Lamellae.[31]

1.4 Self-assembly of block copolymers in solution

The self-assembly of BCPs in solution is driven by the affinity between each block and the solvent. Compared to bulk self-assembly, the system becomes much more complex with a solvent. Generally, two types of solvent are used for self-assembly; one is a good solvent for both blocks A and B, while the other is a selective solvent for one of the blocks. Because the χ-parameters between these solvents and the two blocks in the diblock copolymer must be considered, the theoretical calculation and estimation of morphologies of self-assembled structures in solution becomes challenging.[34]

Polymer chemists have researched the self-assembly of amphiphilic BCPs in aqueous solution using water as a selective solvent. Early in research, the Meijer and Eisenberg groups in 1995 reported the aqueous-solution self-assembly of polystyrene-*block*-dendrimer and polystyrene-*block*-poly(acrylic acid) (PS-*b*-PAA) diblock copolymers, respectively.[14,15] In both systems, the hydrophobic blocks were much larger than the hydrophilic blocks, forming so-called "crew-cut" systems, which developed complex morphologies rather than simple spherical micelles. Afterward, the Eisenberg group published numerous papers on observations of several morphologies formed by the solution self-assembly of "crew-cut" PS-*b*-PAA (Figure 1-5).[17,35,36]

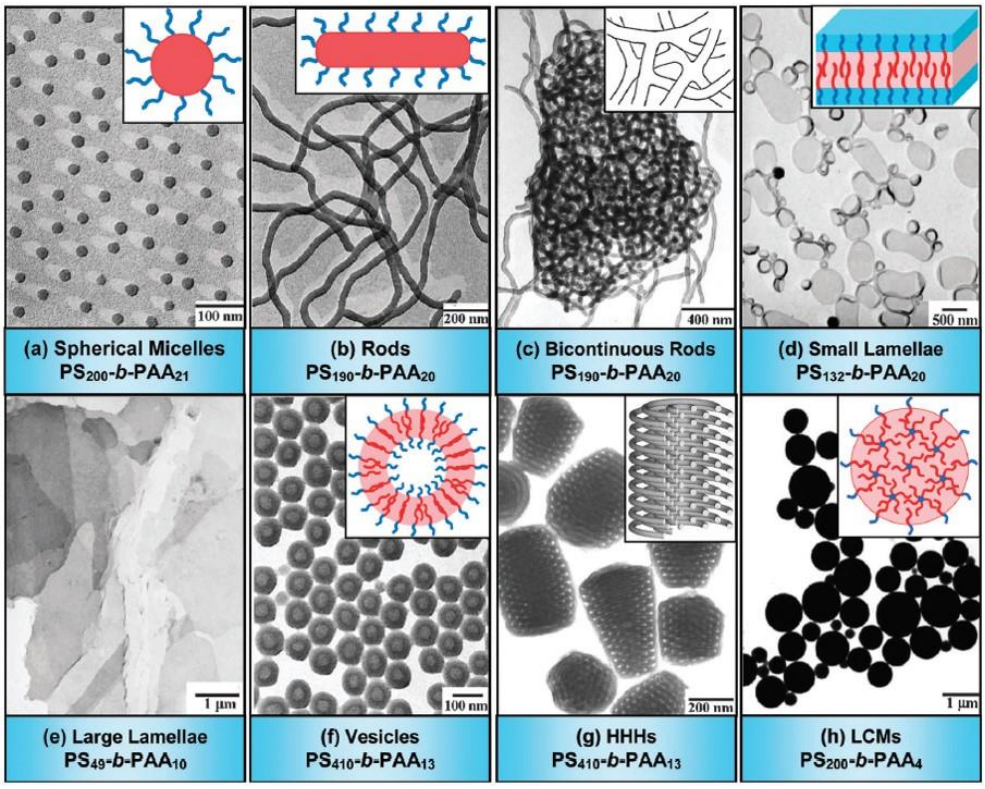

Figure 1-5. TEM images and corresponding schematic diagrams of diverse morphologies from self-assembly of polystyrene-*block*-poly(acrylic acid) copolymers. In the schematic figures, red represents PS blocks and blue indicates PAA blocks. HHHs = hexagonally packed hollow hoops and LCMs = large compound micelles.[36]

Because BCPs have large molecular weights compared to small amphiphilic molecules and many variables are involved, such as the types of good and selective solvents, the BCP components, the block volume fractions, and even the BCP architectures, many morphologies have been observed. In this section, some representative morphologies are introduced with brief explanations and examples. The morphologies detected during the self-assembly of small amphiphilic molecules are also observed in the solution self-assembly of BCPs. They include spherical micelles, cylindrical micelles, vesicles (polymersomes), lamellae, and inverse structures. Finally, a general method to control their morphologies is introduced.

1.4.1 Various morphologies from solution self-assembly of block copolymers

Spherical micelles have spherical cores of the hydrophobic blocks and short coronas of hydrophilic blocks because of their higher affinity to the selective solvent of water. The radius of the spherical core is shorter than the length of the hydrophobic chains. Because of their structural simplicity, spherical micelles are difficult to use in complicated applications. However, they have been utilized as nano-carriers for hydrophobic drugs[37,38] and fluorescence probes[39] because of their concentrated hydrophobic cores.

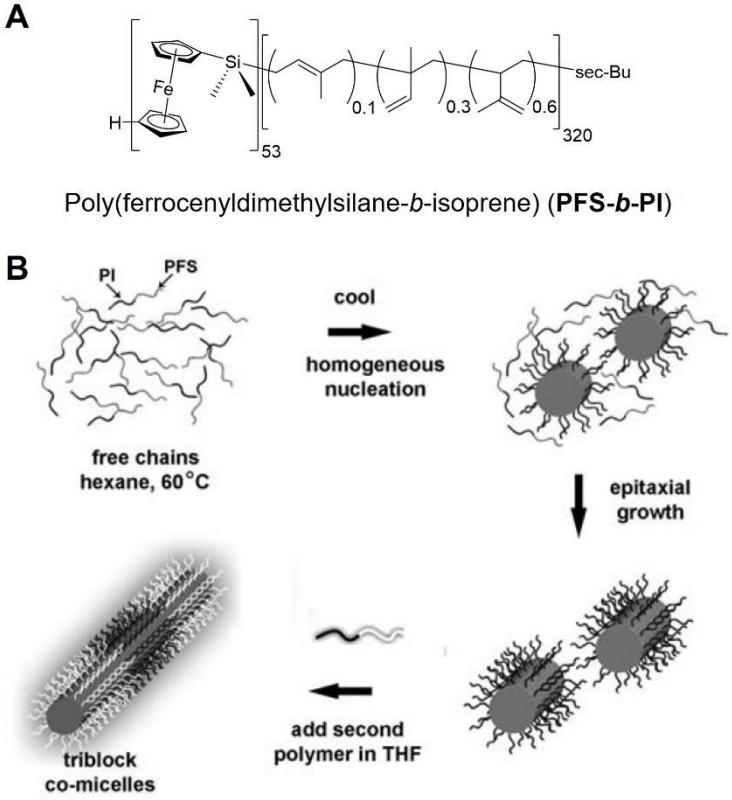

Figure 1-6. (A) A scheme for poly(ferrocenyldimethylsilane-*block*-isoprene) (PFS-*b*-PI) used for the formation of cylindrical micelles. (B) A mechanism for the self-assembly of PFS-*b*-PI and their living self-assembly processes.[40]

Cylindrical micelles have cylindrical cores and coronas surrounding the cores. The core radius remains shorter than the length of the hydrophobic chains for the same reason as for spherical micelles. However, the cylinder length can vary from tens of nanometers to the micrometer scale. Controlling the cylinder length has been a challenge; Manners et al. (2007) reported successful control of the cylinder length by crystallization-driven self-assembly (CDSA) technique (Figure 1-6).[40] They used polyferrocenylsilane-*block*-polyisoprene (PFS-*b*-PI) BCPs to achieve cylindrical micelles.[41] PFS and PI blocks form the core and corona of the cylindrical micelles, respectively. After solution self-assembly, randomly sized cylinders were broken down into extremely short cylinders by sonication. These short cylinders functioned as nucleation cores; additional free polymer chains began to self-assemble at these cores by the epitaxial growth. This process was called "living self-assembly" because of its similarity to living polymerization. Therefore, the cylinder length was controlled by regulating the amount of additional free polymer chains.

Vesicles, also called *polymersomes*, comprise BCP bilayers, like *lamellae*. While lamellae are mostly flat structures, bilayers in polymer vesicles are bent and closed into hollow spheres. Vesicle size varies from tens of nanometers to micrometers because they are thermodynamically stable in structure. Compared to liposomes, polymersomes have much thicker membranes because of their higher molecular weights. Because thick membranes can remain stable for long periods and block the exchange of molecules between the inner and outer space of the vesicle, polymersomes can be exploited as nano-carriers for the delivery of small molecules, including drugs.[42-44] Kim et al. (2012) reported glucose-responsive polymersomes constructed of poly(ethylene glycol)-*block*-polystyreneboroxole (PEG-*b*-PBOx) as insulin-delivery materials (Figure 1-7).[45] The styreneboroxole moiety bonded with monosaccharides, such as glucose and fructose, at physiological pH (~7.4). When monosaccharides became attached to boroxole groups, they acquired negative charges that stabilized their molecular structures, which rendered the hydrophobic blocks soluble in water. Because the polymersomes could not maintain their morphology, the insulin molecules initially located in the polymersome cavity were released to the outside, thus demonstrating a glucose-responsive insulin delivery system.

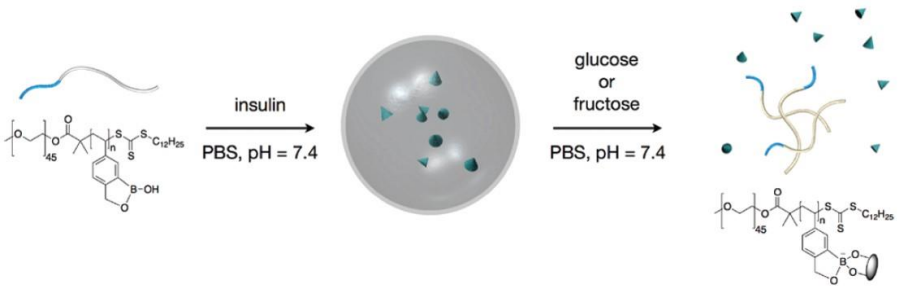

Figure 1-7. Glucose-responsive polymersomes formed by self-assembly of block copolymers containing styreneboroxole and their release of insulin in the presence of monosaccharides.[45]

Inverse structures include large compound vesicles, polymer cubosomes, hexagonal structures, inverse micelles, and more. These structures show much larger sizes and more complicated inner structures compared to those mentioned previously and they have recently attracted specific study. Among such inverse structures, *polymer cubosomes* are considered cutting-edge structures in the field of polymer self-assembly.[46,47] Kim et al. (2014) reported on colloidal inverse bicontinuous cubic membranes (polymer cubosomes) of BCPs and their structural analysis by electron microscopy and small-angle X-ray scattering (SAXS) (Figure 1-8).[48] They used branched-linear PEG-*b*-PS with a high fraction of hydrophobic blocks (~90%). The polymer cubosomes had two bicontinuous water channels with a large crystalline lattice (lattice parameter ~ 50 nm). The internal structures were unique with surface areas sufficiently large to function as carriers; thus, they demonstrated that polymer cubosomes could be used as enzyme carriers by introducing functional groups at the ends of BCPs.

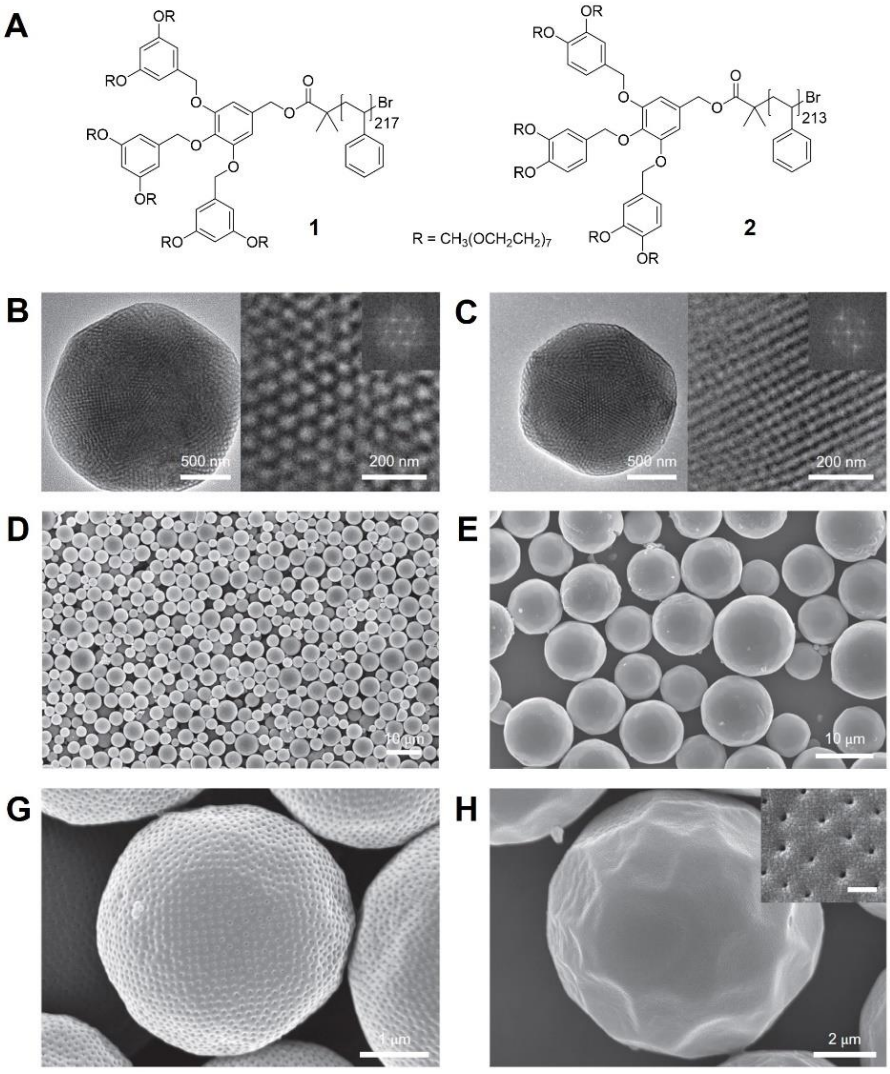

Figure 1-8. (A) Schemes of dendritic-linear PEG-*b*-PS; **1** and **2**. (B, C) TEM images of polymer cubosomes of **1** (B) and **2** (C). (D − H) SEM images of polymer cubosomes of **1** (D, G) and **2** (E, H).[48]

1.4.2 General method to control morphologies

Morphologies generated by the self-assembly of small amphiphilic molecules, like lipids, can be approximated based on the packing parameter (p).[7] However, the solution self-assembly of BCPs cannot be precisely estimated as the assembly of lipids can, because the system is too complex for easy calculation. Regardless, the tendency is similar to that of lipid self-assembly. As the fraction of hydrophobic blocks increases, the morphology of the self-assembled structures becomes larger and more complicated, from spherical micelles, cylindrical micelles, and bilayer structures including vesicles and lamellae to inverse structures. If certain variables, like the BCP components and solvent compositions, are fixed, only the block ratios of the hydrophilic to hydrophobic blocks must be considered to estimate the final morphologies. The most conventional method to control the block ratio is obviously changing the molecular weight of each block. Using this basic rule, various morphologies have been studied until recently.[16,17]

Methods to control the morphologies of self-assembled structures of BCPs, rather than tuning block ratios, are also of interest. One such method enables morphological control by designing molecular architectures; another by introducing external stimuli such as pH transitions and light irradiation.

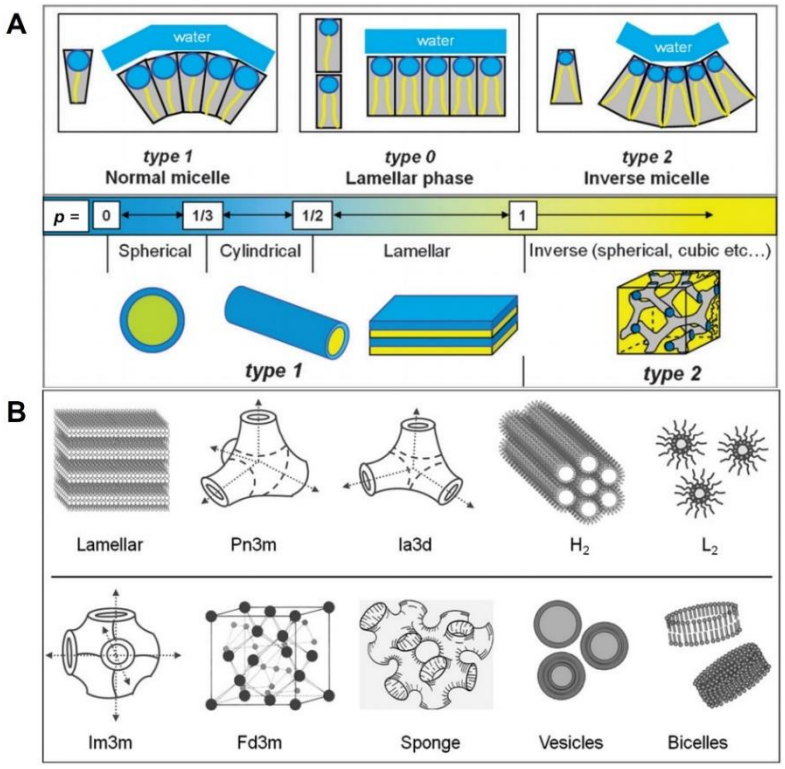

Figure 1-9. (A) A relationship between molecular architectures of amphiphilic lipid molecules and morphologies of self-assembled structures. (B) Various inverse structures that can be observed from self-assembled structures with high molecular packing parameter (p >1). H_2 = hexagonal phases and L_2 = isotropic phases.[6]

1.5 Controlling morphology by molecular design

Most diblock copolymers have linear–linear conformations because these are easily achieved by successive living polymerizations. However, for the self-assembly of amphiphilic lipid molecules, the number of hydrophobic chains can be increased to allow complex structures like bilayers and inverse structures (Figure 1-9). This branching technique is one method to induce the approach of BCP self-assembled structures toward abnormal structures, such as miktoarm polymers[49] and hyperbranched polymers[50], which yield various morphologies that cannot be observed by the conventional self-assembly of linear–linear BCPs. Percec et al. (2010) reported the self-assembly of Janus dendrimers into uniform bilayer structures and other complex structures (Figure 1-10).[51] They used amphiphilic dendrimers with higher molecular weights than lipids but lower weights than amphiphilic BCPs; the important characteristic was the significantly expanded library of amphiphilic molecules because of the introduction of branching to their molecular architectures. From these branched structures, they observed not only vesicles with perfectly uniform size distributions but also other complex structures such as bicontinuous cubic particles, ribbon-like micelles, and disk-like micelles.

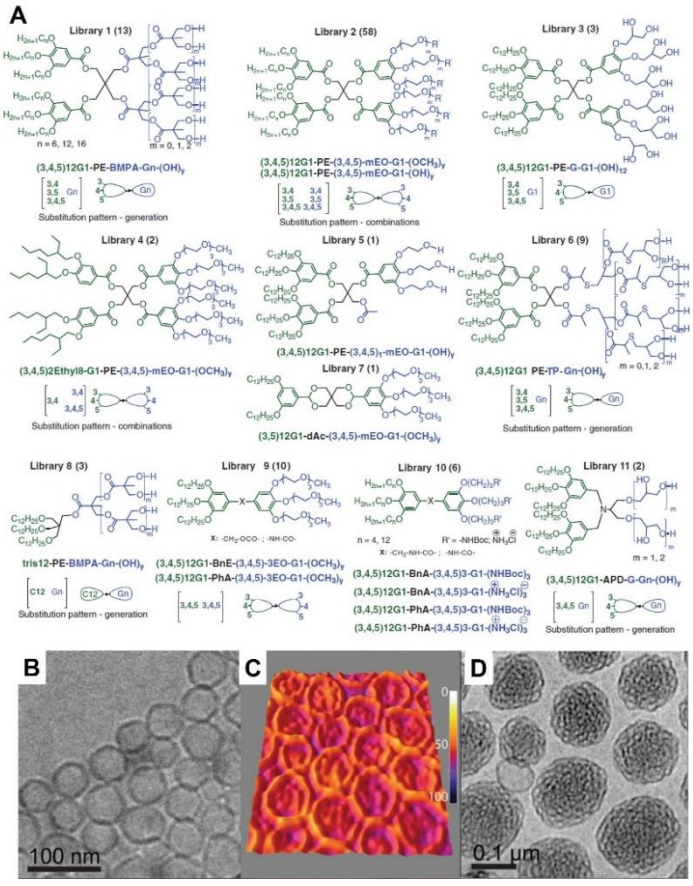

Figure 1-10. (A) Schemes of libraries of amphiphilic Janus dendrimers. (B) TEM image and (C) 3D intensity profile of vesicles with perfectly uniform size distribution. (D) TEM image of bicontinuous cubic particles.[51]

1.6 Controlling morphology by external stimuli

The development of functional materials has been essential in improving the quality of human life; polymers have been designed and synthesized for this purpose. However, at an early stage, the lack of polymerization and organic synthesis tools obstructed access to highly functional polymer materials. As polymerization techniques developed over time, polymers with complicated architectures and functional groups could be synthesized in specified desirable ways. Stimuli-responsive polymers are among a wide range of highly functional polymers that change their physical or chemical properties in response to a target stimulus such as pH changes, the presence of small molecules, light irradiation, and temperature changes.[53,54] Therefore, stimuli-responsive polymers have attracted significant study for many potential applications, including drug delivery and release systems[54] and shape-memory materials.[55] Because of their versatility, stimuli-responsive morphological transitions have also been studied recently. In this section, several stimuli-responsive polymers with morphological transformations are studied.

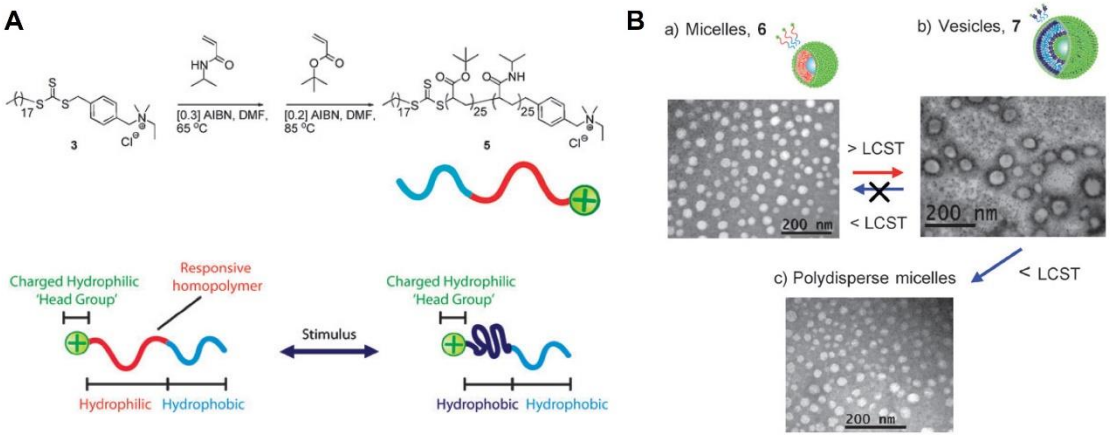

Figure 1-11. (A) Schemes of poly(*t*-butylacrylate)-*block*-poly(*N*-isopropylacrylamide) (PtBA-*b*-PNIPAM) BCPs and their thermo-responsive properties. (B) TEM images of PtBA-*b*-PNIPAM BCPs and their thermos-responsive morphological transitions.[56]

1.6.1 Thermo-responsive morphological transition

O'Reilly et al. (2010) reported on thermos-responsive BCPs and their morphological transitions.[56] They synthesized poly(*t*-butylacrylate)-*block*-poly(*N*-isopropylacrylamide) (PtBA-*b*-PNIPAM) with positively charged end groups by RAFT polymerization (Figure 1-11). PtBA acted as the hydrophobic block, while PNIPAM and the charged end group behaved as the hydrophilic block. The self-assembled structures in an aqueous solution were spherical in morphology. PNIPAM is a popular thermos-responsive polymer with the property of a lower critical solution temperature (LCST). Polymers with LCST points are soluble at temperatures below the LCST and insoluble at temperatures above it. Because the critical temperature of PNIPAM is ~32°C, the PNIPAM block becomes insoluble in water

and behaves hydrophobically as the temperature increases above 32°C. With increasing temperature, the small charged end group remained the only hydrophilic block, thus significantly increasing the block ratio of the hydrophobic block and driving a morphological transition from spherical micelles to vesicles. This structural change was analyzed by dynamic light scattering (DLS) and transmission electron microscopy (TEM). When the temperature was decreased below 32°C, the polymersomes were transformed back to spherical micelles by the inverse process.

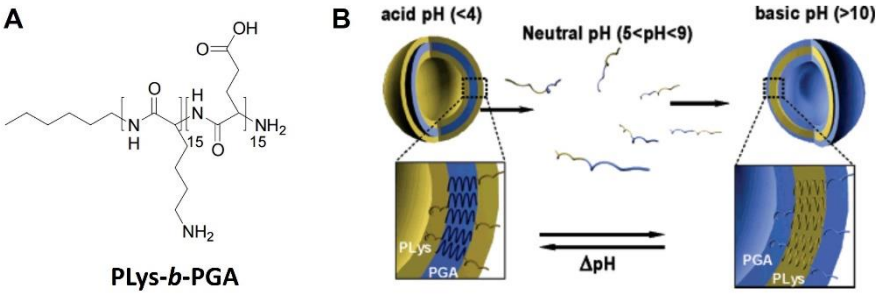

Figure 1-12. (A) A scheme of poly(*L*-lysine)-*block*-poly(glutamic acid) (PLys-*b*-PGA) (B) pH-responsive phase inversion of polymersomes of PLys-*b*-PGA.[57]

1.6.2 pH-responsive morphological transition

Lecommandoux et al. (2005) reported on pH-responsive BCPs and their morphological transitions.[57] They synthesized poly(*L*-lysine)-*block*-poly(glutamic acid) (PLys-*b*-PGA); both blocks respond to pH changes (Figure 1-12). PLys-*b*-PGA is self-assembled into polymersomes with changes in pH. At neutral pH, the BCP has zwitterionic properties solubility in water. In acidic conditions (pH < 4), the PGA blocks lose their charges and form α-helical structures as hydrophobic blocks. In basic conditions (pH > 10), the PLys blocks are neutralized and become hydrophobic. With these solubility transitions, a phase inversion of bilayers is observed by controlling the pH.

Armes et al. (2015) reported on pH-responsive non-ionic diblock copolymers.[58] They synthesized poly(glycerol monomethacrylate)-*block*-poly(2-hydroxypropyl methacrylate) (PGMA-*b*-PHPMA) by RAFT polymerization with two CTAs with carboxylic acid end groups (PETTC) and methyl ester end groups (Me-PETTC) (Figure 1-13). Because both blocks were non-ionic, the only functional group that responds to the external stimulus of pH changes is the carboxylic acid end group in PETTC. PGMA-*b*-PHPMA prepared with PETTC was self-assembled into spherical micelles in neutral conditions because the carboxylate end groups were negatively charged, enhancing the hydrophilicity of the entire BCP. The structure was transformed to cylindrical micelles in acidic solutions because the carboxylate groups became protonated and lost their charge–charge repulsion forces. For control experiments, they also prepared BCPs polymerized by Me-PETTC in which the carboxylic acid end groups were protected by methyl ester groups. In the control BCPs, no morphological transitions were observed.

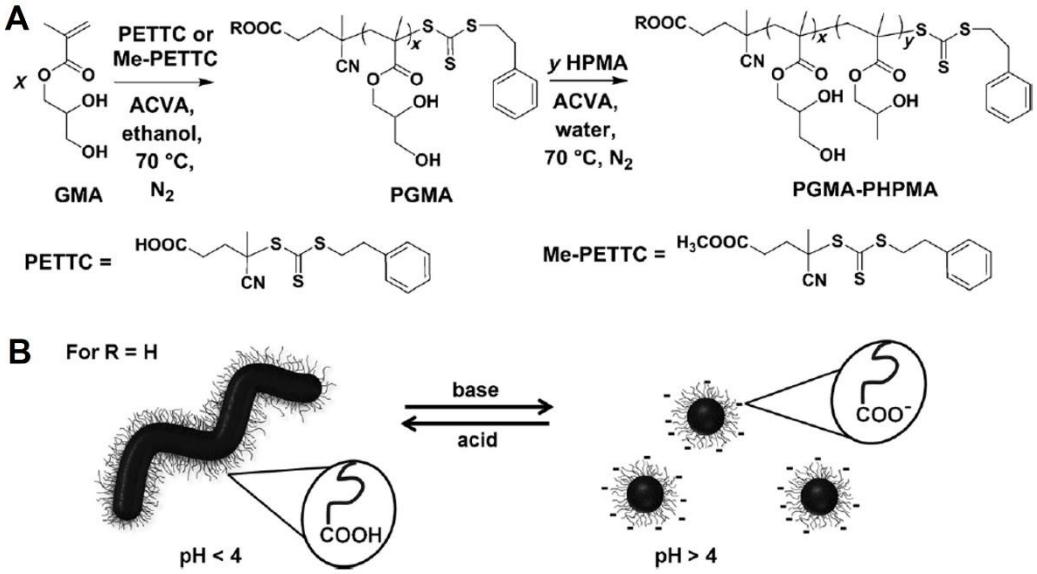

Figure 1-13. (A) Schemes of polymerization of poly(glycerol monomethacrylate)-*block*-poly(2-hydroxypropyl methacrylate) (PGMA-*b*-PHPMA) BCPs and used two chain transfer agents (CTA). (B) pH-responsive morphological transitions between spherical and cylindrical micelles when BCPs with PETTC are subjected to an acidic condition (pH <4).[58]

1.7 Stabilization of morphology by cross-linking

In the above sections, various self-assembly morphologies and methods for morphological control of BCPs are introduced. The physical, chemical, and biological properties of self-assembled structures are essential in the development of potential applications. However, in order to utilize self-assembled structures in harsh environments such as high temperatures, extreme pH, and organic solutions that can dissolve BCPs, the cross-linking of BCPs is necessary. Therefore, polymer chemists are highly interested in the cross-linking of BCPs. Many cross-linking methods have been developed, classified into diverse categories of covalent[59] or non-covalent[60] cross-linking; core[61] or corona[62] cross-linking; and various stimuli-responsive cross-linking mechanisms induced by light[63], complexation with metal precursors[64], and temperature changes[65]. Self-assembled structures cross-linked by these methods can be utilized as nanoscale reactors[66] and stabilized drug-delivery systems.[67]

Among cross-linking methods for BCPs, covalent cross-linking yields networks of polymer chains interconnected by covalent bonds. These covalent bonds are generally induced by the addition of external molecules (cross-linkers) and the initiation of further reactions (cross-linking). For instance, Armes et al. (2012) reported the cross-linking-induced stabilization of vesicles in the presence of a surfactant.[68] They synthesized poly(glycerol monomethacrylate)-*block*-poly(2-hydroxypropyl methacrylate-*co*-glycidyl methacrylate) (PGMA-*b*-P(HPMA-*co*-GlyMA)), which had PGMA as a hydrophilic block, PHPMA as a hydrophobic block, and PGlyMA as a cross-linkable group (Figure 1-14). These BCPs were self-assembled into polymersomes that were extremely unstable at high

concentrations of small-molecule surfactants (1 w/v%). Because the epoxy groups in the hydrophobic blocks could react rapidly with nucleophilic moieties, such as primary amines, under mild conditions, diamine groups were added to a suspension of polymersomes as cross-linking agents. Then the BCPs were cross-linked by multiple epoxy-amine reactions. The resulting cross-linked

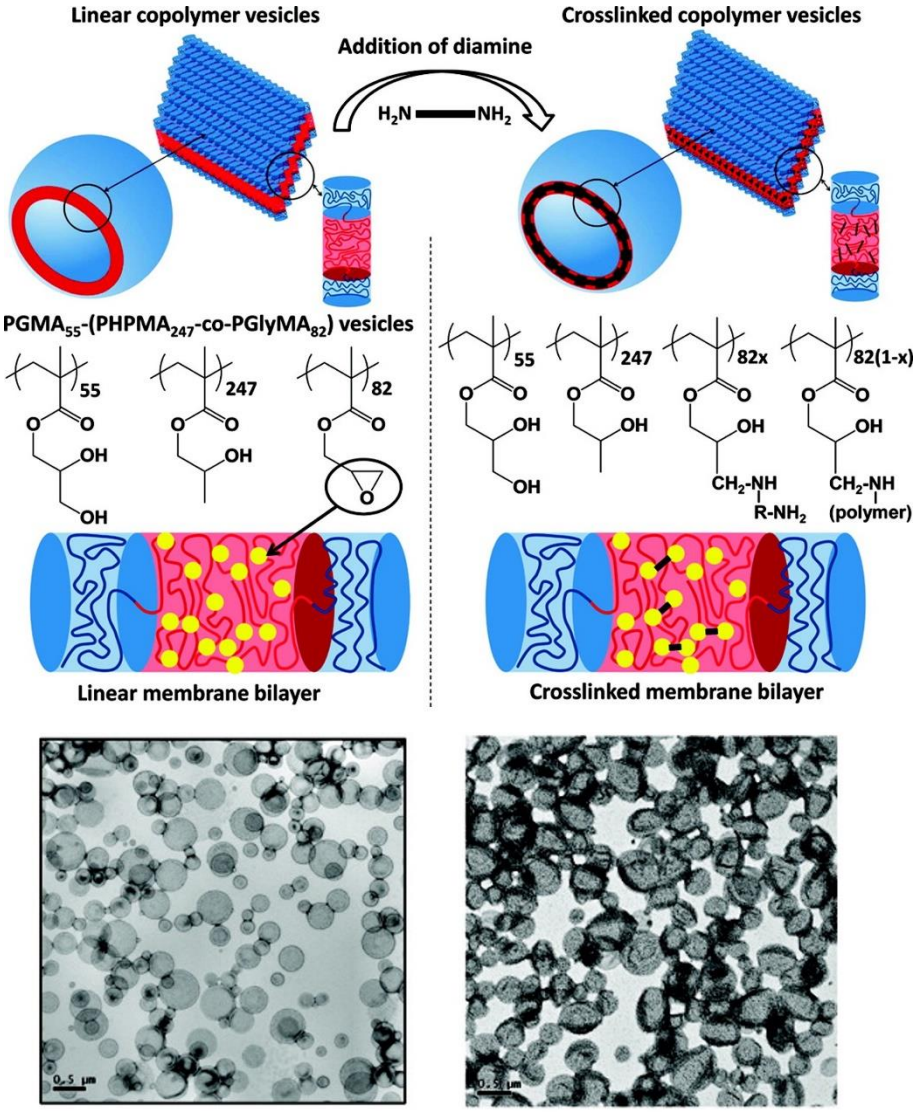

Figure 1-14. Epoxy-amine cross-linking of polymersomes by addition of diamine and TEM images of non-cross-linked (left) and cross-linked polymersomes (right).[68]

1.7.1 Photo-cross-linking of block copolymers

General cross-linking methods require the addition of cross-linkers like diamine, as in the previous example; such processes may destroy the morphologies and modify the shapes of structures. Because of these drawbacks, stimuli-responsive cross-linking systems have been studied extensively; among these, photo-cross-linking systems were attractive to polymer chemists because they offered convenience and versatility.[63] For example, Voit et al. (2014) reported the use of cross-linked

polymersomes as nanoscale reactors for controlled and stabilized enzymatic reactions.[66] They synthesized poly(ethylene glycol)-*block*-poly(diethylaminoethyl methacrylate-*co*-dimethyl maleic imido butyl methacrylate) (PEG-*b*-P(DEAEM-*co*-DMIBM) (Figure 1-15). PDMIBM had photo-cross-linkable groups, while PDEAEM had pH-sensitive groups that became hydrophilic in acidic environments. The BCPs were self-assembled into vesicles; enzymes such as horse radish peroxidase (HRP), glucose oxidase (GOx), and myoglobin (Myo) were simultaneously encapsulated in the inner spaces of the polymersomes. Cross-linking was conducted by the dimerization of double bonds in the PDMIBM blocks under UV irradiation for 40 s. The cross-linked polymersomes showed stability against variable pH solutions pH 6 to 8. For polymersomes in acidic conditions (pH = 6), the bilayer permeability was increased by positive charge–charge repulsion in the hydrophobic blocks, which provided molecular exchange between the inner and outer spaces of the polymersomes. Therefore, enzymatic reactions between the encapsulated enzymes and infiltrated guest molecules were observed with constant activities under repeated reaction cycles.

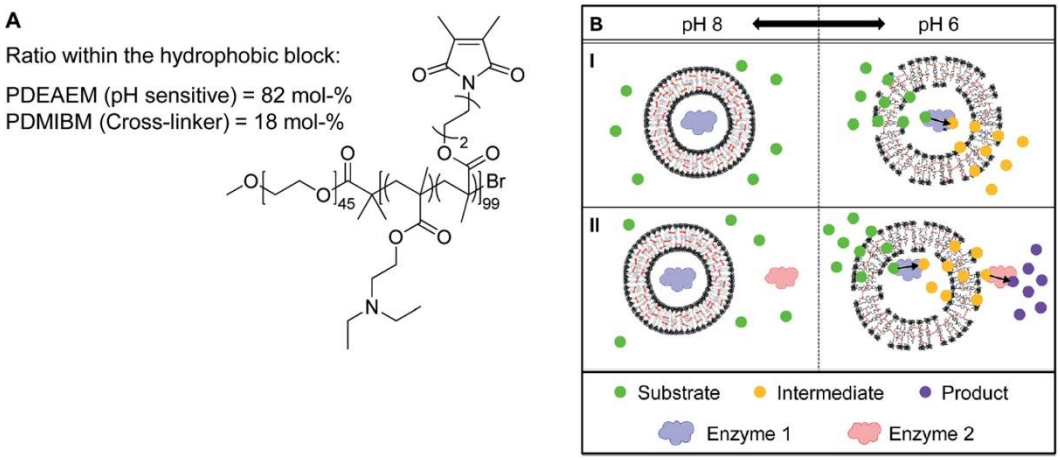

Figure 1-15. (A) A scheme of amphiphilic block copolymers having both photo-cross-linkable and pH-responsive properties. (B) Illustrations of enzymatic reactions with a single enzyme (I) and two enzymes (II).[66]

1.8 Summary of thesis

In the following chapters, BCPs based on PEG-*b*-PS are synthesized and their molecular structures are modified precisely to achieve certain desired characteristics. In chapter 2, dendritic–linear PEG-*b*-PS BCPs are synthesized and their self-assembled structures are observed. Furthermore, their morphologies are compared to those of linear–linear BCPs and the relationships between BCP architectures and their morphologies at fixed block ratios are studied.

In chapter 3, self-assembled structures such as micelles, vesicles, inverse sponge phases, and polymer cubosomes are stabilized by an unusual photo-cross-linking method. The indenylstyrene monomer is newly introduced to the hydrophobic block by co-polymerization with styrene; indene functional groups

are covalently linked by dimerization under UV irradiation. In this way, the stability of cross-linked morphologies is examined under extreme dilution by an organic solvent.

In chapter 4, branched–linear BCPs with high-molecular-weight PS blocks (~200,000 g/mol) are synthesized by ATRP and purified by gradient column chromatography. The BCPs are self-assembled by two methods of co-solvents and solvent diffusion–evaporation. Polymer cubosomes with high lattice parameters, comparable to biological lipid cubic membranes, and their photonic bandgap properties are studied.

In the last chapter, multiple stimuli-responsive morphological transitions are researched. Three pyridine groups are introduced at the junctions of peripheral PEG chains and then branched–linear PEG-*b*-PS BCPs are synthesized by RAFT polymerization. Because of the pyridine groups, the BCPs respond to low pH and metal precursors, yielding various morphologies in diverse conditions.

Some parts of the following chapters were already published

Chapter 2. Jeong, M. G.; van Hest, J. C. M.; Kim, K. T. Self-Assembly of Dendritic-Linear Block Copolymers with the Fixed Molecular Weight and Block Ratio. *Chem. Commun.*, **2012**, *48*, 3590-3592.

Chapter 3. Jeong, M. G.; Kim, K. T. Covalent Stabilization of Inverse Bicontinuous Cubic Structures of Block Copolymer Bilayers by Photodimerization of Indene Pendant Groups of Polystyrene Hydrophobic Blocks. *Macromolecules*, **2017**, *50*, 223-234

1.9 References

1. Lutton, E. S. Phase Behavior of Aqueous Systems of Monoglycerides. *J. Am. Oil Chem.'Soc.* **1965**, *42*, 1068-1070.
2. Sagalowicz, L.; Leser, M. E.; Watzke, H. J.; Michel, M. Monoglyceride Self-Assembly Structures as Delivery Vehicles. *Trends Food Sci. Technol.* **2006**, *17*, 204-214.
3. Ganem-Quintanar, A.; Quintanar-Guerrero, D.; Buri, P. Monoolein: A Review of the Pharmaceutical Applications. *Drug Dev. Ind. Pharm.* **2000**, *26*, 809-820.
4. Fong, C.; Le, T.; Drummond, C. J. Lyotropic liquid crystal engineering–ordered nanostructured small molecule amphiphile self-assembly materials by design. *Chem. Soc. Rev.* **2012**, *41*, 1297-1322.
5. Qiu, H.; Caffrey, M. The Phase Diagram of the Monoolein/Water System: Metastability and Equilibrium Aspects. *Biomaterials* **2000**, *21*, 223.
6. Kulkarni, C. V.; Wachter, W.; Iglesias-Salto, G.; Engelskirchen, S.; Ahualli, S. Monoolein: a magic lipid? *Phys. Chem. Chem. Phys.* **2011**, *13*, 3004-3021.
7. Israelachvili, J. N.; Mitchell, D. J.; Ninham, B. W. Theory of Self-Assembly of Hydrocarbon Amphiphiles into Micelles and Bilayers. *J. Chem. Soc., Faraday Trans. 2* **1976**, *72*, 1525-1568.
8. Israelachvili, J. N.; Mitchell, D. J.; Ninham, B. W. Theory of Self-Assembly of Lipid Bilayers and

Vesicles. *Biochim. Biophys. Acta* **1977**, *470*, 185-201.

9. Nagarajan, R. Molecular Packing Parameter and Surfactant Self-Assembly: The Neglected Role of the Surfactant Tail. *Langmuir* **2002**, *18*, 31-38.
10. Nagarajan, R.; Ruckenstein, E. Theory of Surfactant Self-Assembly: A Predictive Molecular Thermodynamic Approach. *Langmuir* **1991**, *7*, 2934-2969.
11. Szwarc, M. 'Living' Polymers. *Nature* **1956**, *178*, 1168-1169.
12. Matyjaszewski, K. Architecturally Complex Polymers with Controlled Heterogeneity. *Science* **2011**, *333*, 1104-1105.
13. Matyjaszewski, K.; Tsarevsky, N. V. Nanostructured Functional Materials Prepared by Atom Transfer Radical Polymerization. *Nat. Chem.* **2009**, *1*, 276-288.
14. van Hest, J. C. M.; Delnoye, D. A. P.; Baars, M. H. P.; van Genderen, M. H. P.; Meijer, E. W. Polystyrene-Dendrimer Amphiphilic Block Copolymers with a Generation-Dependent Aggregation. *Science* **1995**, *268*, 1592.
15. Zhang, L.; Eisenberg, A. Multiple Morphologies of "Crew-Cut" Aggregates of Polystyrene-*b*-Poly(acrylic acid) Block Copolymers. *Science* **1995**, *268*, 1728.
16. Riess, G. Micellization of Block Copolymers. *Prog. Polym. Sci.* **2003**, *28*, 1107-1170.
17. Mai, Y.; Esienberg, A. Self-Assembly of Block Copolymers. *Chem. Soc. Rev.* **2012**, *41*, 5969-5985.
18. Webster, O. W. Living Polymerization Methods. *Science*, **1991**, *251*, 887-893.
19. Yagci, Y.; Tasdelen, M. A. Mechanistic Transformations Involving Living and Controlled/Living Polymerization Methods. *Prog. Polym. Sci.* **2006**, *31*, 1133-1170.
20. Morton, M.; Fetters, L. J. Anionic Polymerization of Vinyl Monomers. *Rubber Chem. Technol.* **1975**, *48*, 359-409.
21. Hadjichristidis, N.; Pitsikalis, M.; Pispas, S.; Iatrou, H. Polymers with Complex Architecture by Living Anionic Polymerization. *Chem. Rev.* **2001**, *101*, 3747-3792.
22. Aoshima, S.; Kanaoka, S. A Renaissance in Living Cationic Polymerization. *Chem. Rev.* **2009**, *109*, 5245-5287.
23. Braunecker, W. A.; Matyjaszewski, K. Controlled/Living Radical Polymerization: Features, Developments, and Perspectives. *Prog. Polym. Sci.* **2007**, *32*, 93-146.
24. Bielawski, C. W.; Grubbs, R. H. Living Ring-Opening Metathesis Polymerization. *Prog. Polym. Sci.* **2007**, *32*, 1-29.
25. Matyjaszewski, K.; Xia, J. Atom Transfer Radical Polymerization. *Chem. Rev.* **2001**, *101*, 2921-2990.
26. Matyjaszewski, K. Atom Transfer Radical Polymerization (ATRP): Current Status and Future Perspectives. *Macromolecules* **2012**, *45*, 4015-4039.
27. Moad, G.; Chong, Y. K.; Postma, A.; Rizzardo, E.; Thang, S. H. Advances in RAFT Polymerization: the Synthesis of Polymers with Defined End-Groups. *Polymer* **2005**, *46*, 8458-8468.

28. Hawker, C. J.; Bosman, A. W.; Harth, E. New Polymer Synthesis by Nitroxide Mediated Living Radical Polymerizations. *Chem. Rev.* **2001**, *101*, 3661-3688.
29. Nicolas, J.; Guillaneuf, Y.; Lefay, C.; Bertin, D.; Gigmes, D.; Charleux, B. Nitroxide-Mediated Polymerization. *Prog. Polym. Sci.* **2013**, *38*, 63-235.
30. Matsen, M. W.; Schick, M. Self-Assembly of Block Copolymers. *Curr. Opin. Colloid Interface Sci.* **1996**, *1*, 329-336.
31. Bates, F. S.; Fredrickson, G. H. Block Copolymers−Designer Soft Materials. *Phys. Today* **1999**, *52*, 32-38.
32. Leibler, L. Theory of Microphase Separation in Block Copolymers. *Macromolecules* **1980**, *13*, 1602-1617.
33. Khandpur, A. K.; Föster, S.; Bates, F. S.; Hamley, I. W.; Ryan, A. J.; Almdal, K.; Mortensen, K. Polyisoprene−Polystyrene Diblock Copolymer Phase Diagram near the Order−Disorder Transition. *Macromolecules* **1995**, *28*, 8796-8806.
34. He, X.; Liang, H.; Huang, L.; Pan, C. Complex Microstructures of Amphiphilic Diblock Copolymer in Dilute Solution. *J. Phys. Chem. B* **2004**, *108*, 1731-1735.
35. Zhang, L.; Eisenberg, A. Multiple Morphologies and Characteristics of "Crew-Cut" Micelle-like Aggregates of Polystyrene-*b*-poly(acrylic acid) Diblock Copolymers in Aqueous Solutions. *J. Am. Chem. Soc.* **1996**, *118*, 3168-3181.
36. Cameron, N. S.; Corbierre, M. K.; Eisenberg, A. Asymmetric Amphiphilic Block Copolymers in Solution: a Morphological Wonderland. *Can. J. Chem.* **1999**, *77*, 1311-1326.
37. Harada, A.; Kataoka, K. Supramolecular assemblies of block copolymers in aqueous media as nanocontainers relevant to biological applications. *Prog. Polym. Sci.* **2006**, *31*, 949-982.
38. Kataoka, K.; Harada, A.; Nagasaki, Y. Block Copolymer Micelles for Drug Delivery: Design, Characterization and Biological Significance. *Adv. Drug Deliv. Rev.* **2012**, *64*, 37-48.
39. Maysinger, D.; Lovrić, J.; Eisenberg, A.; Savić, R. Fate of Micelles and Quantum Dots in Cells. *Eur. J. Pharm. Biopharm.* **2007**, *65*, 270-281
40. Wang, X.; Guerin, G.; Wang, H.; Wang, Y.; Manners, I.; Winnik, M. A. Cylindrical Block Copolymer Micelles and Co-Micelles of Controlled Length and Architecture. *Science* **2007**, *317*, 644-647.
41. Massey, J. A.; Temple, K.; Cao, L.; Rharbi, Y.; Raez, J.; Winnik, M. A.; Manners, I. Self-Assembly of Organometallic Block Copolymers: The Role of Crystallinity of the Core-Forming Polyferrocene Block in The Micellar Morphologies Formed by Poly(ferrocenylsilane-*b*-dimethylsiloxane) in n-Alkane Solvents. *J. Am. Chem. Soc.* **2000**, *122*, 11577-11584.
42. Discher, D. E.; Eisenberg, E. Polymer Vesicles. *Science* **2002**, *297*, 967-973.
43. Tanner, P.; Baumann, P.; Enea, R.; Onaca, O.; Palivan, C.; Meier, W. Polymer Vesicles: From Drug Carriers to Nanoreactors and Artificial Organelles. *Acc. Chem. Res.* **2011**, *44*, 1039-1049.

44. Kim, K. T.; Meeuwissen, S. A.; Nolte, R. J. M.; van Hest, J. C. M. Smart Nanocontainers and Nanoreactors. *Nanoscale* **2010**, *2*, 844-858.
45. Kim, H.; Kang, Y. J.; Kang, S.; Kim, K. T. Monosaccharide-Responsive Release of Insulin from Polymersomes of Polyboroxole Block Copolymers at Neutral pH. *J. Am. Chem. Soc.* **2012**, *134*, 4030-4033.
46. McKenzie, B. E.; Nudelman, F.; Bomans, P. H. H.; Holder, S. J.; Sommerjijk, N. A. J. M. Temperature-Responsive Nanospheres with Bicontinuous Internal Structures from a Semicrystalline Amphiphilic Block Copolymer. *J. Am. Chem. Soc.* **2012**, *132*, 10256-10259.
47. An, T. H.; La, Y.; Cho, A.; Jeong, M. G.; Shin, T. J.; Park, C.; Kim, K. T. Solution Self-Assembly of Block Copolymers Containing a Branched Hydrophilic Block into Inverse Bicontinuous Cubic Mesophases. *ACS Nano* **2015**, *9*, 3084-3096.
48. La, Y.; Park, C.; Shin, T. J.; Joo, S. H.; Kang, S.; Kim, K. T. Colloidal Inverse Bicontinuous Cubic Membranes of Block Copolymers with Tunable Surface Functional Groups. *Nat. Chem.* **2014**, *6*, 534-541.
49. Khanna, K.; Varshney, S.; Kakkar, A. Miktoarm Star Polymers: Advances in Synthesis, Self-Assembly, and Applications. *Polym. Chem.* **2010**, *1*, 1171-1185.
50. Zhou, Y.; Huang, W.; Liu, J.; Zhu, X.; Yan, D. Self-Assembly of Hyperbranched Polymers and Its Biomedical Applications. *Adv. Mater.* **2010**, *22*, 4567-4590.
51. Percec, V.; Wilson, D. A.; Leowanawat, P.; Wilson, C. J.; Hughes, A. D.; Kaucher, M. S.; Hammer, D. A.; Levine, D. H.; Kim, A. J.; Bates, F. S.; Davis, K. P.; Lodge, T. P.; Klein, M. L.; DeVane, R. H.; Aqad, E.; Rosen, B. M.; Argintaru, A. O.; Sienkowska, M. J.; Rissanen, K.; Nummelin, S.; Ropponen, J. Self-Assembly of Janus Dendrimers into Uniform Dendrimersomes and Other Complex Architectures. *Science* **2010**, *328*, 1009-1014.
52. Alarcón, C. H.; Pennadam, S.; Alexander, C. Stimuli Responsive Polymers for Biomedical Applications. *Chem. Soc. Rev.* **2005**, *34*, 276-285.
53. Stuart, M. A. C.; Huck, W. T. S.; Genzer, J.; Müller, M.; Ober, C.; Stamm, M.; Sukhorukov, G. B.; Szleifer, I.; Tsukruk, V. V.; Urban, M.; Winnik, F.; Zauscher, S.; Luzinov, I.; Minko, S. Emerging Applications of Stimuli-Responsive Polymer Materials. *Nat. Mater.* **2010**, *9*, 101-113.
54. Meng, F.; Zhong, Z.; Feijen, J. Stimuli-Responsive Polymersomes for Programmed Drug Delivery. *Biomacromolecules* **2009**, *10*, 197-209.
55. Meng, H.; Xiao, P.; Gu, J.; Wen, X.; Xu, J.; Zhao, C.; Zhang, J.; Chem, T. Self-Healable Macro/Microscopic Shape Memory Hydrogels Based on Supramolecular Interactions. *Chem. Commun.* **2014**, *50*, 12277-12280.
56. Moughton, A. O.; O'Reilly, R. K. Thermally Induced Micelle to Vesicle Morphology Transition for a Charged Chain End Diblock Copolymer. *Chem. Commun.* **2010**, *46*, 1091-1093.
57. Rodríguez-Hernández, J.; Lecommandoux, S. Reversible Inside−Out Micellization of pH-

responsive and Water-Soluble Vesicles Based on Polypeptide Diblock Copolymers. *J. Am. Chem. Soc.* **2005**, *127*, 2026.

58. Lovett, J. R.; Warren, J. W.; Ratcliffe, L. P. D.; Kocik, M. K.; Armes, S. P. pH-Responsive Non-Ionic Diblock Copolymers: Ionization of Carboxylic Acid End-Groups Induces an Order-Order Morphological Transition. *Angew. Chem. Int. Ed.* **2015**, *54*, 1279-1283.
59. O'Reilly, R. K.; Hawker, C. J.; Wooley, K. L. Cross-Linked Block Copolymer Micelles: Functional Nanostructures of Great Potential and Versatility. *Chem. Soc. Rev.* **2006**, *35*, 1068-1083.
60. Thibault, R. J.; Hotchkiss, P. J.; Gray, M.; Rotello, V. M. Thermally Reversible Formation of Microspheres through Non-Covalent Polymer Cross-Linking. *J. Am. Chem. Soc.* **2003**, *125*, 11249-11252.
61. Shuai, X.; Merdan, T.; Schaper, A. K.; Xi, F.; Kissel, T. Core-Cross-Linked Polymeric Micelles as Paclitaxel Carriers. *Bioconjugate Chem.* **2004**, *15*, 441-448.
62. Read, E. S.; Armes, S. P. Recent Advances in Shell Cross-Linked Micelles. *Chem. Commun.* **2007**, *7*, 3021-3035.
63. Gohy, J. F.; Zhao, Y. Photo-Responsive Block Copolymer Micelles: Design and Behavior. *Chem. Soc. Rev.* **2013**, *42*, 7117-7129.
64. Rupar, P. A.; Chabanne, L.; Winnik, M. A.; Manners, I. Non-Centrosymmetric Cylindrical Micelles by Unidirectional Growth. *Science* **2012**, *337*, 559-562.
65. Zhao, H.-B.; Liu, B.-W.; Wang, X.-L.; Chen, L.; Wang, X.-L.; Wang, Y.-Z. A Flame-Retardant-Free and Thermo-Cross-Linkable Copolyester: Flame-Retardant and Anti-Dripping Mode of Action. *Polymer* **2014**, *55*, 2394-2403.
66. Gräfe, D.; Gaitzsch, J.; Appelhans, D.; Voit, B. Cross-Linked Polymersomes as Nanoreactors for Controlled and Stabilized Single and Cascade Enzymatic Reactions. *Nanoscale* **2014**, *6*, 10752-10761
67. Chen, X.; Ding, X.; Zheng, Z.; Peng, Y. Thermosensitive Cross-Linked Polymer Vesicles for Controlled Release System. *New J. Chem.* **2006**, *30*, 577-582.
68. Chambon, P.; Blanazs, A.; Battaglia, G.; Armes, S. P. How Does Cross-Linking Affect the Stability of Block Copolymer Vesicles in the Presence of Surfactant? *Langmuir* **2012**, *28*, 1196-1205.

Chapter 2. Self-Assembly of Dendritic-Linear Block Copolymers with Fixed Molecular Weight and Block Ratio

2.1 Abstract

Block copolymers built on a dendritic block having fixed molecular weight but different number of peripheral PEG chains were synthesized. At a fixed block ratio, these block copolymers exhibited topological transition of cylindrical micelles depending on the number of PEG chains.

2.2 Introduction

Self-assembly of block copolymers in solution has been a facile way to create a variety of nanostructures.[1,2] So far, the common strategy to create self-assembled structures of a block copolymer with a preferred morphology has been to control the molecular weight of both the hydrophilic and hydrophobic blocks so that the ratio between two blocks lies in the region where the close packing of the block copolymer prefers a desired geometry. Although this strategy, drawn from the analogy to the packing factor theory of amphiphiles,[3] has proven to be effective,[4,5] the flexible conformation of linear block copolymers partly limits a thorough assessment and exploration of the structure–property relationship with respect to self-assembly. Furthermore, a subtle control of self-assembly of block copolymers to obtain more complex topological variants of simple micelles and vesicles such as toroids, branched networks, and shape transformed vesicles has only been realized in a few cases by using specific thermodynamic and kinetic manipulations of the self-assembly process.[6-26]

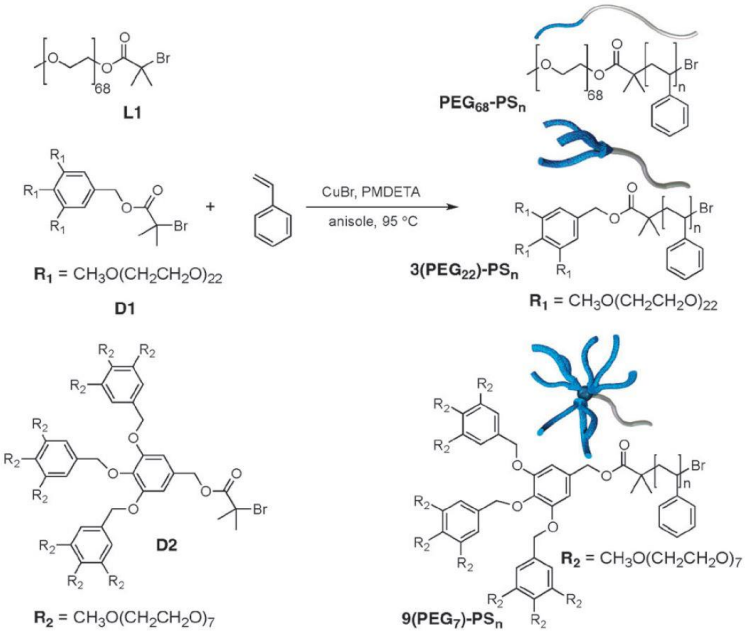

Figure 2-1. Block copolymers containing a linear or dendritic PEG hydrophilic block. The molecular weight of the PEG segment is fixed at ca. 3000 g mol^{-1}

In this chapter, we describe a new design concept to synthesize amphiphilic block copolymers to rationally control the topology of the self-assembled structure. Our design involves a hydrophilic block constructed on a dendritic scaffold[27-30] for which the number of the peripheral hydrophilic chains can be precisely controlled while the overall molecular weight of the hydrophilic segment is unchanged by matching the molecular weight of individual peripheral chains (Figure 2-1). This enables us to induce a change in the molecular packing geometry at the interface of the hydrophobic core of the micelle without significantly altering the weight ratio between two blocks. As a result, we specifically induce a topological change in cylindrical micelles from linear cylinders to either toroidal or lasso (a ring attached to a linear cylinder) micelles, which is caused by differences in the steric effect on the corona of the micelles. Our results contribute to a better understanding of the structure and self-assembly behavior relationship of block copolymers in solution and may provide a new way of a rational control over morphology of self-assembled micellar and vesicular structures.

2.3 Results and Discussion

We chose poly(ethylene glycol) (PEG) as a water-soluble peripheral chain due to its non-ionic character preventing strong chain–chain interaction. Peripheral PEG chains were introduced into the benzyl ether dendrons synthesized according to the literature procedure.[31,32] The molecular weight of the PEG segment was adjusted to ca. 3000 g mol^{-1}. Therefore, 3 PEG chains of M_n = 1000 g mol^{-1} were introduced for the first generation dendron **D1** and 9 PEG chains (M_n = 350 g mol^{-1}) were used for the second generation dendron **D2** (Figure 2-1). By this design, we only changed the number of peripheral PEG chains in the hydrophilic block without varying the molecular weight of the entire PEG segment (Figure 2-2). Block copolymers with the same length as a PS block were synthesized by using these macroinitiators under standard ATRP conditions. All block copolymers revealed a well-defined molecular weight and narrow polydispersity. The number average degree of polymerisation (DP_n) of block copolymers was measured by ^{1}H NMR integration, which coincided with the estimated DP_n values from GPC results (Table 2-1).

All micelle samples were prepared by adding water slowly to a dioxane solution of block copolymers. Formation of cylindrical micelles was pronounced for the dendritic-linear block copolymers for which the molecular weight was in a range of 18 000–21 000 g mol^{-1}. For example, micelle solutions prepared from the dioxane solutions (0.5 wt%) of **3(PEG$_{22}$)–PS$_{152}$** and **9(PEG$_7$)–PS$_{150}$** (the subscript denotes the calculated number average degree of polymerization) showed long cylindrical micelles on TEM (Figure 2-3A and C). In contrast, block copolymers having a linear PEG chain in the same molecular weight range only formed vesicles under the same preparation conditions (Figure 2-4).

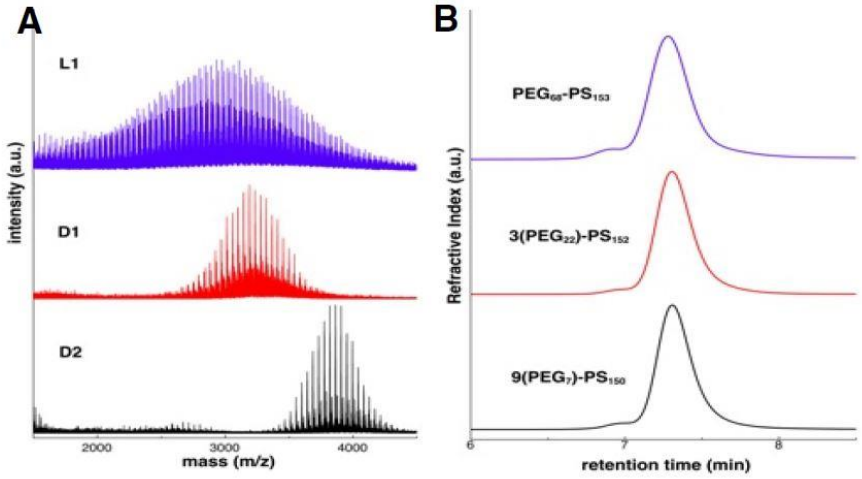

Figure 2-2. (A) MALDI-TOF spectra a linear PEG (**L1**) and PEG-based macroinitiators (**D1**, **D2**). Excluding the dendritic benzyl ether scaffold, the molecular weight of the PEG segment determined by MALDI-TOF was 2998 g mol^{-1} for **D1** and 3140 g mol^{-1} for **D2**, which are close to the molecular weight of the linear PEG analog **L1** (3020 g mol^{-1}). (B) GPC spectra of block copolymers containing a linear and dendritic PEG block.

Table 2-1. Molecular characteristics of the block copolymers

Entry	M_n (GPC) (kg/mol)[a]	$Đ$ (GPC)[a]	DP_n[b]	f_{PEG} (%)[c]
PEG_{68}-PS_{153}	19.2	1.13	159	15.6
PEG_{68}-PS_{170}	20.9	1.08	176	14.3
3(PEG_{22})-PS_{120}	15.8	1.07	114	18.9
3(PEG_{22})-PS_{152}	19.3	1.08	156	15.5
3(PEG_{22})-PS_{171}	21.1	1.08	177	14.2
9(PEG_7)-PS_{121}	16.3	1.07	116	19.3
9(PEG_7)-PS_{150}	19.4	1.08	151	16.2
9(PEG_7)-PS_{166}	21.0	1.08	171	15.0

[a]Molecular weights and polydispersity index measured by gel permeation chromatography (GPC). [b]Calculated number average degree of polymerization from the ^{1}H NMR integration (PEG vs aromatic signal of PS). [c]The calculated weight fraction of a PEG block in the block copolymers based on GPC results.

From the TEM study, we also observed a small number of toroidal cylindrical micelles for the dioxane solutions (0.5 wt%) of **3(PEG_{22})–PS_{152}** and **9(PEG_7)–PS_{150}** (Figure 2-5). Dominant cyclization over a linear growth of micelles has been demonstrated before by designing a tetramer of dodecyltrimethylammonium bromide (DTAB) with a precisely tuned packing factor and a maximized

free energy of the end caps of a cylindrical micelle.[14] This is a crucial prerequisite for cyclization of micelles, which stabilizes the toroidal micelle by the reduction of such a high free energy area through a merger of the two end caps. As observed from cyclization during step-growth polymerization under equilibrium conditions, a low concentration of surfactants in the medium and a low critical micelle concentration have been suggested as important factors to suppress the linear growth of a micelle and to enhance the population of toroidal micelles.[33-35]

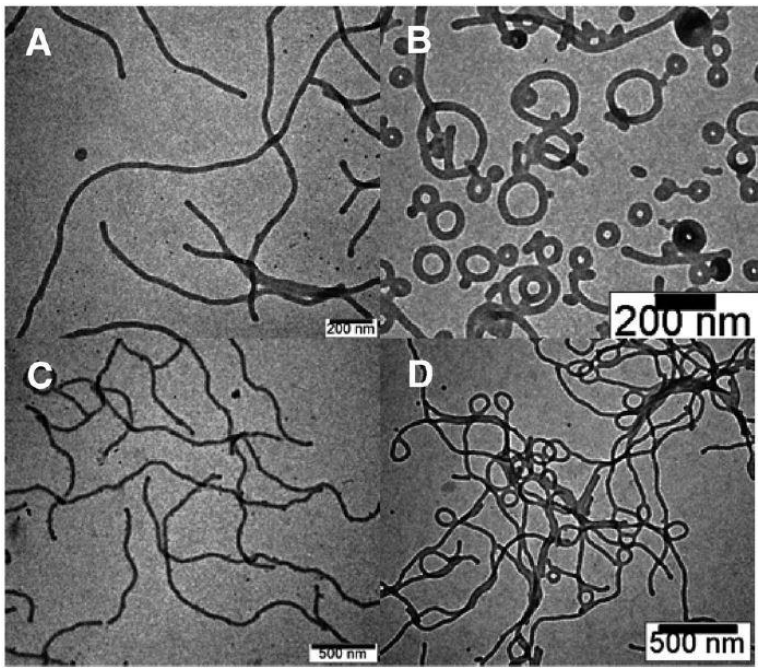

Figure 2-3. TEM images obtained from dried micelle solutions of dendritic-linear block copolymers. (A) **3(PEG$_{22}$)-PS$_{152}$** (0.5 wt%). (B) **3(PEG$_{22}$)-PS$_{152}$** (0.05 wt%). (C) **9(PEG$_{7}$)-PS$_{150}$** (0.5 wt%). (D) **9(PEG$_{7}$)-PS$_{150}$** (0.05 wt%).

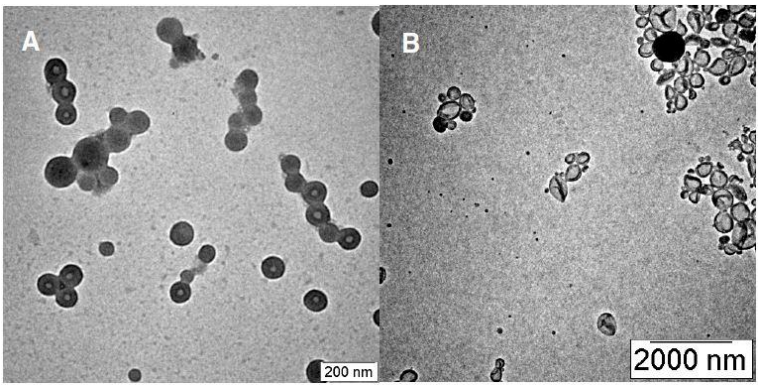

Figure 2-4. TEM images of vesicles of **PEG$_{68}$-P$_{S153}$** prepared from (A) THF and (B) dioxane.

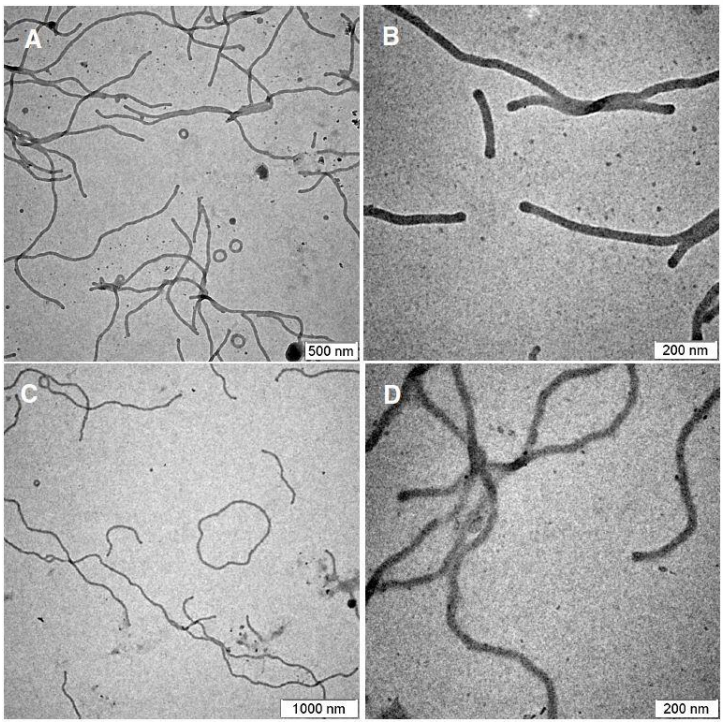

Figure 2-5. Representative TEM images of cylindrical micelles prepared from the dioxane solution (0.5 wt%) of **3(PEG$_{22}$)-PS$_{152}$** (A and B) and **9(PEG$_{7}$)-PS$_{150}$** (C and D)

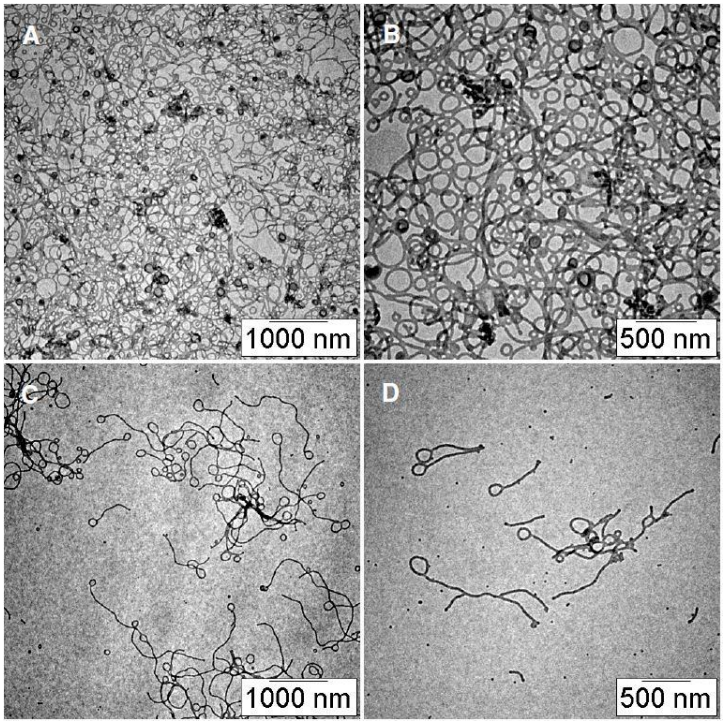

Figure 2-6. Representative TEM images of cylindrical micelles of **3(PEG$_{22}$)-PS$_{152}$** (A and B) and lasso micelles of **9(PEG$_{7}$)-PS$_{150}$** (C and D). The micelle solutions were prepared from the dioxane solution (0.05 wt %) of a block copolymer.

We imagined that our dendritic-linear block copolymers having short PEG peripheral chains may also impose high free energy at the end caps of a cylindrical micelle because of the reduced entropic effect of the hydrophilic corona on the stabilization of micelles.[36,37] In addition, a high molecular weight of the hydrophobic PS block would ensure our dendritic-linear block copolymers to have a low critical micelle concentration. We, therefore, reduced the concentration of the block copolymer in dioxane solution to 0.05 wt% for the preparation of micelles. The TEM study revealed that the population of toroidal micelles was increased from *ca*. 2% to 45–60% after the reduction of the block copolymer concentration of **3(PEG$_{22}$)–PS$_{152}$** (Figure 2-3B, 2-6A and 2-6B). The yield of toroidal micelles was determined by counting the number of the micelles from the TEM images taken from a single grid (a total of 200 micelles were counted). The relative population of toroidal micelles compared to that of linear cylindrical micelles was unchanged even after long hours of stirring in the presence of an organic solvent (water content 25 vol%), suggesting that the cyclization of micelles is more dependent on the architectural effect of the block copolymer rather than kinetic effects such as shear force. These results suggested that **3(PEG$_{22}$)–PS$_{152}$** possesses the packing factor allowing cyclization of micelles owing to the branched architecture of the hydrophilic block.

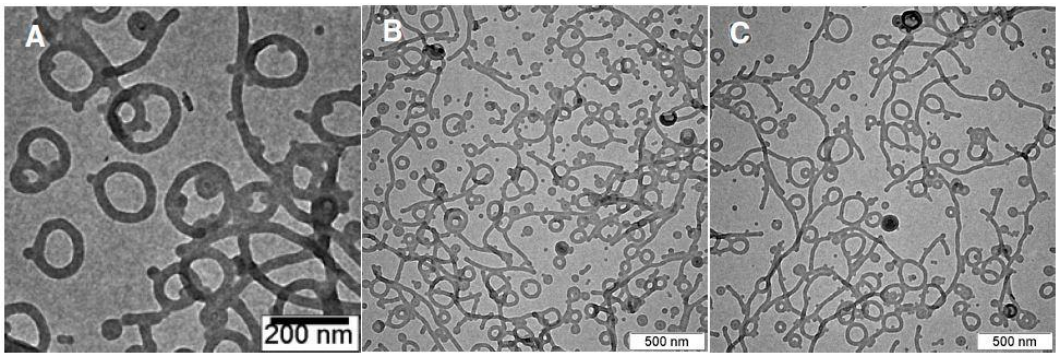

Figure 2-7. Representative TEM images of the micelle solutions of **9(PEG$_7$)-PS$_{150}$** quenched at the water content of 25%.

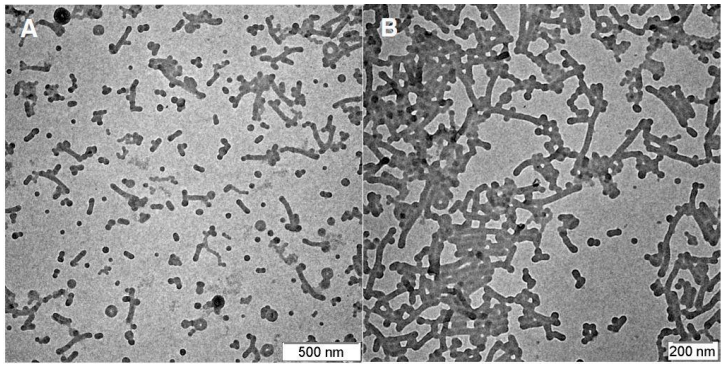

Figure 2-8. Representative TEM images of the micelle solutions of **3(PEG$_{22}$)-PS$_{152}$** quenched at the water content of 25%.

Surprisingly, we observed that all long cylindrical micelles changed their topology to lasso micelles (toroidal micelles with a long linear tail) upon the reduction of the concentration of **9(PEG$_7$)–PS$_{150}$** (Figure 2-3D, 2-6C and 2-6D). The population of lasso micelles was unexpectedly high (490%) compared to the population of toroidal micelles observed from the micelle solution of **3(PEG$_{22}$)–PS$_{152}$**. Based on the topology of a lasso micelle having a ring in the structure, this observation suggested the high free energy at the end of cylindrical micelles of **9(PEG$_7$)–PS$_{150}$**. To unravel the possible pathway of the formation of a lasso micelle, we studied the kinetic effect on the micellization of the block copolymers. From TEM studies of the micelles of **9(PEG$_7$)–PS$_{150}$** quenched and dialyzed at 25 vol% of water in dioxane, we observed toroidal micelles with a small bud or a shortened cylinder on the ring (Figure 2-7). The higher population of toroidal micelles observed than the population of toroids from the quenched micellar solution of **3(PEG$_{22}$)–PS$_{152}$** (Figure 2-8) suggested that **9(PEG$_7$)–PS$_{150}$**, upon self-assembly, imposes a higher free energy on the end caps of cylindrical micelles than **3(PEG$_{22}$)–PS$_{152}$**. This high free energy should facilitate cyclization of cylindrical micelles yielding the dominant toroid formation over linear growth of micelles.

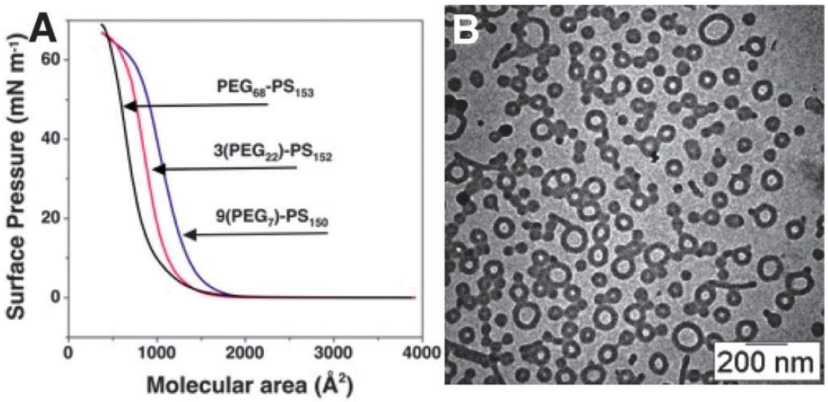

Figure 2-9. (A) Surface pressure to molecular area (Π–A) isotherms of linear and dendritic-linear block copolymers. The molecular areas for block copolymers are 1000 Å^2 for **PEG$_{68}$–PS$_{153}$**, 1210 Å^2 for 3**(PEG$_{22}$)–PS$_{152}$**, and 1475 Å^2 for **9(PEG$_7$)–PS$_{150}$**. (B) A TEM image of toroidal micelles of **9(PEG$_7$)–PS$_{150}$/PEG$_{68}$–PS$_{153}$** (90/10 by weight).

As suggested from the TEM study, formation of lasso micelles might occur from budding on the toroidal micelles, which acts as a growing site for a cylindrical micelle. We presumed that this budding of a toroid of **9(PEG$_7$)–PS$_{150}$** is arising from the steric constraint at the micellar corona due to the close packing of the bulky 2nd generation dendrons upon self-assembly. To prove our hypothesis of the increased steric effect of the dendritic architecture on self-assembly, we measured Π–A isotherms of linear and dendritic block copolymers. It has been reported that the molecular area of PEG-*b*-PS block copolymers exhibited an increase with the increased molecular weight of the PEG block, which

indicates that the hydrodynamic volume of a water-immersed PEG block is a deciding factor for the molecular area of the block copolymer in a compressed monolayer.[38] We found that the molecular area of our block copolymers increases with the number of peripheral PEG chains with the fixed molecular weight of the PEG domain (Figure 2-9A). The increased molecular area obtained from the monolayer of **9(PEG$_7$)–PS$_{150}$** (1475Å^2) compared to the area inferred from the monolayer of **3(PEG$_{22}$)–PS$_{152}$** (1210 Å^2) supports our hypothesis of the increased steric effect on the corona of micelles of **9(PEG$_7$)–PS$_{150}$**, which might induce the budding and the growth of a cylindrical micelle on a toroidal micelle (Figure 2-7).

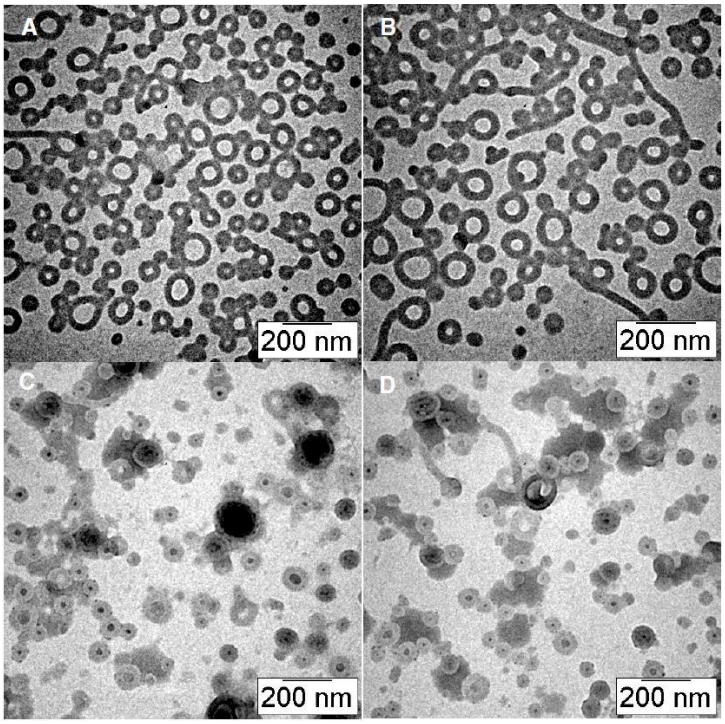

Figure 2-10. Representative TEM images of toroidal micelles prepared from the dioxane solution (0.05 wt%) of **PEG$_{68}$-PS$_{153}$/9(PEG$_7$)-PS$_{150}$**. (C) and (D) are negatively stained TEM images.

We also tested our idea of the steric effect of the dendritic block on self-assembly by co-assembling two block copolymers, **9(PEG$_7$)–PS$_{150}$** and a linear analogue, **PEG$_{68}$–PS$_{153}$**. The TEM images of the micelle solution of **9(PEG$_7$)–PS$_{150}$** containing **PEG$_{68}$–PS$_{153}$** (10 wt% of **9(PEG$_7$)–PS$_{150}$**) revealed that nearly all lasso micelles turned to a toroidal micelle (485% yield, Figure 2-9B and 2-10), indicating that the presence of a linear block copolymer could relieve the steric strains in the corona of the toroidal micelles without a drastic decrease of cyclization of the micelles. This dominant formation of toroidal micelles was only caused by the architectural effect of the block copolymer without using specific interactions between the corona mediated by added molecules[5] or physical forces applied for a long period of time.[6]

2.4 Summary

In summary, we showed a new design of amphiphilic block copolymers possessing a hydrophilic block built on a dendritic scaffold. By adjusting the molecular weight of peripheral hydrophilic polymer chains and the generation of the dendritic scaffold, we specifically induce a change in the molecular packing of the block copolymer upon self-assembly without changing the block ratio between hydrophilic and hydrophobic blocks, which is a deciding factor for the morphology of the micelle. We demonstrated that our strategy enabled the induction of a topological transition of a linear cylindrical micelle to toroid and lasso micelles. We are currently building a library of dendritic hydrophilic blocks having a controlled number of peripheral PEG chains of varying molecular weight to study the topological variations caused by the architecture of the dendritic block. Our efforts may lead to a rational control of morphology of polymeric micelles and vesicles induced by the architecture of the block copolymer building blocks.

2.5 Experimental

Materials and Methods. All reagents and chemicals were purchased from commercial sources and used as received. All reactions were performed under N_2 unless otherwise noted. NMR spectra were recorded on a Varian VNMRS 600 spectrometer with $CDCl_3$ as a solvent. Molecular weights of block copolymers were measured on an Agilent 1260 Infinity GPC system equipped with a PL gel 5 μm mixed C column (Polymer Laboratories) and differential refractive index detectors. THF was used as an eluent with a flow rate of 1 mL/min. A PS standard (Polymer Laboratories) was used for calibration. MALDI-TOF was performed on a Bruker Ultraflex III TOF-TOF mass spectrometer equipped with a nitrogen laser (335 nm) and operating in a reflectance mode. Internal calibration was performed using a Bruker peptide calibration standard (mass range 1000−4000 Da). The analytical sample was obtained by mixing a THF solution of analyte (5-10 mg/mL) with a THF solution of matrix (2,5-dihydroxybenzoic acid, 10 mg/mL) in a 1/5 v/v ratio. The prepared solution of the analyte and matrix (0.5 μL) was loaded on the MALDI plate and allowed to dry at 23 °C before the plated was inserted into the vacuum chamber of the MALDI instrument. The laser steps and voltages applied were adjusted depending on both the molecular weight and the nature of analyte.

Transmission electron microscopy (TEM) was performed on a JEOL 1400 microscope at an acceleration voltage of 100 kV. Sample specimens were prepared by placing a drop of the solution on a carbon-coated Cu grid (200 mesh, EM science). After 30 min, remaining solution on a grid was removed with a filter paper, and the grid was air-dried for 8 h.

The turbidity test was performed on a JASCO V-670 UV-Vis spectrophotometer equipped with a thermostat sample holder with a magnetic stirrer. 1.5 mL of dioxane solution of a block copolymer (0.5 wt%) was stirred while water was added through a syringe pump at a rate of 1.5 ml/h. Absorbance at 480 nm was measured at every 30 second for 1 h.

The surface pressure/area isotherms were performed using a film balance (KSV NIMA) with a platinum Wilhelmy plate. The subphase was prepared from house-purified water which was subsequently passed through a Milli-Q water purification system equipped an organic removal cartridge. The subphase water temperature was maintained at 25 (± 0.5) °C. In a typical experiment 20 μL of the polymer solution (1 mg/mL) was spread evenly over the water surface in small drops. After a further 30 min delay to allow for the evaporation of the solvent, compression at a constant rate of 10 mm/min (12.5 mm^2/s) began.

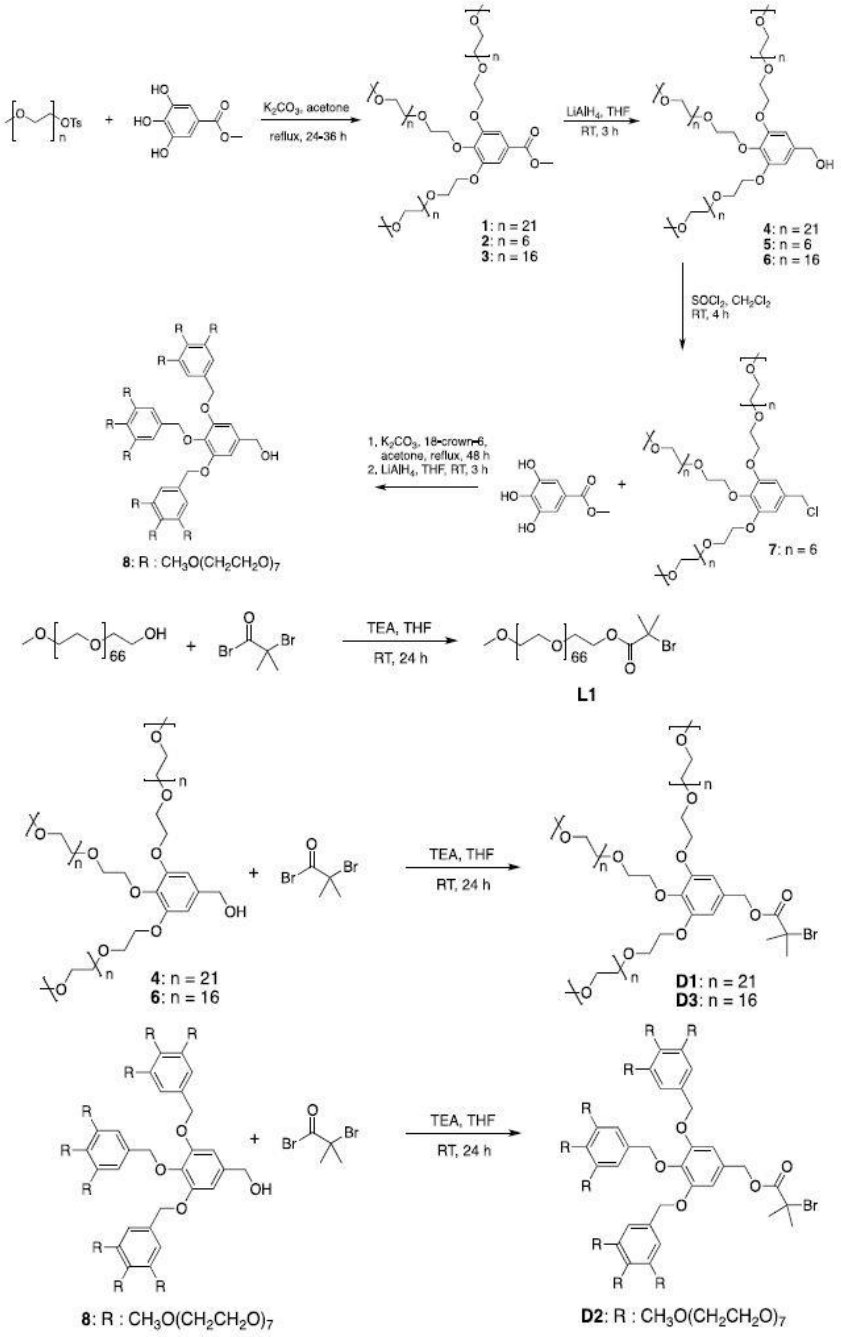

Scheme 2-1. Synthesis of dendritic macroinitiators with peripheral PEG chains.

Synthesis of Dendritic Macroinitiators with Peripheral PEG Chains. Dendrons **1**−**8** and macroinitiators **L1** and **D1**−**D3** were synthesized by following the literature procedure.[31,32,39]

L1. Monomethoxy PEG (1 g, M_n = 3000 g/mol, Polymer Source, Montreal, Canada) and trimethylamine (0.1 mg, 1 mmol) were dissolved in dry THF (50 mL). To this solution was added dropwise α-bromoisobutyryl bromide (0.23 g, 1mmol) in 3 mL dry THF. The solution was stirred for 24 h at room temperature. White solid was removed by filtration. The filtered solution was evaporated on a rotavap and the resulting residue was re-dissolved in CH_2Cl_2 (10 mL), which was precipitated into cold diethyl ether. White solid was collected by vacuum filtration. White solid was obtained after drying in vacuo. Yield 0.9 g, ^{1}H NMR (δ = ppm, 600 MHz, $CDCl_3$) 4.33 (t, 2H), 3.76-3.52 (m, -CH2CH2O-), 3.38 (s, 3H), 1.94 (s, 6H). M_n (GPC) = 4020 g/mol, PDI = 1.08, M_n (MALDI-TOF) = 3125 g/mol.

D1. Yield. 2.4 g, ^{1}H NMR (δ = ppm, 600 MHz, $CDCl_3$) 6.6 (s, 2H), 5.1 (s, 2H), 4.12-4.15 (m, 6H), 3.70-3.54 (m, -CH2CH2O-), 3.38 (s, 3H), 1.95 (s, 6H). M_n (GPC) = 4020 g/mol, PDI = 1.03. M_n (MALDI-TOF) = 3255 g/mol.

D2. Yield 1.8 g, ^{1}H NMR (δ = ppm, 600 MHz, $CDCl_3$) 6.68 (s, 2H), 6.63 (s, 4H), 6.61 (s, 2H), 5.06 (s, 2H), 5.01 (s, 4H), 4.97 (s, 2H), 3.80-3.54 (m, -CH2CH2O-), 3.35 (m, 27H), 1.91 (s, 6H). M_n (GPC) = 3410 g/mol, PDI = 1.04. M_n (MALDI-TOF) = 3702 g/mol.

D3. Yield 3.1 g, ^{1}H NMR (δ = ppm, 600 MHz, CDCl3) 6.60 (s, 2H), 5.10 (s, 2H), 4.16-4.13 (m, 6H), 3.71-3.50 (m, -CH2CH2O-), 3.38 (s, 9H), 1.95 (s, 6H). M_n (GPC) = 3350 g/mol, PDI = 1.04. M_n (MALDI-TOF) = 2736 g/mol.

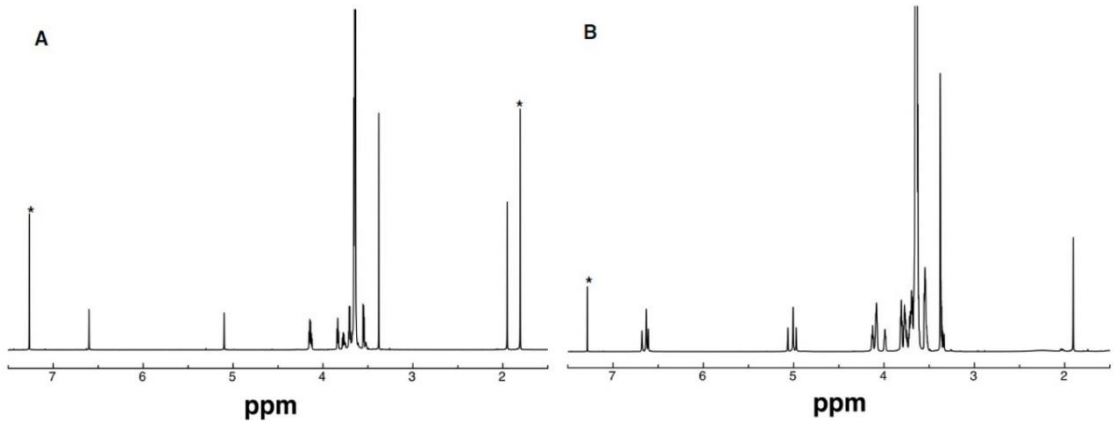

Figure 2-11. ^{1}H NMR spectra of dendritic macroinitiators **D1** (A) and **D2** (B) in $CDCl_3$. * indicates residual solvents.

Synthesis of PEG-*b*-PS block copolymers. Polymerization of styrene was performed with macroinitiators under a standard ATRP condition.[39]

Representative procedure. CuBr (7 mg, 0.05 mmol) and *N*,*N*,*N*',*N*'',*N*''-pentamethyldiethylene-triamine (PMDETA) (12 mg, 0.075 mmol) were mixed with 1 mL of anisole in a 20 mL Schlenk tube

with a magnetic bar. The tube was sealed with a rubber septum. This mixture was bubbled with N_2 for 15 min with gentle stirring. To this solution, the solution of styrene (5 mL) and **D1** (120 mg, 0.035 mmol) was added via a syringe. The green solution was degassed by bubbling N_2 for 20 min. After degassing, the tube was immersed in a preheated oil bath (95 ℃) and the polymerization was proceed at this temperature. The progress of polymerization was monitored by taking GPC at an interval of 1 h. When the molecular weight of the block copolymer reached to the desired value, the reaction was quenched by exposing the solution to air in an ice/water bath and diluted with $CHCl_3$ (15 mL). The cooled solution was filtered through a pack of aluminum oxide (basic) with $CHCl_3$ to remove the Cu catalyst. The filtered solution was concentrated on a rotavap, and the resulting residue was diluted with 20 mL CH_2Cl_2. This solution was precipitated into methanol (400 mL). White powder was collected by vacuum filtration and dried in vacuo. All block copolymers were characterized by ^{1}H NMR and GPC to evaluate the molecular weight and the size distribution. The molecular characteristics of the block copolymers are listed in **Table 2-1**.

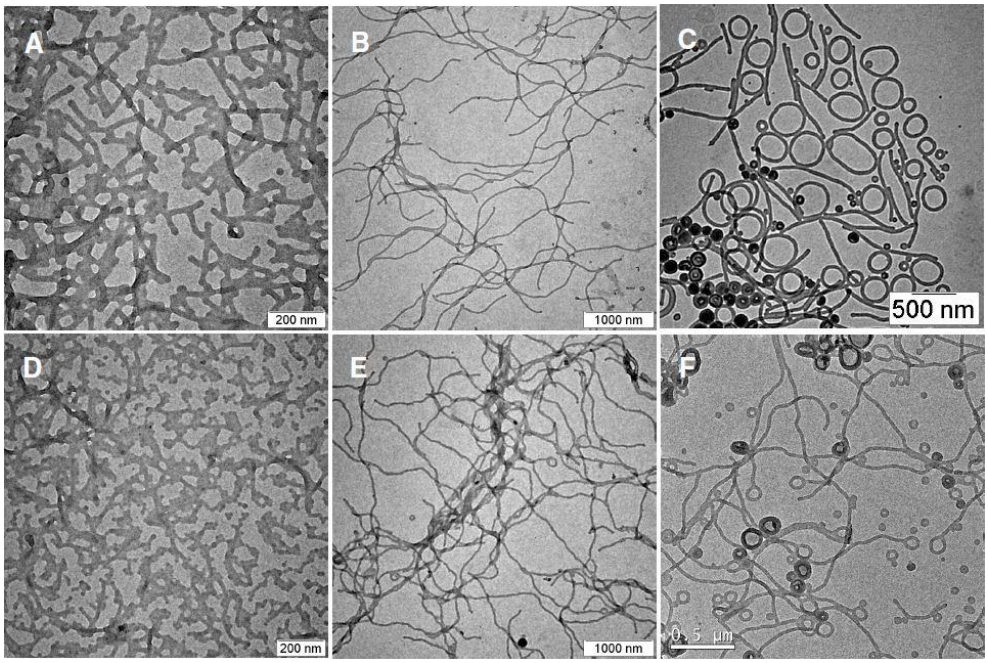

Figure 2-12. TEM images of micelles of (A) **3(PEG$_{22}$)-PS$_{120}$**, (B) **3(PEG$_{22}$)-PS$_{152}$**, (C) **3(PEG$_{22}$)-PS$_{171}$**, (D) **9(PEG$_7$)-PS$_{121}$**, (E) **9(PEG$_7$)-PS$_{150}$**, (F) **9(PEG$_7$)-PS$_{166}$**. All micelle solutions were prepared from a dioxane solution (0.5 wt %) of a block copolymer.

Preparation of Micelle Solutions. Doubly distilled water (MilliQ, 18.1 MΩ) was used throughout the experiments. A typical procedure is described: **3(PEG$_{22}$)-PS$_{152}$** (10 mg) was dissolved in 1,4-dioxane (dioxane) (2 mL) in a 15 mL capped vial with a magnetic stirrer. The solution was stirred for 3 h at room temperature. A syringe pump was calibrated to deliver water with a speed of 2 mL/h. The vial cap was replaced by a rubber septum. 2 mL of water was added to the organic solution with vigorous

stirring (850 rpm) by a syringe pump with a 5 mL syringe equipped with a steel needle. After adding 2 mL of water, 50 μL of the suspension was taken and added at once in 2 mL of pure water with stirring. This ensured a rapid quenching of the PS domain of micelles. The remaining solution was subjected to dialysis (SpectraPor, molecular weight cut-off: 12,000−14,000 Da) against water for 24 h with a frequent change of water. After dialysis, all organic solvents were replaced with water. Dialysis performed longer than 24 h did not change morphology of micelles. In all cases, the morphology of the micelles after rapid quenching and dialysis for 24 h was identical based on the TEM observation.

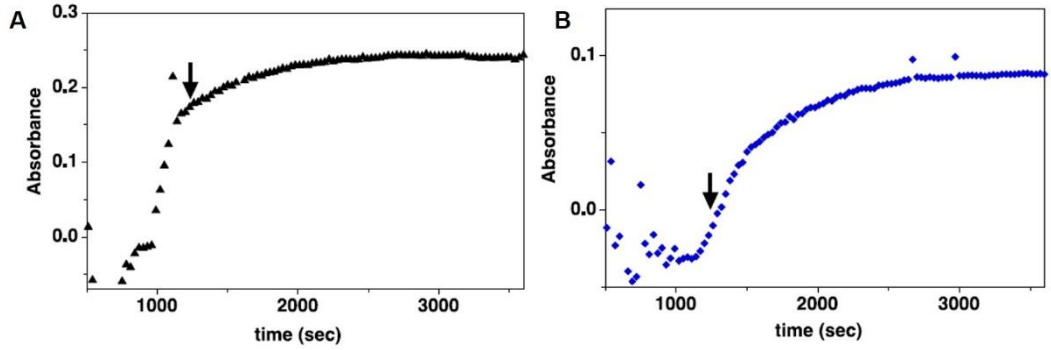

Figure 2-13. Absorbance change of the dioxane solution (0.5 wt%) of **3(PEG$_{22}$)-PS$_{152}$** (A) and **9(PEG$_{7}$)-PS$_{150}$** (B) during water addition. The arrow indicates the water content of 25%.

2.6 References

1. Hirsh, A. R.; Escuder, B.; Miravet, J. F.; Smith, D. K. *Angew. Chem. Int. Ed.* **2008**, *47*, 8002
2. Holder, S. J.; Sommerdijk, N. A. J. M. *Polym. Chem.* **2011**, *2*, 1018
3. Israelachivili, J. N. *Intermolecular and Surface Forces*, Academic Press, London, **2001**
4. Zhang, L.; Eisenberg, A. *Science* **1995**, *268*, 1728
5. van Hest, J. C. M.; Delnoye, D. A. P.; Baars, M. H. P.; van Genderen, M. H. P.; Meijer, E. W. *Science* **1995**, *268*, 1592
6. Pochan, D. J.; Chen, Z.; Cui, H.; Hales, K.; Qi, K.; Wooley, K. L. *Science* **2004**, *306*, 94
7. Chen, Z.; Cui, H.; Hales, K.; Qi, K.; Pochan, D. J. *J. Am. Chem. Soc.* **2005**, *127*, 8592
8. Cui, H.; Chen, Z.; Wooley, K. L.; Pochan, D. J. *Soft Matter*, **2009**, *5*, 1269
9. Zhu, J.; Liao, Y.; Jiang, W. *Langmuir*, **2004**, *20*, 3809
10. Jiang, Y.; Zhu, J.; Liang, H. *J. Phys. Chem. B.* **2005**, *109*, 21549
11. Yu, H.; Jiang, W. *Macromolecules* **2009**, *42*, 3399
12. Wang, Z.; Jiang, W. *Soft Matter* **2010**, *6*, 3743
13. Huang, H.; Chung, B.; Jung, J.; Park, H.-W.; Chang, T. *Angew. Chem. Int. Ed.* **2009**, *48*, 4594
14. Liu, C.; Chen, G.; Sun, H.; Xu, J.; Feng, Y.; Zhang, Z.; Wu, T.; Chen, H. *Small* **2011**, *7*, 2721

15. Jain, S.; Bates, F. S. *Science* **2003**, *300*, 460
16. Jian, S.; Bates, F. S. *Macromolecules* **2004**, *37*, 1511
17. Zhang, L.; Bartels, C.; Yu, Y.; Shen, H.; Eisenberg, A. *Phys. Rev. Lett.* **1997**, *79*, 5034
18. McKenzie, B. E.; Nudelman, F.; Bomans, P. H. H.; Holder, S. J.; Sommerdijk, N. A. J. M. *J. Am. Chem. Soc.* **2010**, *132*, 10256
19. Kim, K. T.; Zhu, J.; Meeuwissen, S. A.; Cornelissen, J. J. L. M.; Pochan, D. J.; Nolte, R. J. M.; van Hest, J. C. M. *J. Am. Chem. Soc.* **2010**, *132*, 12522
20. Meeuwissen, S. A.; Kim, K. T.; Chen, Y.; Pochan, D. J.; van Hest, J. C. M. *Angew. Chem. Int. Ed*. **2011**, *50*, 7070
21. Zhu, Z.; Hayward, R. C. *J. Am. Chem. Soc.* **2008**, *130*, 7496
22. Hayward, R. C.; Pochan, D. J. *Macromolecules* **2010**, *43*, 3577
23. Wang, X.; Guerin, G.; Wang, H.; Wang, Y.; Manners, I.; Winnik M. A. *Science* **2007**, *317*, 644
24. Gädt, T.; Ieong, N. S.; Cambridge, G.; Winnik, M. A.; Manners, I. *Nat. Mater.* **2009**, *8*, 144
25. Gilroy, J. B.; Gädt, T.; Whittell, G. R.; Chabanne, L.; Mitchels, J. M.; Richardson, R. M.; Winnik, M. A.; Manners, I. *Nat. Chem.* **2010**, *2*, 566
26. Qian, J.; Zheng, M.; Manners, I.; Winnik, M. A. *Trends Biotechnol.* **2009**, *28*, 84
27. Percec, V.; Wilson, D. A.; Leowanawat, P.; Wilson, C. J.; Hughes, A. D.; Kaucher, M. S.; Hammer, D. A.; Levine, D. H.; Kin, A.; Bates, F. S.; Davis, K. P.; Lodge, T. P.; Klein, M. L.; Devane, R. H.; Rosen, B. M.; Argintaru, A. O.; Sienkowska, M.; Rissanen, K.; Nummelin, S.; Ropponen, J. *Science*, **2010**, *328*, 1009
28. Trappmann, B.; Ludwig, K.; Radowski, M. R.; Shukla, A.; Mohr, A.; Rehage, H.; Böttcher, C.; Haag, R. *J. Am. Chem. Soc*. **2010**, *132*, 1119
29. Park, C.; Lee, J.; Kim, C. *Chem. Commun*. **2011**, *47*, 12042
30. Soliman, G. M.; Sharma, A.; Maysinger, D.; Kakkar, A. *Chem. Commun.* **2011**, *47*, 9572
31. Percec, V.; Johansson, G.; Ungar, G.; Zhou, J. *J. Am. Chem. Soc.* **1996**, *118*, 9855
32. Oar, M. A.; Serin, J. M.; Dichtel, W. R.; Fréchet, J. M. J.; Ohulchanskyy, T. Y.; Prasad, P. N. *Chem. Mater.* **2005**, *17*, 2267
33. In, M.; Aguerre-Chariol, O.; Zana, R. *J. Phys. Chem. B* **1999**, *103*, 7747
34. Cates, M. E.; Candau, S. J. *J. Phys.: Condens. Matter* **1990**, *2*, 6869
35. Petschek, R. G.; Pfeuty, P.; Wheeler, J. C. *Phys. Rev. A* **1986**, *34*, 2391
36. Zhulina, E. B.; Adam, M.; LaRue, I.; Sheiko, S. S.; Rubinstein, M. *Macromolecules* **2005**, *38*, 5330
37. LaRue, I.; Adam, M.; Zhulina, E. B.; Rubinstein, M.; Pitsikalis, M.; Hadjichristidis, N.; Ivanov, D. A.; Gearba, R. I.; Anokhin, D. V.; Sheiko, S. S. *Macromolecules* **2008**, *41*, 6555
38. Cox, J. K.; Yu, K.; Constantine, B.; Eisenberg, A.; Lennox, R. B. *Langmuir* **1999**, *15*, 7714
39. Kim, K. T.; Cornelissen, J. J. L. M.; Nolte, R. J. M.; van Hest, J. C. M. *Adv. Mater.* **2009**, *21*, 278

Chapter 3. Covalent Stabilization of Inverse Bicontinuous Cubic Structures of Block Copolymer Bilayers by Photodimerization of Indene Pendant Groups of Polystyrene Hydrophobic Blocks

3.1 Abstract

We report the cross-linking of hydrophobic compartments of complex self-assembled structures of amphiphilic block copolymers (BCPs) by the [2π + 2π]-cycloaddition of indene moieties present in a hydrophobic block based on polystyrene (PS). A photodimerizable indene group was introduced to the PS block by controlled radical copolymerization of indanolylstyrene, which was subsequently dehydrated to indenylstyrene using the Burgess reagent. This mild conversion producing the photodimerizable indene pendant groups ensured the synthesis of BCPs with a photo-cross-linkable PS block. We demonstrate that the micellar structures and complex inverse bicontinuous bilayers of BCPs containing hydrophobic PS cores could be covalently cross-linked in aqueous solutions upon irradiation with long-wavelength UV light (λ = 365 nm). The procedure formed an infinite polymer network within the hydrophobic compartments of the self-assembled nanostructures without using any additional reagents or causing morphological changes during the cross-linking. A wide variety of self-assembled structures retained their structural integrity in common organic solvents after cross-linking of the hydrophobic PS blocks.

3.2 Introduction

Self-assembly of block copolymers (BCPs) in a block-selective solvent generates size- and shape-defined nanostructures with desired functions that originate from the structures and architectures of the building blocks.[1–4] Simple low-dimensional structures (e.g., micelles and vesicles) and complex three-dimensional (3-D) and periodic nanostructures were generated by the solution self-assembly of BCPs with well-defined architectures.[5] Recently, complex nanostructures have attracted interest because of their potential applications for drug delivery, separation, catalysis, and nanotemplating.[6–9] Application of these nanostructures could benefit from covalent cross-linking of the BCP building blocks that consist of self-assembled structures; this would impart structural robustness to otherwise transient structures in harsh environments (extreme dilution, presence of organic solvents, and extreme temperature and pH condition).[10–16] In addition, covalent stabilization of polymer micelles and vesicles caused a reversible change in the sizes and shapes of the resulting nanogels and polymersomes in response to the external stimuli such as the presence of chemical reactions, and pH and temperature changes.[17–23] The use of photochemical reactions such as the cyclodimerization of conjugated alkenes is of particular interest to induce covalent bonds between BCPs. The [2π + 2π]-cycloaddition of coumarin derivatives, introduced as pendant groups of polymer chains, has been utilized to stabilize polymer micelles and vesicles and

install reversible gates on mesoporous materials.[24–26] Photochemical reactions of the BCP pendant functional groups require no additional reagents (e.g., initiators, cross-linkers or catalysts) unlike the coupling reactions used for shell- or core-cross-linking of polymer micelles and vesicles.[27,28]

Polystyrene (PS) has been widely used as a hydrophobic polymer block to construct self-assembling BCPs because of its physical properties, chemical inertness, and ease of synthesis by various controlled polymerization methods. Cross-linked PS prepared by chemical cross-linking using divalent cross-linkers, such as divinylbenzene, is an indispensable material for use as the stationary phase for solid-phase synthesis and separation.[29] Irradiation of PS chains using short-wavelength UV light (λ = 254 nm) generates radicals: PS might be cross-linked in bulk by the recombination of these radicals.[30] The uncontrolled cross-linking of the PS domains of the BCP self-assembled structures, such as microphase-separated nanostructures and polymer micelles deposited on the substrate, can provide robust self-assembled structures upon exposure to solvents.[31] However, the cross-linking of PS chains in solution has not been performed in a controlled manner using photochemistry (e.g., cycloaddition). Self-assembled BCPs containing PS hydrophobic blocks can produce a variety of morphologies. The controlled radical polymerization of styrenic monomers with photo-curable pendant groups could benefit the synthesis of well-defined BCPs form self-assembled nanostructures with diverse shapes that could be covalently stabilized at harsh conditions.

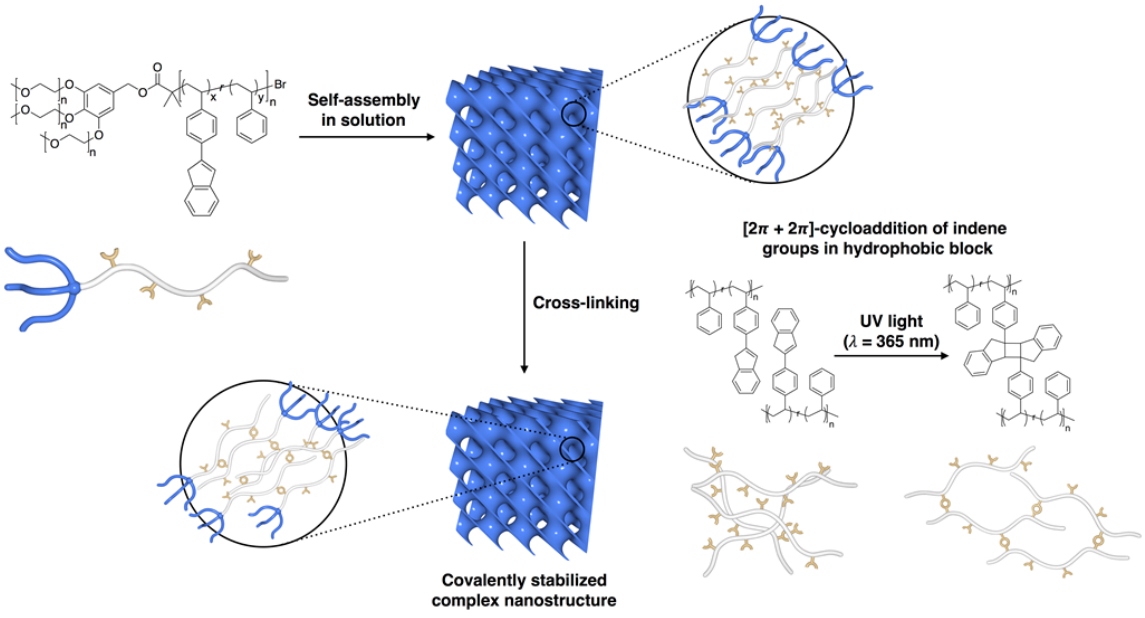

Figure 3-1. A scheme of branched-linear block copolymers containing polystyrene hydrophobic blocks with indene pendant groups and their self-assembly toward complex inverse bicontinuous bilayers. The self-assembled structures were cross-linked by [2π + 2π]-cycloaddition of indene groups with irradiation of long-wavelength UV light (λ = 365 nm).

We report core cross-linking of complex, self-assembled structures of BCPs by the [2π + 2π]-cycloaddition of indene moieties[32,33] present in a hydrophobic block based on PS. A photodimerizable indene group was introduced to PS using controlled radical polymerization of indanolylstyrene, which was subsequently dehydrated to indene pendant groups using the Burgess reagent as a mild reagent.[34] The mild conversion to photodimerizable indene pendant groups ensured the synthesis of BCPs with a photo-cross-linkable PS block. We demonstrate that the micellar structures and complex inverse bicontinuous bilayers of BCPs containing the hydrophobic PS polymer block with indene pendant groups could be covalently stabilized in aqueous solutions upon irradiation with long-wavelength UV light (λ = 365 nm). This process cross-links the hydrophobic compartments of the self-assembled nanostructures without any additional reagents or morphological changes during the cross-linking (Figure 3-1). Consequently, these complex cross-linked structures retain their structural integrity in common organic solvents that dissolves PS.

3.3 Results and Discussion

We implemented the photo-dimerizable indene groups into the PS chain using trimethylsilyl-indanolylstyrene (**1-TMS)** as a monomer for the controlled radical copolymerization of styrene by atom-transfer radical polymerization (ATRP) (Scheme 3-1). The direct polymerization of indanolylstyrene or indeneylstyrene by ATRP and reversible addition-fragmentation chain-transfer polymerization were unsuccessful because of the sluggish propagation or unwanted cross-linking during polymerization. In contrast, **1-TMS** could be polymerized to poly(TMS-indanolylstyrene) (**P1-TMS**) with a moderate conversion (up to ~50%) at standard ATRP conditions with CuBr as a catalyst. The controlled nature of ATRP for **1-TMS** was confirmed by measuring the linear increase of the molecular weight of **P1-TMS** over the polymerization time and the consumption of the monomer (Figure 3-2). The polydispersity index (*Đ*) of **P1-TMS** measured by GPC remained low (*Đ* <1.35) until the conversion of **1-TMS** exceeded ~50%, indicating the well-controlled nature of ATRP for **1-TMS** (Figure 3-2D). For conversions above 50%, the propagation of **1-TMS** became noticeably slower, and the molecular weight distribution broadened. This polymerization behavior may be partly caused by steric hindrance from the bulky indanol pedant group of **1-TMS**. This steric hindrance could be reduced by co-polymerizing **1-TMS** with styrene (50 mol%) at standard ATRP conditions. These conditions provided a high conversion (~70%) for the copolymerization of these monomers without a significant increase in the *Đ* value of the resulting random copolymer, poly(styrene-*ran*-TMS-indanolylstyrene) (**P2-TMS**) (Figure 3-2C and D). The composition ratio and feed ratio of **1-TMS** to styrene were determined by integrating the ^{1}H NMR spectrum of **P2-TMS** (Figure 3-3); both ratios were similar.

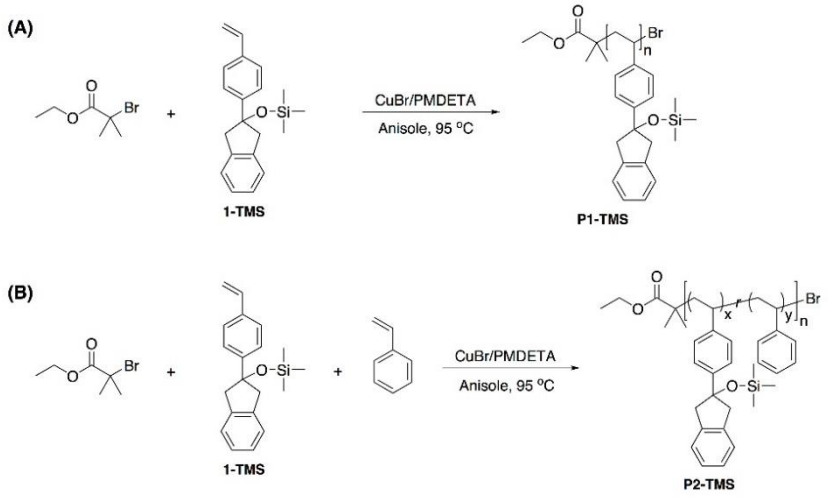

Scheme 3-1. Polymerization of trimethylsilane-indanolylstyrene (**1-TMS**) for (A) the homopolymer and (B) random copolymer with styrene using atom transfer radical polymerization.

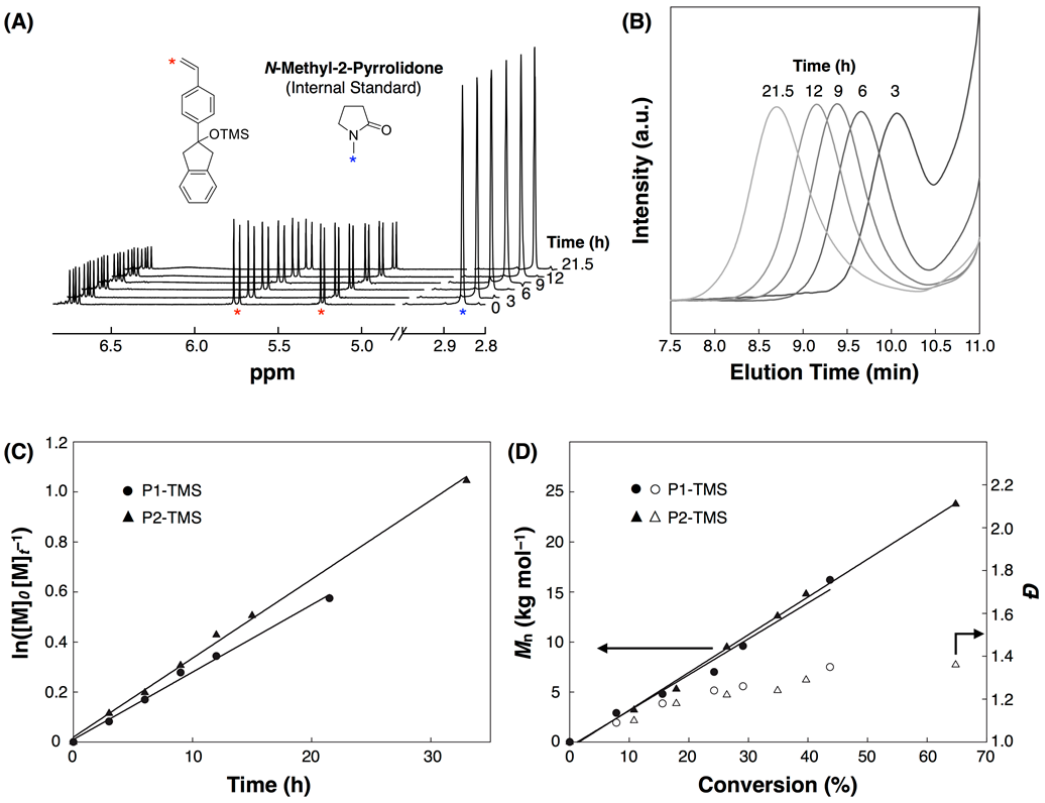

Figure 3-2. (A) ^{1}H NMR and (B) gel permeation chromatography (GPC) spectra showing the progress of polymerization for **P1-TMS** during the polymerization time. (C) Plots of polymerization time vs. $\ln([M]_0\ [M]_t^{-1})$ for the polymerization of **P1-TMS** and **P2-TMS**. $[M]_0$ and $[M]_t$ indicate the concentration of monomers at times 0 and t, respectively. (D) Plots of reaction conversion vs. the number-averaged molecular weight (M_n) and polydispersity index ($Đ$) for **P1-TMS** and **P2-TMS**. Filled circles and triangles indicate M_n and opened circles and triangles indicate $Đ$.

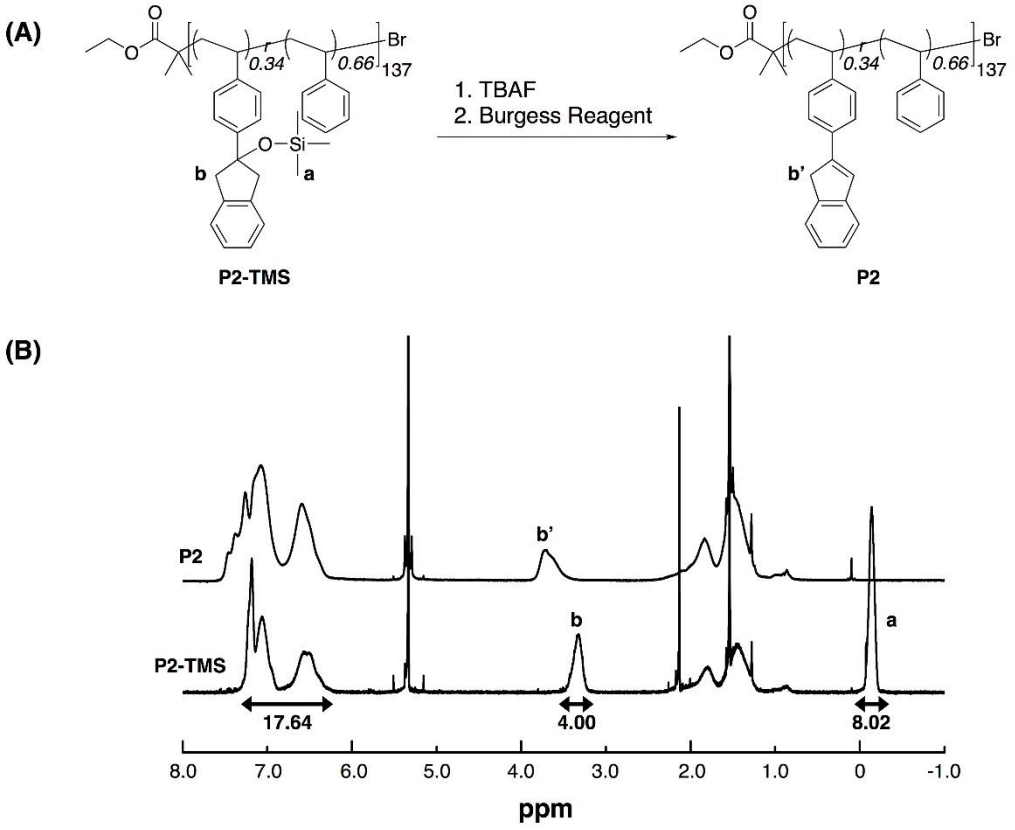

Figure 3-3. (A) A scheme for post-modification of **P2-TMS** to **P2**. (B) ^{1}H NMR spectra of **P2-TMS** and **P2**. The DP_n ratio was calculated based on the **P2-TMS** spectrum.

The TMS-protected indanol pendant groups present in **P1-TMS** and **P2-TMS** could be deprotected and dehydrated in the presence of HCl (6 M) in toluene to yield the indene-containing polymer We used a dehydration method by employing the mild Burgess reagent at room temperature to preserve the structural integrity of the polymers with complex architectures and functional groups during the conversion of TMS-indanol to indene pendants. After removing the TMS protecting group using TBAF, the resulting indanol-containing polymers were dehydrated in the presence of the Burgess reagent (methyl *N*-(trimethylammoniumsulfonyl)carbamate) in anhydrous benzene at room temperature (Figure 3-4A). The complete conversion of indanol to the indene moiety was confirmed by ^{1}H NMR spectroscopy (Figure 3-4B). The formation of the indene pendant groups of the polymers was also observed using UV-Vis spectroscopy by the emergence of the peak (λ_{max} = 310 nm), corresponding to the π-π* transition of the indene ring (Figure 3-4C). From the GPC analysis, the number-averaged molecular weights (M_n) of the indene-containing polymers, **P1** and **P2,** were slightly less than that of the pristine polymers, **P1-TMS** and **P2-TMS**, with small changes in the $Đ$ values (Table 3-1, Figure 3-5).

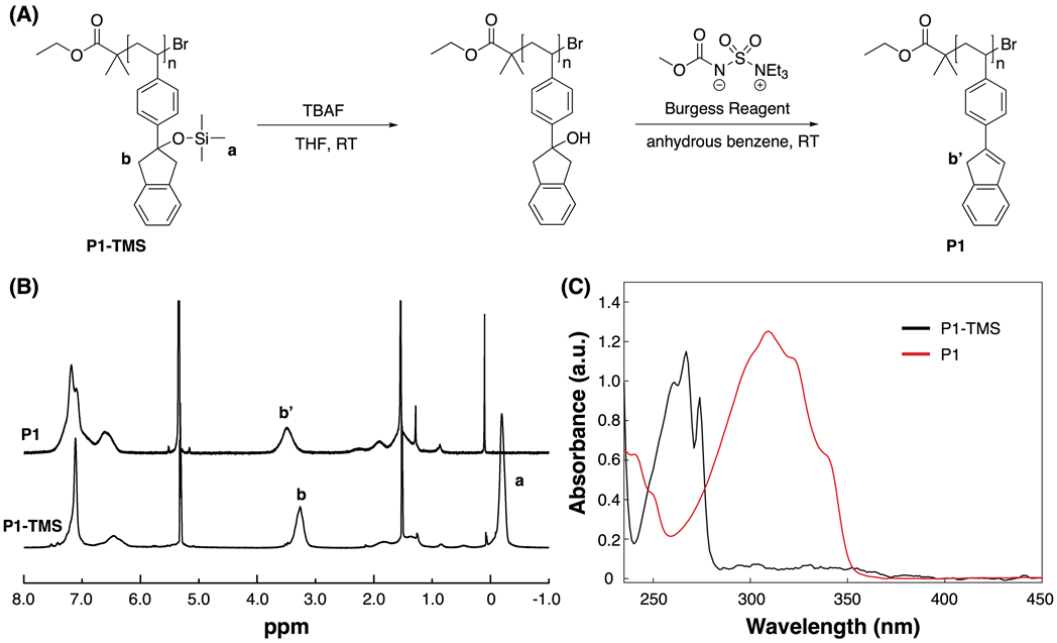

Figure 3-4. (A) Schematic procedures for post-modification of **P1-TMS** toward **P1** using deprotection and the Burgess reaction. (B) ^{1}H NMR spectra of **P1-TMS** and **P1** ("a" and "b" show the characteristic peak changes). (C) UV-Vis spectra of the **P1-TMS** and **P1** solutions in CH_2Cl_2.

Table 3-1. Molecular weight (M_n) and polydispersity index ($Đ$) of **P1-TMS**, **P2-TMS**, **P1** and **P2**.

Sample	M_n (kg/mol)[a]	$Đ$[a]
P1-TMS	17.9	1.34
P1	12.1	1.50
P2-TMS	23.8	1.36
P2	21.6	1.38

[a]Molecular weights and polydispersity index measured by gel permeation chromatography (GPC)

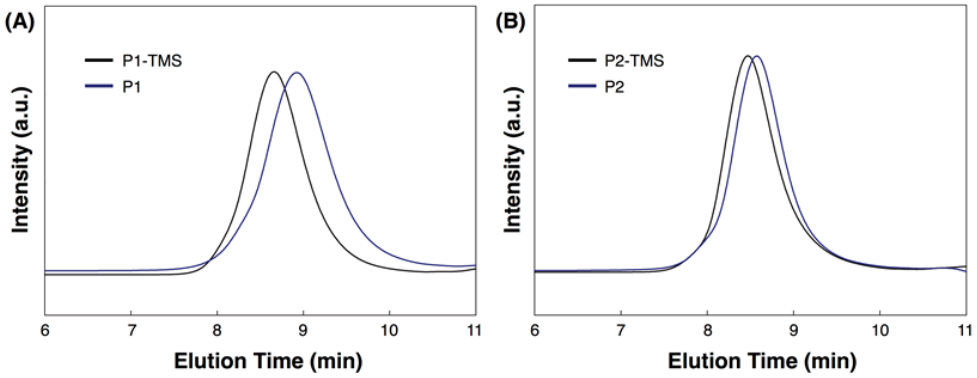

Figure 3-5. GPC spectra of (A) **P1-TMS**, **P1** and (B) **P2-TMS**, **P2**.

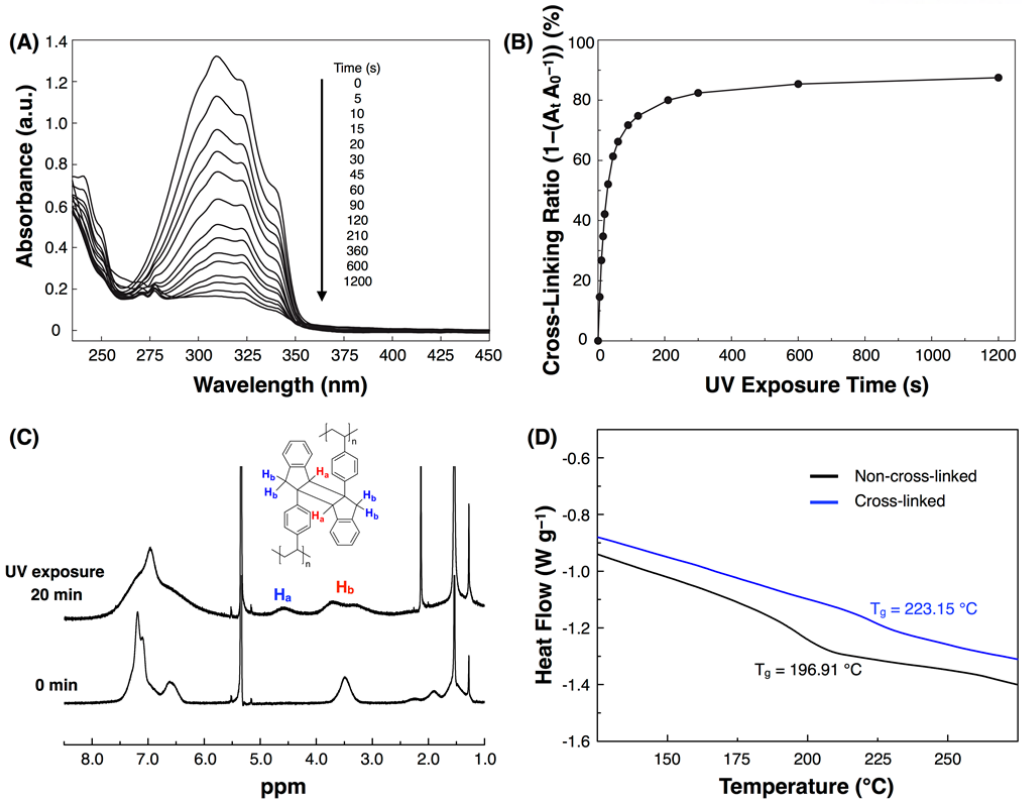

Figure 3-6. (A) UV-Vis spectra of **P1** in CH_2Cl_2 (0.01 mg mL^{-1}) with irradiation of long-wavelength UV light (λ = 365 nm) for different exposure times. (B) Plot of the UV exposure time against the cross-linking ratio ($1 - (A_t\ A_0^{-1})$), where A_0 and A_t are the absorbance values at 310 nm at time 0 and t, respectively. The cross-linking ratio at t = 20 min was 87.5%. (C) ^1H NMR spectra of **P1** in CD_2Cl_2 (1 mg mL^{-1}) with (20 min) and without UV irradiation. (D) Differential scanning calorimetry spectra of non-cross-linked and cross-linked **P1**.

The photodimerization of the indene pendant groups of the polymer chains under UV irradiation was studied in solution. The [2 + 2]-cycloaddition of the pendant indene groups of **P1** in CH_2Cl_2 (0.01 mg mL^{-1}) was observed by UV-Vis absorption with UV light irradiation (λ = 365 nm, 6 W); there was a gradual decrease of the peaks corresponding to π–π* transitions of indene (Figure 3-6A and B). The [2 + 2]-cycloaddition of the pendant indene groups of **P1** and the formation of the cyclobutane linkage were clearly observed from the ^1H NMR analysis after irradiation of **P1** in CD_2Cl_2 (1 mg mL^{-1}) (Figure 3-6C). We also investigated the cross-linking of the bulk state of **P1**. The photo-cross-linking of the **P1** films only yielded intractable solids, which were insoluble in common organic solvents. UV-Vis absorption spectra of the cross-linked film of **P1** showed a decrease of the peak (λ = 310 nm), indicating the formation of cyclobutane linkages of the indene dimer (Figure 3-7). DSC of crosslinked **P1** showed a glass transition temperature (T_g) at 223 °C, which was substantially higher than that (T_g = 197 °C) of pristine **P1** without UV irradiation (Figure 3-6D). These results confirmed that the [2 + 2]-cycloaddition of the indene pendant groups of **P1** and **P2** induced cross-linking of the polymer chains in solution and

bulk with mild irradiation of long-wavelength UV light. The irradiation of short-wavelength UV (λ = 254 nm, 6 W) to cross-linked **P1** did not provide a noticeable retro-cycloaddition of indene dimers, which was in contrast to the partial retro-cyclization of indene dimers into the model compound 4-indenylstyrene in benzene at the same irradiation condition (Figure 3-8 and 3-9).

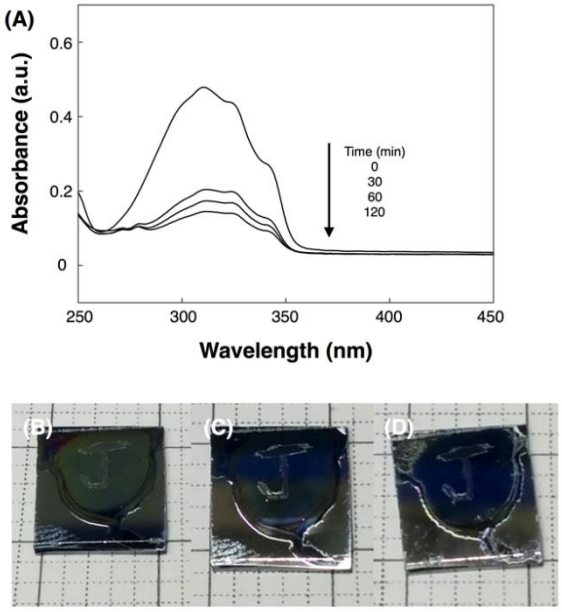

Figure 3-7. (A) UV-Vis spectra of polymer film of **P1** spin-coated onto square quartz plate (2 cm x 2 cm) at irradiation of UV light (λ >300 nm, 200 W) for different exposure time. (B-D) Photographs of polymer film of **P1** spin-coated onto silicon wafer (1 cm x 1 cm) with scratch. (B) Polymer film of **P1** before and (C) after 2 h of UV light irradiation. (D) Cross-linked polymer film of **P1** after soaking in THF for 1 h.

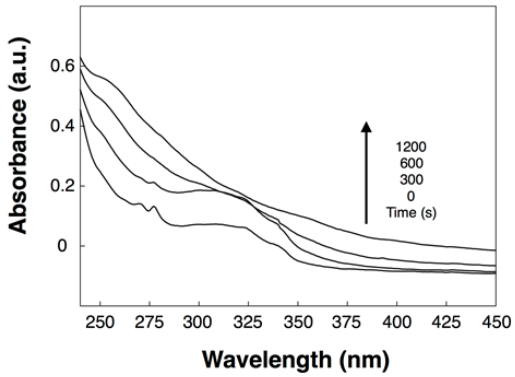

Figure 3-8. UV-Vis spectra of cross-linked **P1** in CH_2Cl_2 at short-wavelength UV light (λ = 254 nm, 6 W) irradiation for different exposure times.

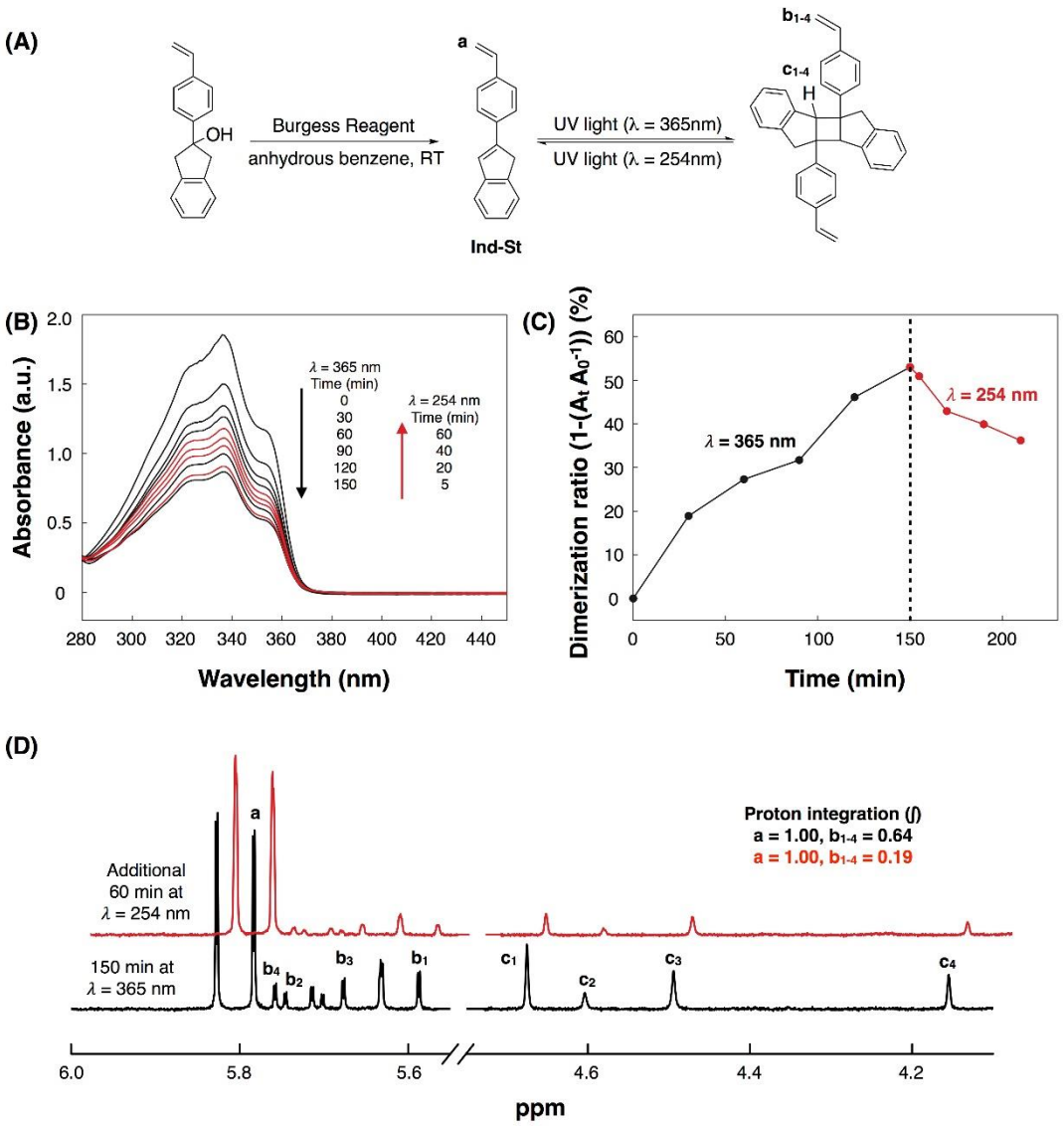

Figure 3-9. (A) Schematic procedures for preparation of a model compound 4-indenylstyrene (**Ind-St**) and its [2 + 2]-cycloaddition at long-wavelength UV light (λ = 365nm) and retro-cyclization of indene dimers at short-wavelength UV light (λ = 254 nm). (B) UV-Vis spectra of **Ind-St** in benzene (1 mg mL^{-1}) with irradiation of long-wavelength UV light (black) and short-wavelength UV light (red), sequentially, for different exposure times. (C) Plot of the UV exposure time against the dimerization ratio (1 - (A_t A_0^{-1})), where A_0 and A_t are the absorbance values at 337 nm at time 0 and t, respectively. The dimerization ratio at t = 150 min was 53.0% and t = 210 min was 36.2%. (D) ^{1}H NMR spectra of **Ind-St** solution after irradiation of long-wavelength UV light (black) and short-wavelength UV light (red), sequentially. "b_{1-4}" and "c_{1-4}" are caused by 4 different isomers of indene dimers.[41] The dimerization ratio calculated by the proton integration (($\int$ b) ($\int$ a + $\int$ b)$^{-1}$) was 39.0% at t = 150 min and was 16.0% at t = 210 min.

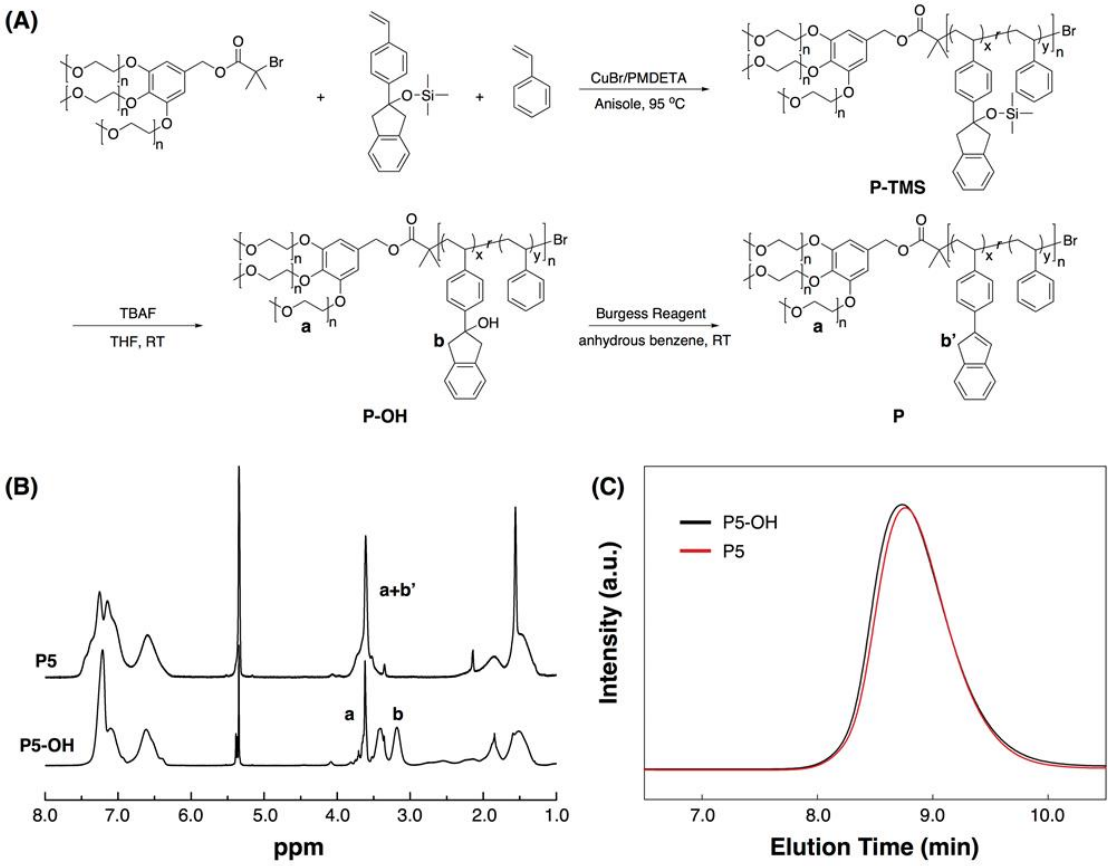

Figure 3-10. (A) Schematic procedures for random copolymerization of **1-TMS** and styrene with the PEG macro-initiator by atom-transfer radical polymerization and their post-modification by deprotection and the Burgess reaction. (B) Representative ^{1}H NMR spectra of deprotected block copolymers (BCPs) (**P5-OH**) and dehydrated BCPs (**P5**) showing their characteristic peak shifts. (C) Representative gel permeation chromatography spectra of **P5-OH** and **P5**.

Amphiphilic BCPs spontaneously form micelles, vesicles, and complex nanostructures in aqueous solutions. Covalent stabilization of polymer micelles and vesicles has been used to permanently fix the transient structures in harsh environments. We confirmed the photo-cross-linking of the PS chains containing indene pendants in solution and investigated the possibility for covalent stabilization of self-assembled BCP nanostructures with the indene-containing PS block as a hydrophobic block. We synthesized the amphiphilic BCPs using branched PEG-based macro-initiators for the ATRP of styrene and **1-TMS** (Figure 3-10A). The resulting BCPs, **P3**–**P6**, showed well-defined molecular weights and narrow size distributions, as determined by GPC (Table 3-2). The pendant groups of the PS block were converted to indene groups in the presence of the Burgess reagent at room temperature. This mild dehydration method preserved the functional groups in the BCPs, which could be compromised at harsh dehydration conditions using strong acids (e.g., HCl) and high temperatures (e.g., reflux condition). ^{1}H NMR and GPC analyses clearly showed the complete conversion of the pendant groups to indene

without any degradation of the BCPs (Figure 3-10B and C).

BCPs were self-assembled by adding water, which is a selective solvent for the hydrophilic PEG block, into a dioxane solution of the BCPs (typically 1 wt%). The organic solvent was removed by dialysis against water for 24 h. The resulting aqueous suspensions of self-assembled structures were studied using DLS, SEM, and TEM. We used three branched PEG hydrophilic blocks with peripheral PEG branches of different molecular weights. As the molecular weight fraction of the hydrophilic PEG domain (f_{PEG}) of the BCP was decreased, the morphology of the self-assembled structure transformed from spherical micelles to cylindrical micelles and polymer vesicles. When the molecular weight of the PEG branches of the hydrophilic block were reduced to 550 g mol^{-1} (DP_n = 12), we observed that the resulting BCPs self-assembled into inverse mesophases such as sponge-phase particles and polymer cubosomes after decreasing the f_{PEG} values by increasing DP_n of the hydrophobic indene-containing PS block (Table 3-2).

Table 3-2. Characterization of polymers containing indene species.

Sample	Initiator	DP_n (St)[b]	DP_n (Ind-St)[b]	f_{Ind} (%)[b]	f_{PEG} (%)[c]	M_n (kg mol^{-1}) ^{1}H NMR[b]	M_n (kg mol^{-1}) GPC	$Đ$ GPC	Phase[f]
P1	EBIB[a]	0	58	100	0	-	17.9[d]	1.34	-
P2	EBIB[a]	91	46	33.6	0	-	23.8[d]	1.36	-
P3	$(PEG1000)_3$	44	62	58.5	16.5	21.2	18.1[e]	1.08	m
P4	$(PEG750)_3$	59	55	48.3	12.3	20.5	13.5[e]	1.15	v
P5	$(PEG550)_3$	43	55	56.4	10.0	18.2	15.3[e]	1.14	s
P6	$(PEG550)_3$	72	41	36.3	10.0	18.2	15.6[e]	1.11	c

[a]EBIB = ethyl α-bromoisobutyrate. [b]Degree of polymerization (DP_n), indenylstyrene ratio of hydrophobic block (f_{Ind}) and M_n were calculated from the ^{1}H NMR integration of the deprotected polymers (**P-OH**). [c]The molecular weight ratio of the PEG domain (f_{PEG}) to that of the hydrophobic block (3000 g mol^{-1}, 2250 g mol^{-1}, and 1650 g mol^{-1} for $(PEG1000)_3$, $(PEG750)_3$, and $(PEG550)_3$ initiators, respectively). [d]Gel permeation chromatography (GPC) data were measured from the protected polymer (**P-TMS**) [e]GPC data were measured from the deprotected polymers (**P-OH**). [f]m: micelles, v: vesicles, s: sponge phase (L_3), c: polymer cubosomes

Self-assembled structures of the BCPs in water were readily cross-linked by irradiating the aqueous dispersion with UV light (λ >300 nm, 200 W) for 5 h. The cross-linking of the micelles of BCP **P3** by photo-dimerization of indene pendant groups within the hydrophobic domains was confirmed by changing the dispersion medium from water to THF. The non-cross-linked micelles were completely dissociated into individual BCPs in THF, as evidenced by the drastic decrease in the scattered light intensity during the DLS measurement (Figure 3-11A and B). In contrast, the dispersions irradiated with UV light for 5 h showed strong scattering in the DLS experiment after replacing the solvent. The hydrodynamic diameters of the cross-linked polymer micelles in THF were slightly larger than that in water, suggesting that the self-assembled structures swelled in THF. The change of the morphology of

the polymer micelles after cross-linking was visualized by TEM. Spherical and cylindrical micelles of **P3** retained their shape after photo-cross-linking in water (Figure 3-11C and D), indicating that the photodimerization of indene pendants of **P3** did not cause any change to the morphology of the micelles. The photo-cross-linking of the **P4** polymer vesicles also caused the polymer vesicles to retain their size and morphology in THF (Figure 3-12). The critical content of indenylstyrene in the hydrophobic block for photo-cross-linking might be ~30% (estimated from the solvent exchange after photo-cross-linking of the polymer vesicles of the derivatives of **P4** with the hydrophobic block synthesized from the monomer mixtures of different feed ratios (Table 3-3, 3-4, Figure 3-13, 3-14)).

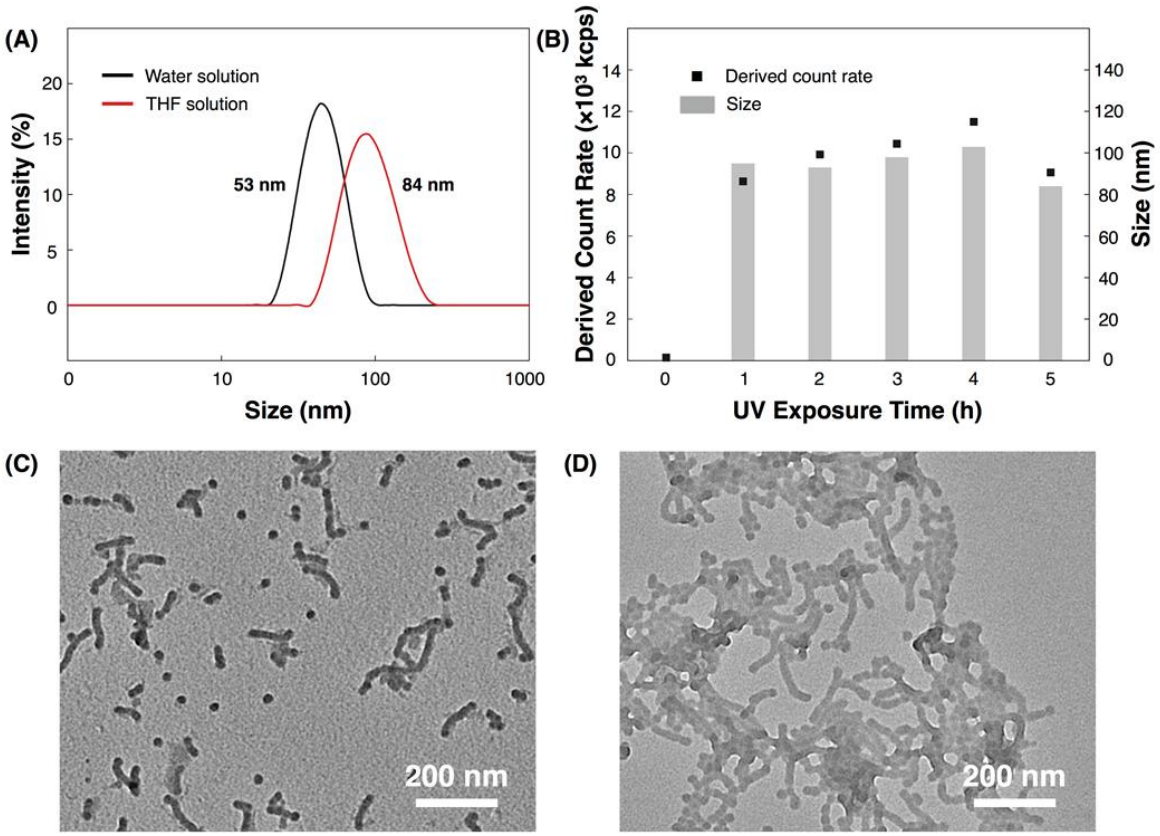

Figure 3-11. (A) Dynamic light scattering (DLS) size plots of the self-assembled structures of **P3** in an aqueous solution (black) and cross-linked **P3** in a tetrahydrofuran (THF) solution (red). (B) Plots of the DLS-derived count rate (light intensity) and size of the cross-linked self-assembled structures of **P3** in THF with increasing UV irradiation times. (C, D) TEM images of (C) non-cross-linked micelles of **P3** and (D) cross-linked micelles after changing the dispersion solvent to THF.

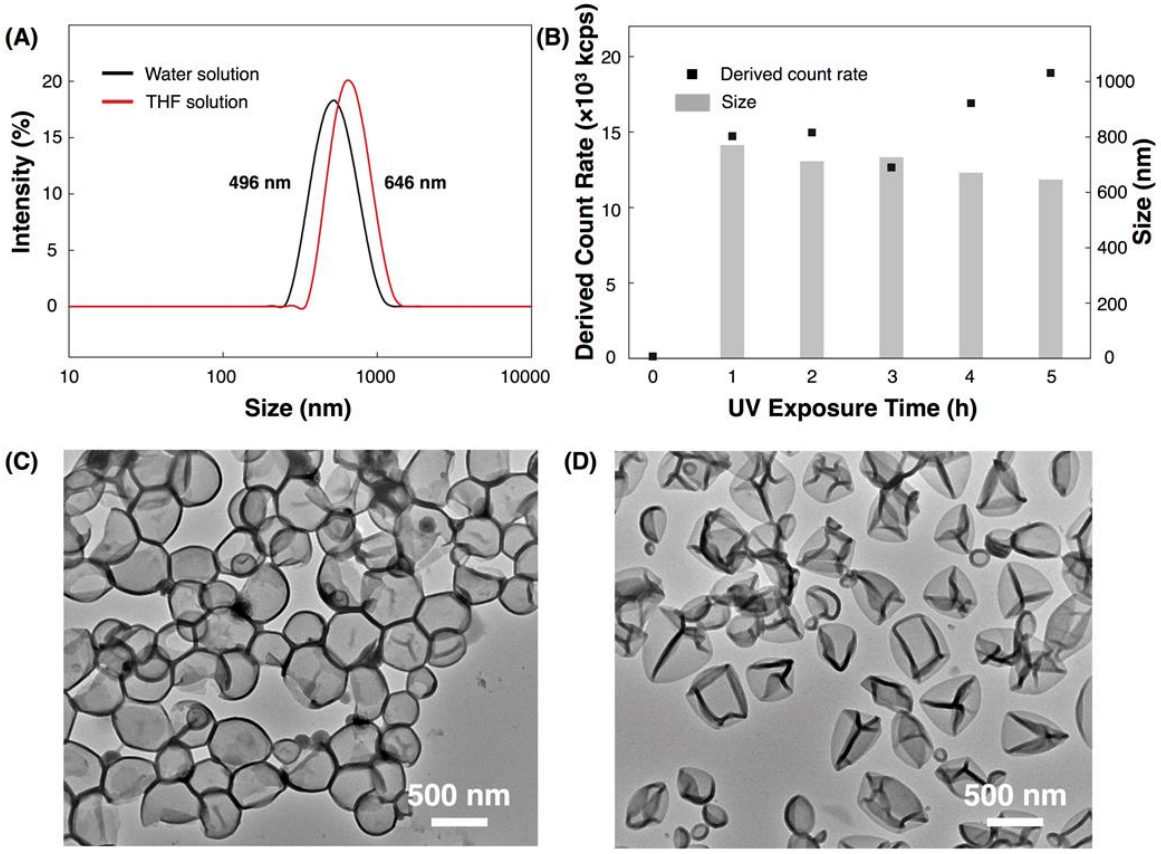

Figure 3-12. (A) Dynamic light scattering (DLS) size plots of the self-assembled structures of **P4** in an aqueous solution (black) and cross-linked **P4** in a tetrahydrofuran (THF) solution (red). (B) Plots of the DLS-derived count rate (light intensity) and size of the cross-linked self-assembled structures of **P4** in THF with various UV irradiation times. (C, D) TEM images of (C) non-cross-linked vesicles of **P4** and (D) cross-linked vesicles after changing the dispersion solvent to THF.

Table 3-3. Characterization of additional polymers containing indene species

Sample	Initiator	DP_n (St)[a]	DP_n (Ind-St)[a]	f_{Ind} (%)[a]	f_{PEG} (%)[b]	M_n (kg mol^{-1}) ^{1}H NMR[a]	M_n (kg mol^{-1}) GPC[c]	$Đ$ GPC
P1S	$(PEG550)_3$	169	10	5.6	8.1	22.0	25.0[e]	1.12
P2S	$(PEG550)_3$	175	21	10.7	7.2	24.6	21.7[e]	1.09
P3S	$(PEG550)_3$	126	33	20.7	7.7	23.0	20.5	1.08

[a]Degree of polymerization (DP_n), indenenylstyrene ratio of hydrophobic block (f_{Ind}) and M_n were calculated from ^{1}H NMR integration of deprotected polymers (**P-OH**). [b]The molecular weight ratio of the PEG domain (f_{PEG}) to that of the hydrophobic block (1650 g mol^{-1} for $(PEG550)_3$ initiator). [c]GPC data were measured from deprtected polymers (**P-OH**).

Table 3-4. DLS count rates of cross-linked polymer vesicles with various indenylstyrene ratio.

Sample	f_{ind} (%)	Count rate (× 10^3 Kcps)[a]		Relative count rate
		diluted in water	diluted in THF	THF/Water (%)
P1S	5.6	106.6	2.8	2.6
P2S	10.7	134.2	14.7	11.0
P3S	20.7	80.2	29.9	37.3
P6	36.3	49.0	44.8	91.4
P5	56.4	50.0	46.2	92.4

[a]Same amount of cross-linked vesicles were diluted in water and THF respectively.

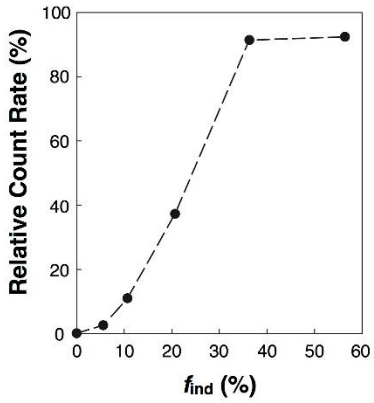

Figure 3-13. Plot of f_{ind} vs. relative count rate. Critical content of indenylstyrene in the hydrophobic block for decent cross-linking was around 30%.

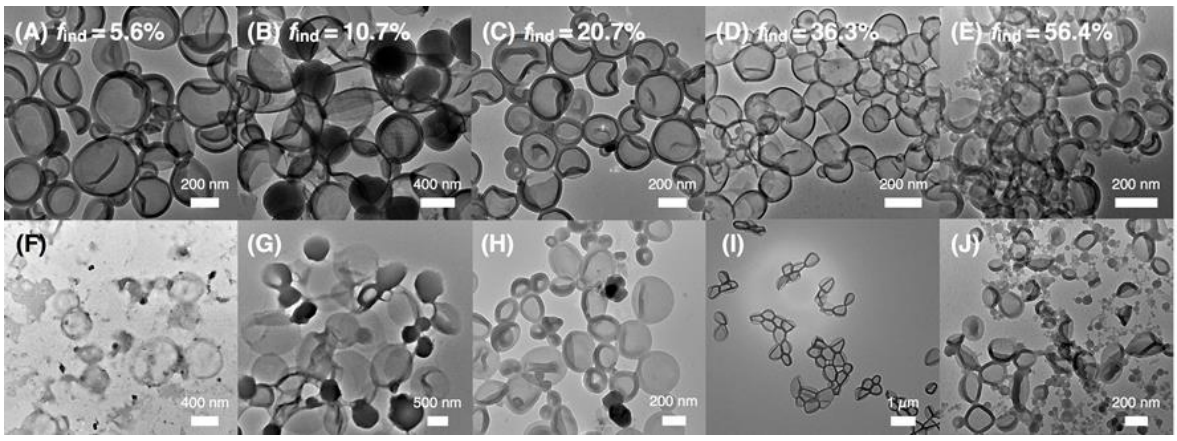

Figure 3-14. (A-E) TEM images of non-cross-linked vesicles of (A) **P1S** (f_{ind} = 5.6%), (B) **P2S** (f_{ind} = 10.7%), (C) **P3S** (f_{ind} = 20.7%), (D) **P6** (f_{ind} = 35.3%) and (E) **P5** (f_{ind} = 56.4%). (F-J) TEM images of cross-linked vesicles of (F) **P1S**, (G) **P2S**, (H) **P3S**, (I) **P6** and (J) **P5** after changing the dispersion solvent to THF.

We reported that amphiphilic BCPs comprised a branched PEG hydrophilic block and a linear hydrophobic PS block preferentially self-assembled into inverse bicontinuous cubic mesophases in solution, which yielded micro-sized colloidal particles (polymer cubosomes)[36–39] and monolithic films (cubofilms)[40] consisting of triply periodic minimal surfaces of BCP bilayers. These inverse bicontinuous cubic structures of polymer bilayers formed periodic minimal surfaces with a large surface area arising from 3-D nanochannels embedded within the minimal surfaces. [2 + 2]-Cycloaddition of indene groups used for the covalent stabilization of self-assembled nanostructures of BCPs in solution could readily cross-link the hydrophobic domain with irradiation of low-energy UV light without requiring any additional reagents or catalysts, which made this method of cross-linking particularly interesting for covalent stabilization of complex 3-D structures with continuous hydrophobic PS-rich cores.

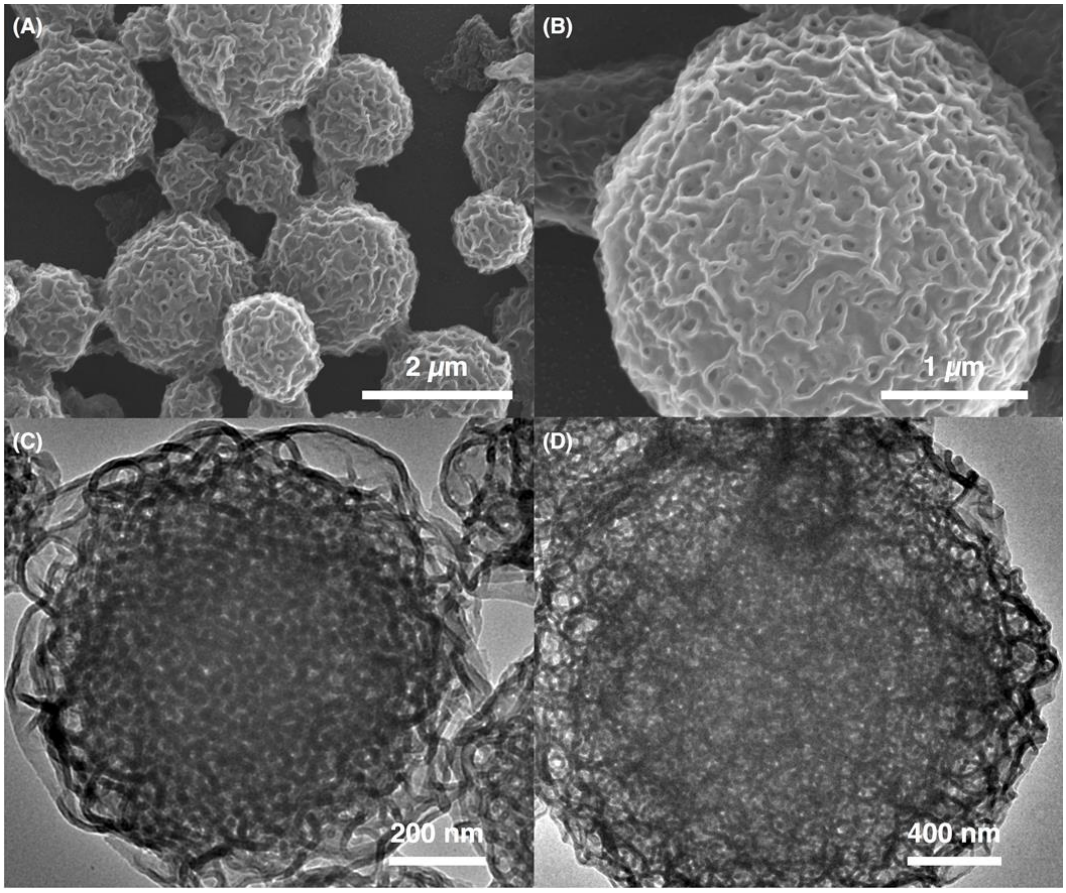

Figure 3-15. SEM and TEM images of (A, C) the self-assembled sponge phase particles of **P5** and (B, D) cross-linked sponge phase of **P5** after soaking in tetrahydrofuran.

The morphologies of the self-assembled structures of a series of BCPs sharing the branched PEG block $(PEG550)_3$ **P5** and **P6** were investigated by electron microscopy. **P5** (f_{Ind} = 56.4%, f_{PEG} = 10.0%) self-assembled into "sponge phase" (L_3) particles comprising bicontinuous inverse structures of BCP

bilayers without any crystalline order (Figure 3-15). SEM and TEM images of the "sponge phase" particles revealed that the internal pore networks with no crystalline order were connected to the environment by surface pores on the crust of the particles (Figure 3-15A and C). After irradiation with UV light for 1 h, the dispersion medium was changed with THF. The particles remained intact in THF for at least three days, indicating that the cyclodimerization of the indene pendant groups of the hydrophobic PS block made the continuous hydrophobic domain of the bilayer membrane covalently cross-linked and insoluble in common organic solvents. SEM and TEM images of the cross-linked particles showed that the morphology of the particles remained unchanged and the internal pore networks were unaffected by the photodimerization of the indene pendant groups and the presence of THF (Figure 3-15B and D).

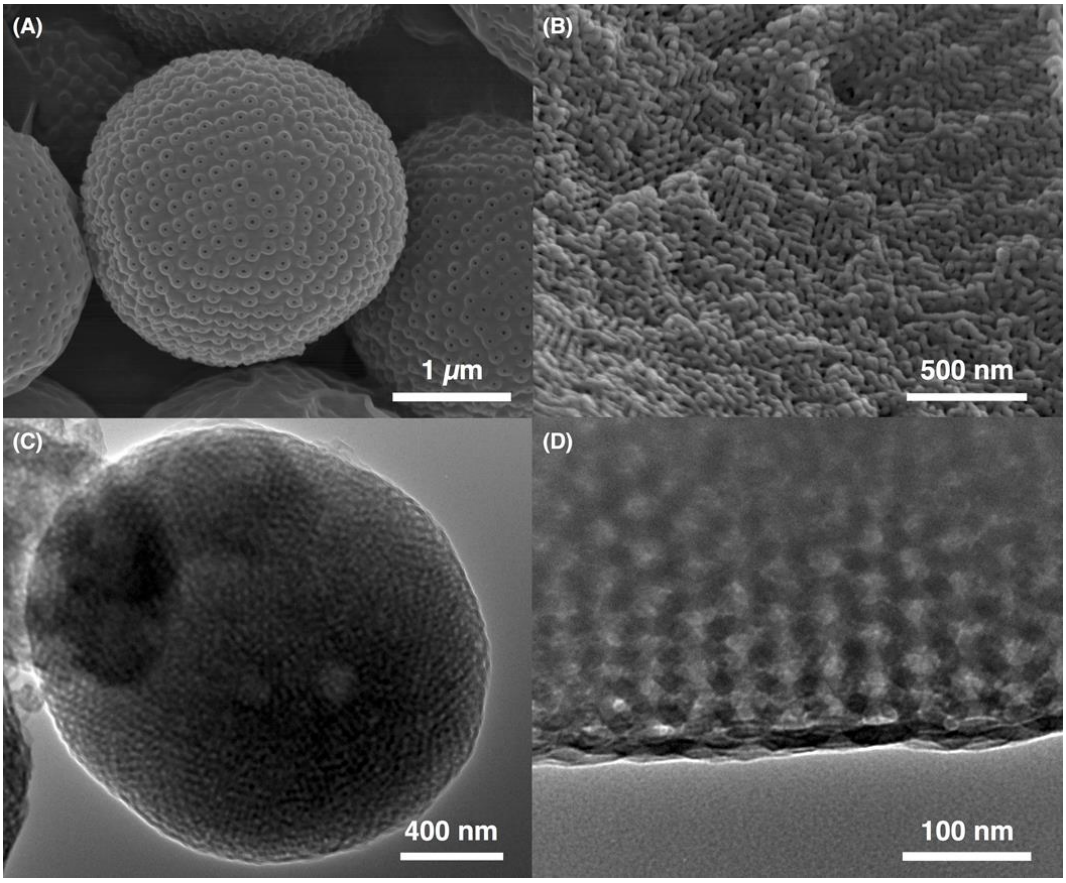

Figure 3-16. (A, B) SEM images of the polymer cubosomes of **P6** showing (A) the spherical shape with surface pores and (B) internal structures. (C, D) TEM images of the polymer cubosomes of **P6** showing internal mesoporous channels.

BCP **P6** (f_{Ind} = 36.3%, f_{PEG} = 10.0%) self-assembled into polymer cubosomes consisting of periodic minimal surfaces of BCP bilayers with crystalline order (Figure 3-16). The internal structure was observed by electron microscopy and SAXS (*Pn3m* space group, lattice parameter a = 41.6 nm). Two

non-intersecting mesoporous channels residing within the polymer cubosomes were clearly observed in the SEM and TEM images (Figure 3-16B and D). The diameter of the internal mesoporous channels was estimated to be ~ 32 nm by analyzing the TEM images of the polymer cubosomes of **P6**.

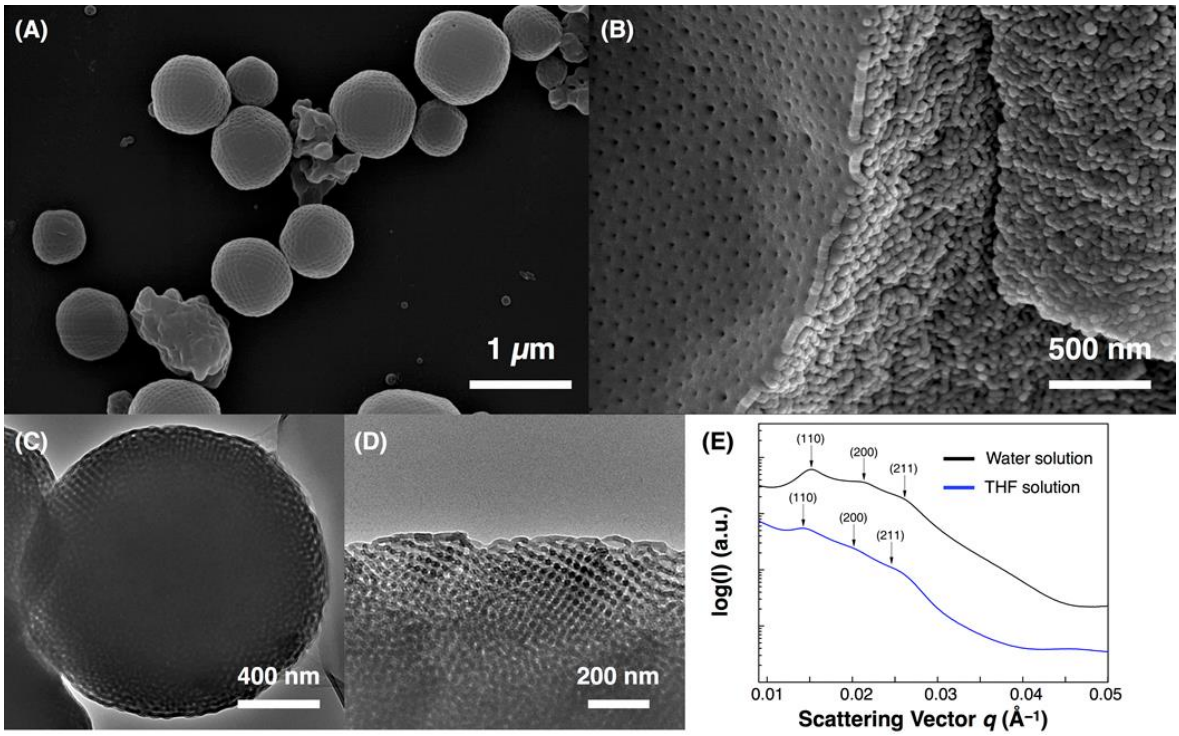

Figure 3-17. (A, B) SEM images and (C, D) TEM images of the cross-linked polymer cubosomes of **P6** showing unchanged crystalline structures after replacing the dispersion solvent in tetrahydrofuran (THF) for at least three days. (E) Small-angle X-ray scattering results obtained from the dried non-cross-linked polymer cubosome of **P6** (*Pn3m* symmetry, a = 41.6 nm) and cross-linked polymer cubosome of **P6** after soaking in THF (*Pn3m* symmetry, a = 44.2 nm).

The polymer cubosomes of **P6** in water were irradiated with UV light for 1 h at room temperature to induce photodimerization of the indene pendant groups within the hydrophobic compartment of the bilayer. After cross-linking and changing the solvent from water to THF, the polymer cubosomes retained the morphology and internal nanostructure in THF for at least three days (Figure 3-17). SEM and TEM images of the cross-linked polymer cubosomes of **P6** dried from the THF solution showed well-defined periodic minimal surface structures of the polymer cubosomes; these structures were stabilized and did not show any significant changes. In addition, SAXS results of the cross-linked polymer cubosomes showed identical peaks corresponding to double diamond structures (*Pn3m* space group, a = 44.2 nm), indicating that the photodimerization of indene pendant groups could covalently stabilize the complex 3-D periodic nanostructures constructed from the inverse bicontinuous structures of BCP bilayers.

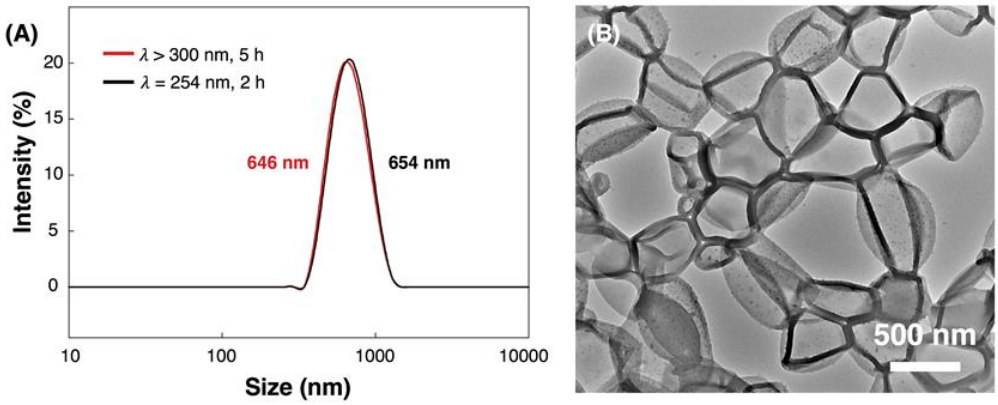

Figure 3-18. (A) Dynamic light scattering size plots of the self-assembled structures of **P4** exposed to long-wavelength UV light (λ >300 nm, 5 h) in a tetrahydrofuran (THF) solution (red) and sequentially exposed to short-wavelength UV light (λ = 254 nm, 2 h) in a THF solution (black). (B) TEM image of vesicles of **P4** exposed to short-wavelength UV light after changing the dispersion solvent to THF.

3.4 Summary

In summary, we synthesized photochemically cross-linkable amphiphilic BCPs by the [2π + 2π]-cycloaddition of indene moieties present in a hydrophobic block based on PS. A photodimerizable indene group was introduced to the PS hydrophobic blocks by controlled radical copolymerization of indanolylstyrene, which was subsequently dehydrated to indenylstyrene using the Burgess reagent as a mild reagent for conversion. We demonstrated that simple low-dimensional structures (e.g., micelles and vesicles) and complex 3-D structures generated by solution self-assembly of BCPs containing indene pendant groups could be stabilized in aqueous solutions upon irradiation with long-wavelength UV light (λ = 365 nm). This process formed an infinite polymer network within the hydrophobic cores of the self-assembled nanostructures without using any additional reagents. After cross-linking of the hydrophobic blocks, the self-assembled structures maintained their morphologies in common organic solvents. These results suggest that the complex periodic nanostructures created by solution self-assembly of BCPs could be used as platforms for application such as nanoreactors and nanotemplating in harsh conditions by simple and facile photo-cross-linking of indene groups in PS hydrophobic blocks.

3.5 Experimental

Materials. All reagents and chemicals were used as received unless otherwise noted. Styrene was purified by passing through a basic alumina column before polymerization. CH_2Cl_2 was dried (using CaH_2 under N_2 atmosphere) and distilled. Tetrahydrofuran (THF) was refluxed with Na and benzophenone under N_2 atmosphere and distilled before use. All reactions were performed in an inert atmosphere unless otherwise noted.

Methods. ^{1}H NMR and ^{13}C NMR spectra were recorded by Agilent 400-MR DD2 Magnetic Resonance System and Varian/Oxford As-500 using CD_2Cl_2 and $CDCl_3$ as solvents and internal standards. Molecular weights and polydispersity indices of polymers and block copolymers were measured by Agilent 1260 Infinity gel permeation chromatography (GPC) system equipped with a PL gel 5 μm MiniMIX-D column (Agilent Technologies) and differential refractive index detectors. THF was used as an eluent with a flow rate of 0.3 mL min^{-1} at 35 °C. A PS standard kit (Agilent Technologies) was used for calibration. Differential scanning calorimetry (DSC) was carried out under N_2 gas at a scan rate of 15 °C min^{-1} with TA Instruments Q10. Transmission electron microscopy (TEM) was performed on a Hitachi 7600 operating at 100 kV and JEOL JEM-2100 operating at 200 kV. Specimens were prepared by placing a drop of the solution on a carbon-coated Cu grid (200 mesh, EM science). After 30 min, remaining solution on a grid was removed with a filter paper, and the grid was dried overnight. Scanning electron microscopy (SEM) was performed on a Hitachi S-4300 operating at 15 kV. Suspension was cast and dried on a slide glass, and coated with Pt by using a Hitachi E-1030 ion sputter. UV-Vis spectrometry (UV-Vis) was measured on a Jasco V-630 spectrophotometer. Dynamic light scattering (DLS) was performed at a Malvern Zetasizer Nano-S. Synchrotron small-angle X-ray scattering (SAXS) data were obtained on the SAXS beamline (PLS-II 6D, 11.18 keV, 6.5 m) at Pohang Accelerator Laboratory. The concentrated suspension of the polymer cubosome was dried for a day in a freeze-dryer. Ti-SBA standard was used. UV light sources were Vilber VL-6.LC (254 nm/365 nm, 6 W), Uvitec Cambridge LF-215.LM (365 nm/312 nm, 15 W) and Ushio Spot Cure SP9-250DB (200 W) with 300 nm longpass cutoff filter.

Synthesis of indanolylstyrene.[32] 4-bromostyrene (21.6 mL, 165 mmol) was added to a dry THF (150 mL) in a Schlenk flask (500 mL) and degassed for 20 min by nitrogen bubbling. The solution temperature was decreased below −70 °C using a dry ice/acetone bath. Then, *n*-BuLi (1.6 M in hexane, 103 mL, 165 mmol) was added dropwise, and the yellow viscous solution was stirred for 30 min for lithiation. A THF solution of 2-indanone (21.8 g, 165 mmol) was slowly added to the reaction flask using a double-tip needle. Then, the reaction mixture was stirred for 1 h at −70 °C, and the temperature was slowly increased to room temperature by removing the dry ice/acetone bath. The reaction mixture was quenched by adding water (100 mL) and concentrated HCl (10 mL). The organic phase was separated and the aqueous phase was extracted using diethyl ether (50 mL × 3 times). The organic phases were collected, dried over $MgSO_4$; the solvents were removed under reduced pressure. The crude product was purified by column chromatography using CH_2Cl_2 as an eluent. Recrystallization in hexane gave a white crystalline solid. Yield 9.02 g (38.2 mmol, 23.2%). ^{1}H NMR (δ = ppm, 400 MHz, CD_2Cl_2) 7.54 (d, 2H, *J* = 8.4 Hz), 7.43 (d, 2H, *J* = 8.4 Hz), 7.30 – 7.19 (m, 4H), 6.74 (dd, 1H, *J* = 17.6, 11.2 Hz), 5.77 (d, 1H, *J* = 17.6), 5.25 (d, 1H, *J* = 10.8), 3.51 (d, 2H, *J* = 16.4 Hz), 3.24 (d, 2H, *J* = 16.4 Hz), 2.14 (s, 1H)

Synthesis of trimethylsilyl-indanolylstyrene (1-TMS). 2-(4-Vinylphenyl)indane-2-ol (7.00 g, 29.6 mmol) and sodium iodide (110 mg, 0.74 mmol) were dissolved in CH_2Cl_2 (200 mL) in a Schlenk flask (500 mL). Triethylamine (7.49 g, 10.3 mL, 74.0 mmol) and chlorotrimethylsilane (TMSCl) (8.04 g, 9.39 mL, 74.0 mmol) were added sequentially to this solution and the mixture was stirred for 15 h at room temperature. When the reaction was complete, sodium acetate (6.07 g, 74.0 mmol) was added and refluxed for 30 min to remove excess amount of TMSCl. The reaction mixture was quenched by adding water and extracted with CH_2Cl_2 (50 mL × 3 times). The organic phases were collected, dried over $MgSO_4$, and evaporated under reduced pressure. The mixture was purified by column chromatography with basic alumina and CH_2Cl_2. The first fraction was collected and dried at a reduced pressure. Recrystallization in hexane at 20 °C gave a yellowish solid. Yield 7.7 g (25.0 mmol, 84.4%). ^{1}H NMR (δ = ppm, 400 MHz, CD_2Cl_2) 7.47 (d, 2H, *J* = 8.4 Hz), 7.39 (d, 2H, *J* = 8.4 Hz), 7.26 – 7.17 (m, 4H), 6.74 (dd, 1H, *J* = 17.6, 10.8 Hz), 5.76 (d, 1H, *J* = 17.6), 5.24 (d, 1H, *J* = 10.8), 3.41 (q, 4H, *J* = 16.0 Hz), -0.06 (s, 9H). ^{13}C NMR (δ = ppm, 100 MHz CD_2Cl_2) 146.87, 141.43, 136.38, 136.09, 126.50, 125.85, 125.72, 124.44, 113.27, 85.81, 49.11, 1.40.

Polymerization and post-modification of the homopolymer and block copolymer containing 1-TMS (representative procedure). All polymerization were performed according to the same procedure. The following procedure outlines the polymerization of **P1-TMS** as an example. CuBr (22 mg, 0.15 mmol) and *N,N,N',N'',N''*-pentamethyldiethylenetriamine (26 mg, 0.15 mmol) were mixed with anisole (0.5 mL) in a 20 mL Schlenk tube. A solution of **1-TMS** (601 mg, 1.95 mmol), ethyl α-bromoisobutyrate (2.9 mg, 15 μmol) and *N*-methyl-2-pyrrolidone (96 μL, 0.97 mmol; internal standard) in anisole (0.7 mL) was added to the Schlenk tube. The solution was degassed by bubbling N_2 for 15 min. After degassing, the tube was immersed in a preheated oil bath (95 °C) and the polymerization proceeded at this temperature. The polymerization progress was monitored using GPC and ^{1}H NMR at 3 h intervals. When the molecular weight of the BCP reached the desired value, the reaction was quenched by exposing the solution to air in an ice/water bath and diluted with $CHCl_3$ (5 mL). The quenched solution was filtered through alumina (basic, 20 mL) using $CHCl_3$ as an eluent. The filtered solution was evaporated under reduced pressure and precipitated into methanol (30 mL). The white powder was collected by vacuum filtration and dried. For BCPs, the branched poly(ethylene glycol) (PEG) macroinitiators were used for polymerization.[35]

Representative procedure for indenylation of the pendant indanol group. P5-TMS (840 mg) and tetrabutylammonium fluoride trihydrate (TBAF) (3.7 g, 4 equiv. of **1-TMS** groups) were dissolved in THF (7 mL) and stirred at ambient condition for 4 h. Then, the solution was precipitated in methanol (40 mL) and the product was concentrated by centrifugation (4,500 rpm, 10 min). A white solid (**P5-OH**) was collected and dried at a reduced pressure. **P5-OH** (300 mg) and methyl *N*-

(triethylammoniumsulfonyl)carbamate (Burgess reagent, 786 mg, 3 equiv. of **1-OH** groups) were dissolved in anhydrous benzene (8 mL) and the solution was degassed by bubbling N_2 for 15 min. The solution was stirred in the dark at room temperature for 36 h. When the reaction was complete, the solution was precipitated in methanol (30 mL). A yellowish white powder was collected by vacuum filtration and dried. The molecular weight and composition of the polymers were characterized by ^{1}H NMR and GPC.

Cross-linking of indene-containing polymers. The **P1** solution in CH_2Cl_2 (2 mL, 0.01 mg mL^{-1}) was prepared in a quartz cuvette and exposed to long-wavelength UV light (λ = 365 nm, 6 W) located 3 cm from the cuvette. UV-Vis spectra were directly measured along the exposure time. After 20 min, the solution was exposed to UV light at a different wavelength (λ = 254 nm, 6 W) located 3 cm from the cuvette and UV-Vis spectra were also measure along the exposure time.

Self-assembly of block copolymers (P3 to P6) and photo-cross-linking of self-assembled structures. The polymer (10 mg) was dissolved in 1,4-dioxane or THF (2 mL) in a 20 mL capped vial with a magnetic bar. The solution was stirred for 1 h at room temperature (765 rpm). A syringe pump was calibrated to deliver water at a speed of 0.5 mL h^{-1}. The vial cap was replaced by a rubber septum and water was added to the polymer solution for 4 h using a syringe pump with a 6 mL syringe equipped with a steel needle. The resulting suspension was subjected to dialysis (molecular weight cutoff 12 to 14 kDA (SpectraPor, Rancho Dominguez, California)) against water for 24 h. The dialyzed suspension (1 mL) was transferred to 4 mL capped vial with a magnetic bar. The suspension was exposed to UV light (λ >300 nm, 200 W) with mild stirring. For tracing, 0.05 mL of the sample was collected and diluted, using water or THF, 40 times to its original volume to prepare the sample for DLS.

3.6 References

1. Zhang, L.; Eisenberg, A. Multiple Morphologies of "Crew-Cut" Aggregates of Polystyrene-b-Poly(Acrylic Acid) Block Copolymers. *Science* **1995**, *268*, 1728-1731.
2. van Hest, J. C. M.; Delnoye, D. A. P.; Baars, W. P. L.; van Genderen, M. H. P.; Meijer, E. W. Polystyrene-Dendrimer Amphiphilic Block Copolymers with a Generation-Dependent Aggregation. *Science* **1995**, *268*, 1592-1595.
3. Mai, Y.; Eisenberg, A. Self-Assembly of Block Copolymers. *Chem. Soc. Rev.* **2012**, *41*, 5969-5985.
4. Raffa, P.; Wever, D. A.; Picchioni, F.; Broekhuis, A. A. Polymeric Surfactants: Synthesis, Properties, and Links to Applications. *Chem. Rev.* **2015**, *115*, 8504-8563.
5. Holder, S. J.; Sommerdijk, N. A. J. M. New Micellar Morphologies from Amphiphilic Block Copolymers: Disks, Toroids and Bicontinuous Micelles. *Polym. Chem*. **2011**, *2*, 1018-1028.
6. Elsabahy, M.; Wooley, K. L. Design of Polymeric Nanoparticles for Biomedical Delivery

Applications. *Chem. Soc. Rev.* **2012**, *41*, 2545-2561.

7. Schacher, F. H.; Rupar, P. A.; Manners, I. Functional Block Copolymers: Nanostructured Materials with Emerging Applications. *Angew. Chem. Int. Ed*. **2012**, *51*, 7898-7921.
8. Blanazs, A.; Armes, S. P.; Ryan, A. J. Self-Assembled Block Copolymer Aggregates: From Micelles to Vesicles and Their Biological Applications. *Macromol. Rapid Commun*. **2009**, *30*, 267-277.
9. Förster, S.; Antonietti, M. Amphiphilic Block Copolymers in Structure-Controlled Nanomaterial Hybrids. *Adv. Mater.* **1998**, *10*, 195-217.
10. O'Reilly, R. K.; Hawker, C. J.; Wooley, K. L. Cross-Linked Block Copolymer Micelles: Functional Nanostructures of Great Potential and Versatility. *Chem. Soc. Rev.* **2006**, *35*, 1068-1083.
11. van Nostrum, C. F. Covalently Cross-Linked Amphiphilic Block Copolymer Micelles. *Soft Matter* **2011**, *7*, 3246-3259.
12. Thurmond, K. B. II; Kowalewski, T.; Wooley, K. L. Water-Soluble Knedel-Like Structures: The Preparation of Shell-Cross-Linked Small Particles. *J. Am. Chem. Soc.* **1996**, *118*, 7239-7240.
13. Nardin, C.; Hirt, T.; Leukel, J.; Meier, W. Polymerized ABA Triblock Copolymer Vesicles. *Langmuir* **2000**, *16*, 1035-1041.
14. Kim, B. J.; Chang, J. Y. Preparation of Carbon Nanospheres from Diblock Copolymer Micelles with Cores Containing Curable Acetylenic Groups. *Macromolecules* **2006**, *39*, 90-94.
15. Lê, D.; Liénafa, L.; Phan, T. N. T.; Deleruyelle, D.; Bouchet, R.; Maria, S.; Bertin, D.; Gigmes, D. Photo-Cross-Linked Diblock Copolymer Micelles: Quantitative Study of Photochemical Efficiency, Micelles Morphologies and Their Thermal Behavior. *Macromolecules* **2014**, *47*, 2420-2429.
16. Yan, X.; Liu, G.; Liu, F.; Tang, B. Z.; Peng, H.; Pakhomov, A. B.; Wong, C. Y. Superparamagnetic Triblock Copolymer/Fe2O3 Hybride Nanofibers. *Angew. Chem. Int. Ed.* **2001**, *40*, 3593-3596.
17. Du, J.; Armes, S. P. pH-Responsive Vesicles Based on a Hydrolyticaly Self-Cross-Linkable Copolymer. *J. Am. Chem. Soc.* **2005**, *127*, 12800-12801.
18. Huang, H.; Hoogenboom, R.; Leenen, M. A. M.; Guillet, P.; Jonas, A. M.; Schubert, U. S.; Gohy, J.-F. Solvent-Induced Morphological Transition in Core-Cross-Linked Block Copolymer Micelles. *J. Am. Chem. Soc.* **2006**, *128*, 3784-3788.
19. Zhang, J.; Jiang, X.; Zhang, Y.; Li, Y.; Liu, S. Facile Fabrication of Reversible Core Cross-Linked Micelles Possessing Thermosensitive Swellability. *Macromolecules* **2007**, *40*, 9125-9132.
20. Walther, A.; Goldmann, A. S.; Yelamanchili, R. S.; Drechsler, M.; Schmalz, H.; Eisenberg, A.; Muller, A. H. E. Multiple Morphologies, Phase Transitions, and Cross-Linking of Crew-Cut Aggregates of Polybutadiene-block-Poly(2-Vinylpyridine) Diblock Copolymers. *Macromolecules* **2008**, *41*, 3254-3260.
21. Gaitzsch, J.; Appelhans, D.; Grafe, D.; Schwille, P.; Voit, B. Photo-Crosslinked and pH Sensitive Polymersomes for Triggering the Loading and Release of Cargo. *Chem. Commun.* **2011**, *47*, 3466-

3468.

22. Chen, X.; Ding, X.; Zheng, Z.; Peng, Y. Thermosensitive Cross-Linked Polymer Vesicles for Controlled Release System. *New J. Chem.* **2006**, *30*, 577-582.
23. Du, J.; O'Reilly, R. K. Advances and Challenges in Smart and Functional Polymer Vesicles. *Soft Matter* **2009**, *5*, 3544-3561.
24. Jiang, J.; Qi, B.; Lepage, M.; Zhao, Y. Polymer Micelles Stabilization on Demand through Reversible Photo-Cross-Linking. *Macromolecules* **2007**, *40*, 790-792.
25. He, J.; Tong, X.; Tremblay, L.; Zhao, Y. Corona-Cross-Linked Polymer Vesicles Displaying a Large and Reversible Temperature-Responsive Volume Transition. *Macromolecules* **2009**, *42*, 7267-7270.
26. Abe, E.; Pennycook, S. J.; Tsai, A. P. Direct Observation of a Local Thermal Vibration Anomaly in a Quasicrystal. *Nature* **2003**, *421*, 347-350.
27. Kaur, G.; Johnston, P.; Saito, K. Photo-Reversible Dimerisation Reactions and Their Applications in Polymeric Systems. *Polym. Chem.* **2014**, *5*, 2171-2186.
28. Gohy, J. F.; Zhao, Y. Photo-Responsive Block Copolymer Micelles: Design and Behavior. *Chem. Soc. Rev.* **2013**, *42*, 7117-7129.
29. Millar, J. R.; Smith, D. G.; Marr, W. E.; Kressman, T. R. E. Solvent-Modified Polymer Networks. Part I. The Preparation and Characterisation of Expanded-Network and Macroporous Styrene-Divinylbenzene Copolymers and Their Sulphonates. *J. Chem. Soc.* **1963**, 218-225.
30. Yan, M.; Harnish, B. A Simple Method for the Attachment of Polymer Films on Solid Substrates. *Adv. Mater.* **2003**, *15*, 244-248.
31. Chada, S.; Yan, M. Self-Assembled Nanostructures from Homopolymer Induced by UV and Solvent Exposure. *Soft Matter* **2008**, *4*, 2164-2167.
32. Hoffmann, F.; Wolff, T.; Minko, S.; Stamm, M. Photochemical Structuring and Fixing of Structures in Binary Polymer Brush Layers Via 2p+2p Photodimerization. *J. Colloid Interface Sci.* **2005**, *282*, 349-358.
33. Hoffmann, F.; Wolff, T. Photochemical Fixation of Structures in Binary Polymer Brushes-Influence of Layer Thickness and Grafting Method. *J. Colloid Interface Sci.* **2008**, *322*, 434-447.
34. George M. Atkins, J.; Burgess, E. M. The Reactions of an N-Sulfonylamine Inner Salt. *J. Am. Chem. Soc.* **1968**, *90*, 4744-4745.
35. Jeong, M. G.; van Hest, J. C. M.; Kim, K. T. Self-Assembly of Dendritic-Linear Block Copolymers with Fixed Molecular Weight and Block Ratio. *Chem. Commun.* **2012**, *48*, 3590-3592.
36. La, Y.; Park, C.; Shin, T. J.; Joo, S. H.; Kang, S.; Kim, K. T. Colloidal Inverse Bicontinuous Cubic Membranes of Block Copolymers with Tunable Surface Functional Groups. *Nat. Chem.* **2014**, *6*, 534-541.
37. An, T. H.; La, Y.; Cho, A.; Jeong, M. G.; Shin, T. J.; Park, C.; Kim, K. T. Solution Self-Assembly of Block Copolymers Containing a Branched Hydrophilic Block into Inverse Biocntinuous Cubic

Mesophases. *ACS Nano* **2015**, *9*, 3084-3096.

38. La, Y.; An, T. H.; Shin, T. J.; Park, C.; Kim, K. T. A Morphological Transition of Inverse Mesophases of a Branched-Linear Block Copolymer Guided by Using Cosolvents. *Angew. Chem. Int. Ed.* **2015**, *54*, 10483-10487.
39. Cho, A.; La, Y.; Shin, T. J.; Park, C.; Kim, K. T. Structural Requirements of Block Copolymers for Self-Assembly into Inverse Bicontinuous Cubic Mesophases in Solution. *Macromolecules* **2016**, *49*, 4510-4519.
40. Park, C.; La, Y.; An, T. H.; Jeong, H. Y.; Kang, S.; Joo, S. H.; Ahn, H.; Shin, T. J.; Kim, K. T. Mesoporous Monoliths of Inverse Bicontinuous Cubic Phases of Block Copolymer Bilayers. *Nat. Commun.* **2015**, *6*, 6392-6400.
41. Wolff, T.; Schmidt, F.; Volz, P. Regioselectivity and Stereoselectivity in the Photodimerization of Rigid and Semirigid Stilbenes. *J. Org. Chem*. **1992**, *57*, 4255-4262.

Chapter 4. Polymer Cubosomes with Lattice Parameters Comparable to Biological Lipid Cubic Membranes

4.1 Abstract

Lipid cubic membranes found in biology often exhibited lattice parameters close to the wavelengths of visible light. These highly swollen cubic membranes, the ordered smooth endoplasmic reticulum (OSER), serve as templates for the synthesis of biophotonic crystals in the wing scales of butterflies and the cuticles of weevils and beetles. To achieve the length scale exhibited by biophotonic structures, the molecular weight of the constituting polymer blocks of the block copolymer (BCP) which forms cubic mesophases in solution should be substantially larger than the conventional BCPs that have so far been used to synthesize cubic mesophases. Here we report the synthesis of branched-linear BCPs with a high molecular weight polystyrene (PS) block by the atom-transfer radical polymerization (ATRP) of styrene with a branched poly(ethylene glycol) (PEG) macroinitiator. A series of branched-linear BCPs with a hydrophobic PS block having 1600–2400 repeating units with a narrow molecular weight distribution ($Đ$ < 1.3) was successfully synthesized, which was successfully isolated from the reaction mixture containing homo-polystyrene as a byproduct in large quantity by gradient chromatography. The solution self-assembly of these high molecular weight BCPs confirmed that the proportionality between the degree of polymerization of the PS block and the chain dimension dictated the lattice dimension of the resulting BCP mesophases such as polymer cubosomes and hexosomes. Consequently, polymer cubosomes with large periodicity (> 190 nm) were synthesized, which exhibited an optical reflection arising from the triply periodic minimal surfaces inside the polymer cubosomes.

4.2 Introduction

Fabrication of polymer nanostructures with spatial arrangements of chemical compositions in desired lattices and periodicities is a crucial effort for applications such as lithography, separation, filtration, and optoelectronics[1-4]. In particular, three-dimensionally (3-D) periodic structures composed of cubic lattices having periodicity commensurate with the wavelength of visible light have been pursued as photonic crystals exhibiting a large omni-directional optical band gap[5-7]. Most of these structures have been prepared by interference lithography, multi-step fabrications, or templated synthesis within porous scaffolds such as colloidal crystals[8-10]. Direct self-assembly of block copolymers (BCPs) into 3-D ordered structures with a cubic or gyroid symmetry is an alternative to the top-down fabrication of triply periodic structures[11-13]. In order to achieve a large periodicity (> 200 nm) by self-assembly of BCPs in the bulk, the molecular weight of the polymer blocks constituting the BCP is required to be very high to increase the chain dimension and the lattice parameter of the resulting self-assembled structure[14,15]. Sequential anionic polymerization has been utilized to synthesize BCPs with very high molecular

weight, which self-assembled into 2-D lamellar and 3-D gyroid structures in bulk[16]. Recently, ring-opening metathesis polymerization (ROMP) of norbornene-derivatives has been successfully used to synthesize high molecular weight bottle-brush copolymers[17-19]. Also, controlled radical polymerization of acrylates produced high molecular weight BCPs with complex architectures and topologies[20].

Inverse bicontinuous cubic mesophases formed by self-assembly of BCPs in solution are emerging 3-D periodic structures[21-24]. Analogous to lipid cubic mesophases and complex biological membrane[25-28], BCPs spontaneously form highly defined cubic crystalline structures composed of BCP bilayers in solution. The resulting triply periodic minimal surfaces (TPMSs) of the BCP bilayers, such as Schwarz P (primitive cubic, *Im3m* space group) and D (double diamond, *Pn3m* space group) surfaces, exhibited cubic lattices with large periodicities (40–90 nm), which are an order of magnitude larger than those of the lipid cubic mesophases formed in vitro[29,30]. Polymer cubic mesophases and their colloidal particles (polymer cubosomes) have been predicted to have an optical band gap if the lattice parameter approaches to the wavelength of visible light. Cubic membranes of lipid bilayers found in biology often exhibited lattice parameters commensurate with the wavelength of visible light[31,32]. These highly swollen cubic membranes, such as the ordered smooth endoplasmic reticulum (OSER), serve as templates for the synthesis of biophotonic crystals found in nature, from the wing scales of butterflies to the cuticles of weevils and beetles[33,34]. However, the cubic membranes with these large lattices have not yet been prepared by the self-assembly of lipids and BCPs.

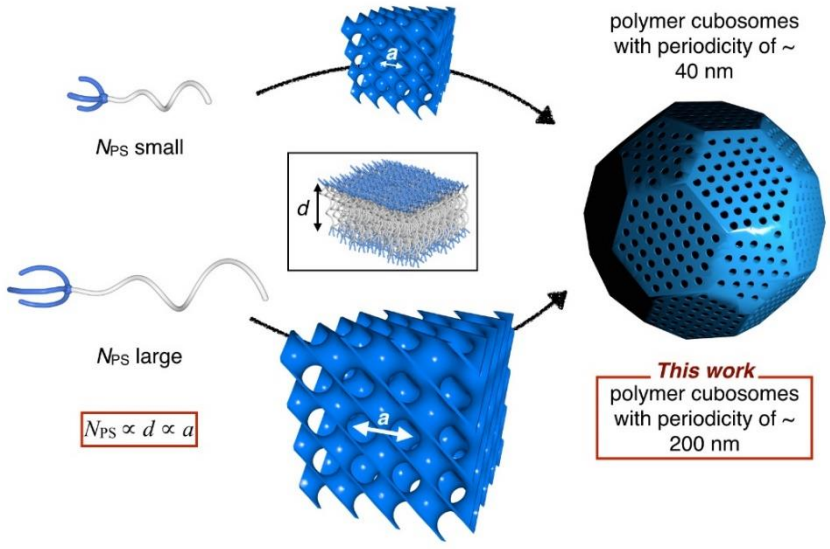

Figure 4-1. Schematic on the self-assembly of high molecular weight branched-linear BCPs into polymer cubosomes with internal double diamond structure (*Pn3m* symmetry group). N_{ps} is the degree of polymerization of a PS block of a BCP. *d* and *a* indicate the thickness of the BCP bilayer and the lattice parameter of the double diamond lattice, respectively.

4.3 Results and Discussion

Our strategy to achieve BCP cubic mesophases with the length scale of biological cubic membranes is based on the assumption that the BCPs with a branched poly(ethylene glycol) (PEG) hydrophilic block and a linear polystyrene (PS) block will self-assemble into polymer cubosomes, regardless of the overall molecular weight, if the block ratio (the molecular weight fraction of the PEG block, f_{PEG}) is adjusted to a value (< 5%) that guides the self-assembly to preferentially form inverse mesophases (Figure 4-1)[22,23]. After screening the reported polymerization methods for synthesizing a PS block of greater than 1200 repeating units, we chose Cu(I)-catalyzed ATRP of styrene in the bulk as the polymerization method because of fast propagation of styrene with a high loading of the catalyst. In order to synthesize high molecular weight branched-linear BCPs, we used the macroinitiator PEG2000$_3$-Br (**1**) which has three peripheral PEG chains (M_n = 2,000 g/mol) for the ATRP of styrene (Scheme 4-1). The purity of **1** (> 99%) was confirmed by ^{1}H NMR and MALDI-TOF mass spectrometry (Figure 4-2).

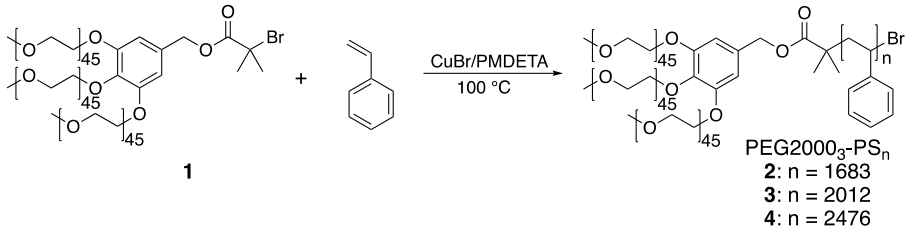

Scheme 4-1. Synthesis of high molecular weight of BCPs

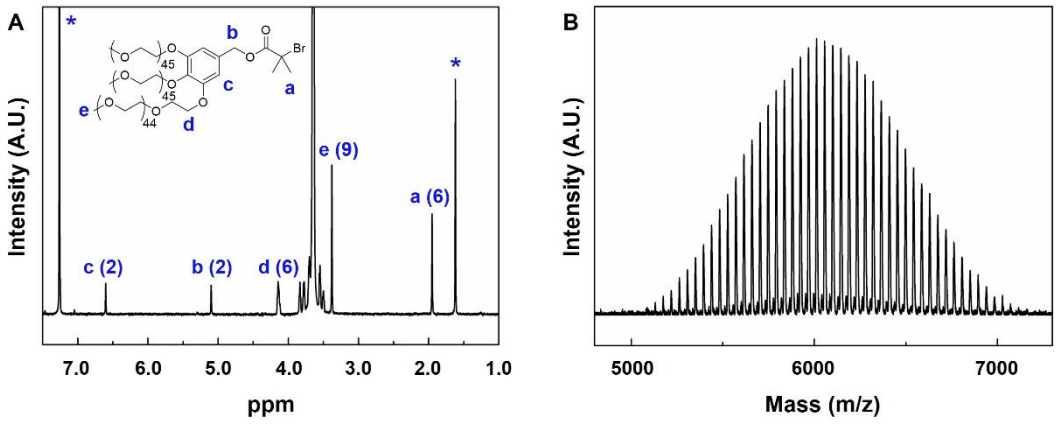

Figure 4-2. (A) ^{1}H NMR spectrum of the macroinitiator PEG2000$_3$-Br, **1**. (B) MALDI-TOF-MS spectrum of the precursor of the macroinitiator, PEG2000$_3$-OH.

Initially, polymerization was carried out in the presence of CuBr/pentamethyldiethyltriamine (PMDETA) (5 eq. to **1**) in neat styrene at 100 °C (Scheme 4-1). Time-interval monitoring of the ATRP by GPC revealed a slow propagation over the reaction time. Polymerization over an extended period of

time (> 12 h) further increased the molecular weight distribution without increasing the molecular weight, which suggested that the control of the ATRP process deteriorated as the reaction time increased. Therefore, we optimized the stoichiometry of CuBr and **1** for achieving the desired degree of polymerization (DP_n > 1200) within the reaction time of 12 h. In the presence of 20 equivalents of CuBr to **1**, the ATRP of styrene resulted in the formation of BCPs with M_n of 60,000 g/mol within 8 h, with a significantly broad molecular weight distribution ($Đ$ > 1.5), as monitored by GPC. At 12 h after initiation, the GPC results for the crude solution showed a peak indicating M_n = 81,600 g/mol ($Đ$ = 1.60) (Figure 4-3).

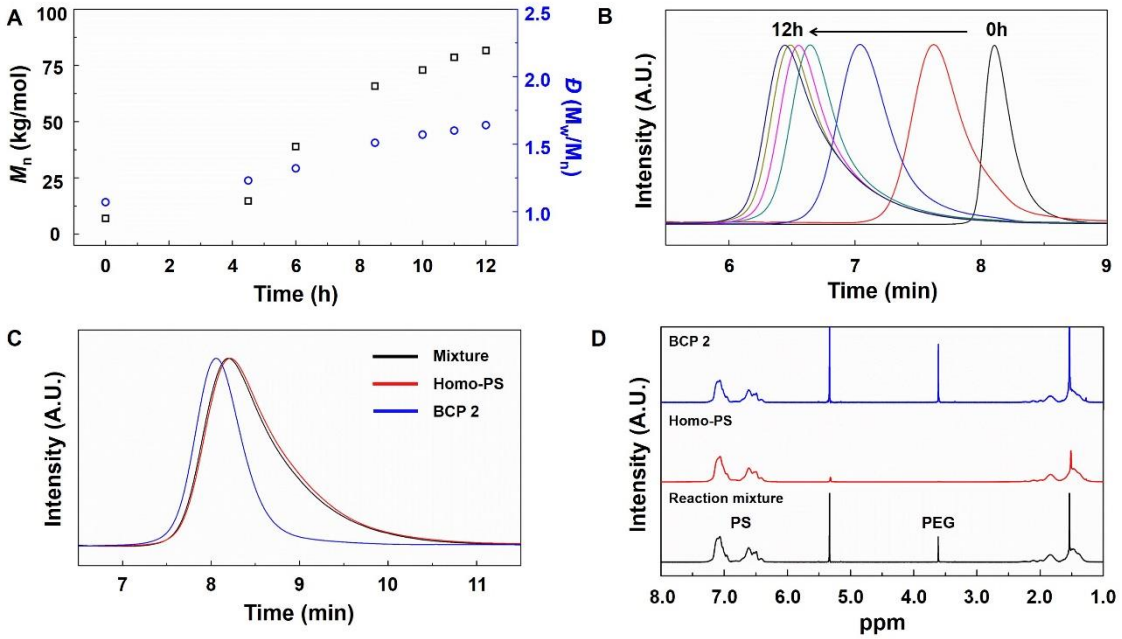

Figure 4-3. (A) Plot of polymerization time vs the number average of molecular weight (M_n) and polydispersity index ($Đ$) for **2**. (B) GPC (THF as an eluent) results showing the progress during the polymerization time for **2**. (C) GPC (DMF as an eluent) and (D) ^{1}H NMR spectra showing the reaction mixture before purification process (black), the homo-PS separated as a first fraction of the gradient chromatography (red), and **2** separated as the second fraction (blue).

After precipitation, we realized that the polymerization had produced homo-polystyrene (homo-PS) as a major product and, thus, the isolated yield of the polymers after precipitation substantially exceeded the expected value calculated by assuming the complete conversion of **1** into the BCP. We purified the precipitated solid by performing the gradient chromatography on SiO_2 with a CH_2Cl_2/MeOH mixture (100:0 to 96:4 v/v) as an eluent utilizing the marked difference of the affinity of PEG and PS blocks toward silica (Figure 4-4). The gradient chromatography of the precipitated polymers yielded homo-PS as the first fraction using CH_2Cl_2 as an eluent, and, then, the desired BCP as the second fraction eluted with a mixed solvent (CH_2Cl_2:MeOH = 96:4 v/v). A trace amount of the low molecular weight BCP

later appeared when the fraction of MeOH in the eluent was increased to 10%. (Figure 4-5). The GPC analysis of each fraction obtained from the gradient chromatography revealed that the BCP (M_n = 158,700 g/mol, $Đ$ = 1.21) retained a well-controlled architecture even though the major product was homo-PS (M_n = 82,900 g/mol, $Đ$ = 1.57) (Figure 4-3C). The absolute yield of the BCP after purification was 9%, while the isolated yield of the homo-PS was 90%. Assuming the complete conversion of the macroinitiator **1** into the BCP by ATRP, the isolated yield of the purified BCP **2**, $PEG2000_3$-PS_{1683} was 17.7%.

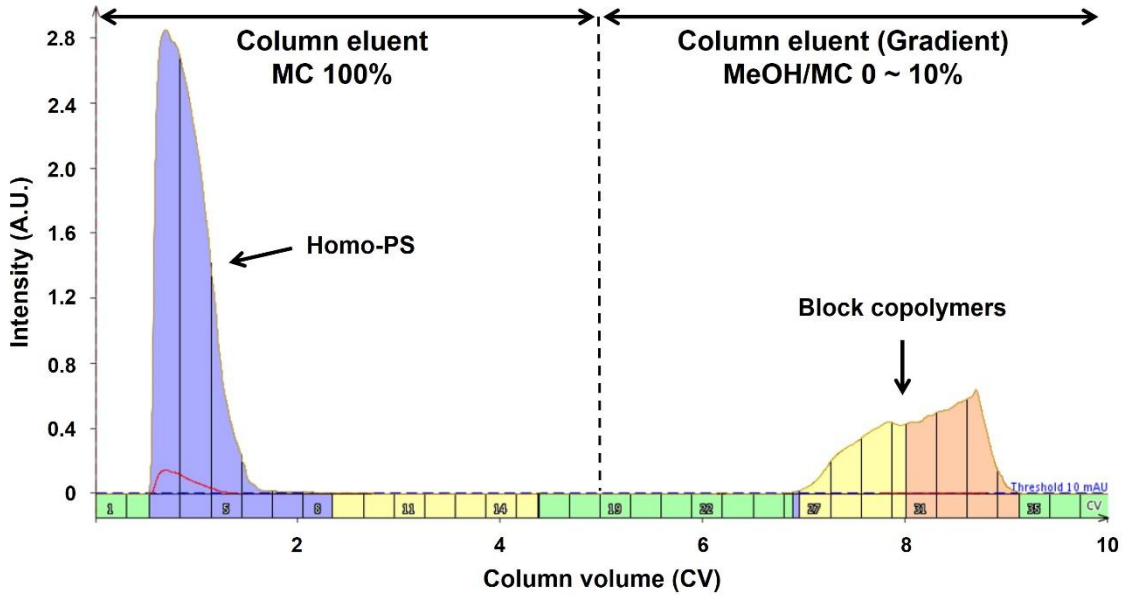

Figure 4-4. Plot of column volume vs intensity of the entire absorbance of gradient column chromatography by Isolera™ Specktra system showing a successful separation of homo-PS and target BCP.

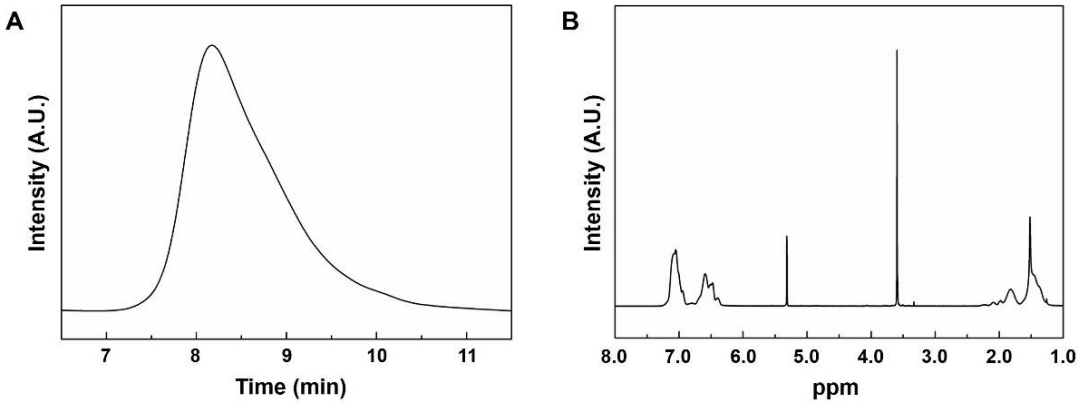

Figure 4-5. (A) GPC and (B) ^{1}H NMR spectrum of residual BCPs from the gradient column chromatography of reaction mixture of **2** (M_n = 81,700 g/mol, $Đ$ = 1.65)

Our ^{1}H NMR results for the fractions obtained from the chromatography suggested that the formation of the homo-PS during the ATRP might not be initiated by the macroinitiator **1** (Figure 4-3D). We suspected that the prevalent generation of homo-PS during the ATRP in the presence of **1** might arise from the autopolymerization of bulk styrene at the elevated temperature we used for the polymerization (100 ºC)[35]. We adjusted the temperature of the ATRP to 90 ºC while maintaining all the other variables unchanged. However, we observed the formation of homo-PS as a major product at this temperature only with the reduced rate of propagation. We also carried out the polymerization of neat styrene at 100 °C in the presence of the macroinitiator **1** without CuBr/PMDETA; this resulted in no detectable polymerization. However, surprisingly, when the polymerization was conducted in the presence of CuBr/PMDETA without **1**, the reaction yielded homo-PS (M_n = 131,200 g/mol, $Đ$ = 1.86) in large quantities after 8 h (Figure 4-6A). Time-interval traces of GPC peaks indicated that the molecular weight of the homo-PS gradually increased during the polymerization in spite of the absence of the macroinitiator (Figure 4-6B).

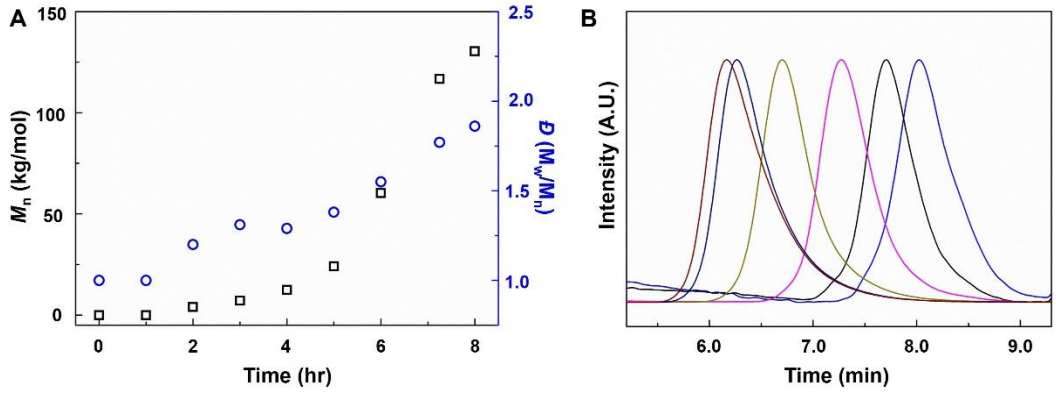

Figure 4-6. (A) Plot of polymerization time vs the number of molecular weight (M_n) and polydispersity index ($Đ$) and (B) GPC spectra showing the progress during the polymerization of the control polymerization in the presence of CuBr/PMDETA without the macroinitiator **1**.

The exact mechanism for the appearance of homo-PS in a substantial quantity without being initiated by the macroinitiator is not yet understood. Our results suggested that the predominant production of homo-PS during the ATRP of neat styrene with an excess amount of CuBr (20 eq. to **1**) might occur as a result of a single electron transfer from the Cu catalyst to styrene[36,37]. The presence of bulky PEG chains around the active center of **1** could render the propagation kinetically challenging, and, therefore, the rate of electron transfer from Cu(I) to the monomer might become competitive with the activation of the propagating center to the active species by the electron transfer from the Cu-catalyst. Nevertheless, it is noteworthy that, in spite of the prevalent formation of homo-PS in the background, the propagation of **1** was unperturbed, yielding the desired BCP in a controlled manner[38].

Under the optimized ATRP conditions (20 eq. of CuBr/PMDETA to **1** in bulk styrene), we synthesized

and isolated a series of BCPs having the overall molecular weights in the range of 158–245 kg/mol ($Đ$ < 1.26) (Table 4-1 and Figure 4-7). The M_n of the BCP was adjusted by controlling the duration of the polymerization reaction. The highest molecular weight BCP, PEG2000$_3$-PS$_{2476}$ (**4**) was obtained by quenching the ATRP at 12 h. ^{1}H NMR spectra of these BCPs confirmed that the presence of PEG chains in the hydrophilic block connected to the long PS chain. The values of the block ratio (f_{PEG}), determined via ^{1}H NMR integration, were in the range of 2.4–3.5%.

Table 4-1. Characterization of BCPs

BCP	M_n (kg/mol)[a]	$Đ$ (GPC)[a]	DP_n[b]	M_n (kg/mol)[b]	f_{PEG} (%)[c]
2	158.7	1.21	1,683	181.2	3.5
3	186.9	1.25	2,012	215.4	3.0
4	245.9	1.26	2,476	263.7	2.4

[a]Determined by GPC using DMF as an eluent. [b]Calculated by ^{1}H NMR integration assuming the M_n of PEG chains of 6000 g/mol. [c]Calculated by f_{PEG} = (M_n of PEG/M_n of a BCP).

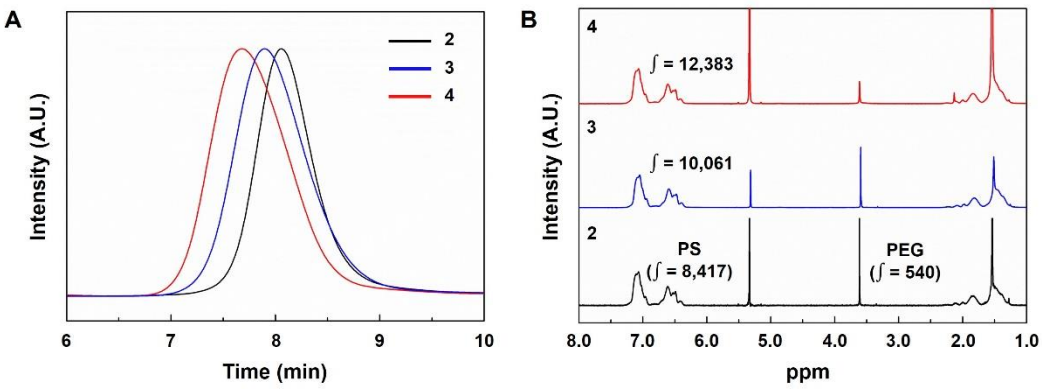

Figure 4-7. (A) GPC (DMF as an eluent) and (B) ^{1}H NMR in CD_2Cl_2 spectra of BCPs

These high molecular weight branched-linear BCPs underwent self-assembly in solution. First, we used a co-solvent method to allow the BCPs to assemble by adding water at a slow rate (0.5 mL/h) to a dioxane solution (2 mL, 0.5 wt % of BCP). When the water content reached to 50 vol%, the suspension was dialyzed against water for 48 h with frequent exchange of the medium. The resulting nanostructures were examined by transmission electron microscopy (TEM), scanning electron microscopy (SEM), and dynamic light scattering (DLS) (Figure 4-8A, B). PEG2000$_3$-PS$_{1683}$ (**2**) (f_{PEG} = 3.5%) self-assembled to polymersomes (polymer vesicles) with an average diameter of 557 nm (polydispersity = 0.125) (Figure 4-9). The bilayer thickness of the polymersomes of PEG2000$_3$-PS$_{1683}$ (**2**) was measured as 74 ± 5 nm by TEM, which is a 2.7-fold increase on that of the bilayer of a linear BCP, PEG2000-PS$_{228}$ (28 nm, Figure 4-10)[23]. The increased thickness of the bilayer of BCP **2** is agreed with the proportionality of the

end-to-end distance of a PS chain to the square root of its DP_n.[39] This result supports our assumption that the dimension of the self-assembled structure of a BCP is proportional to the molecular weight of the hydrophobic polymer block of the BCP.

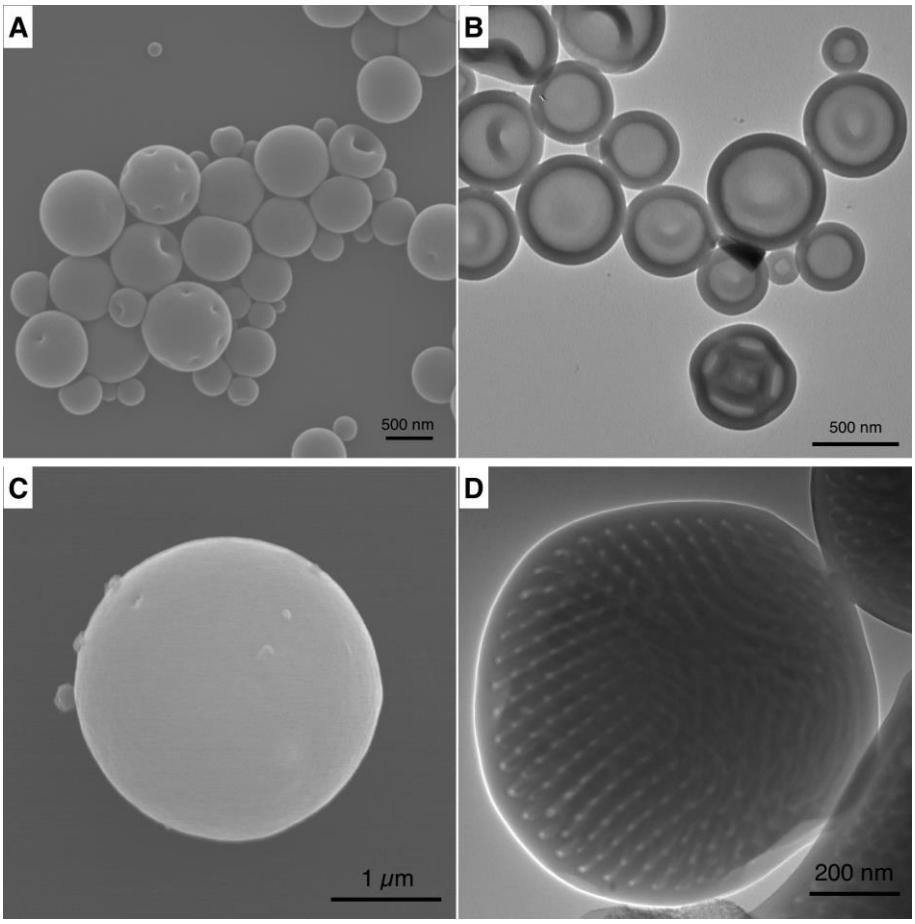

Figure 4-8. (A) SEM and (B) TEM images of polymersomes of **2** self-assembled by co-solvent method. (C) SEM and (D) TEM images of hexosomes of **4** self-assembled by solvent diffusion-evaporation self-assembly method.

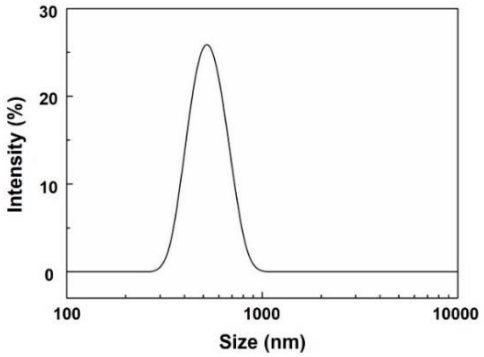

Figure 4-9. DLS plot of the polymersomes of **2** by the co-solvent method.

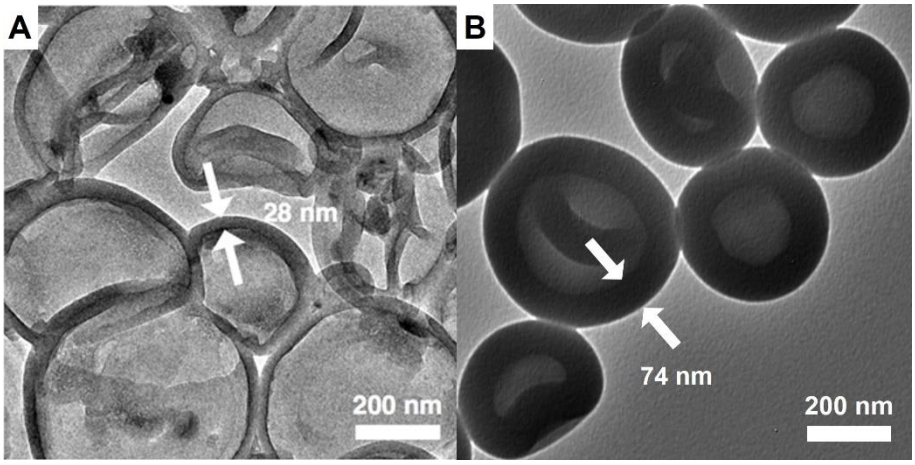

Figure 4-10. TEM images of the polymersomes of (A) PEG2000-PS_{228}^{22} and (B) $PEG2000_3$-PS_{1683} (**2**) showing the thickness of the bilayer membrane.

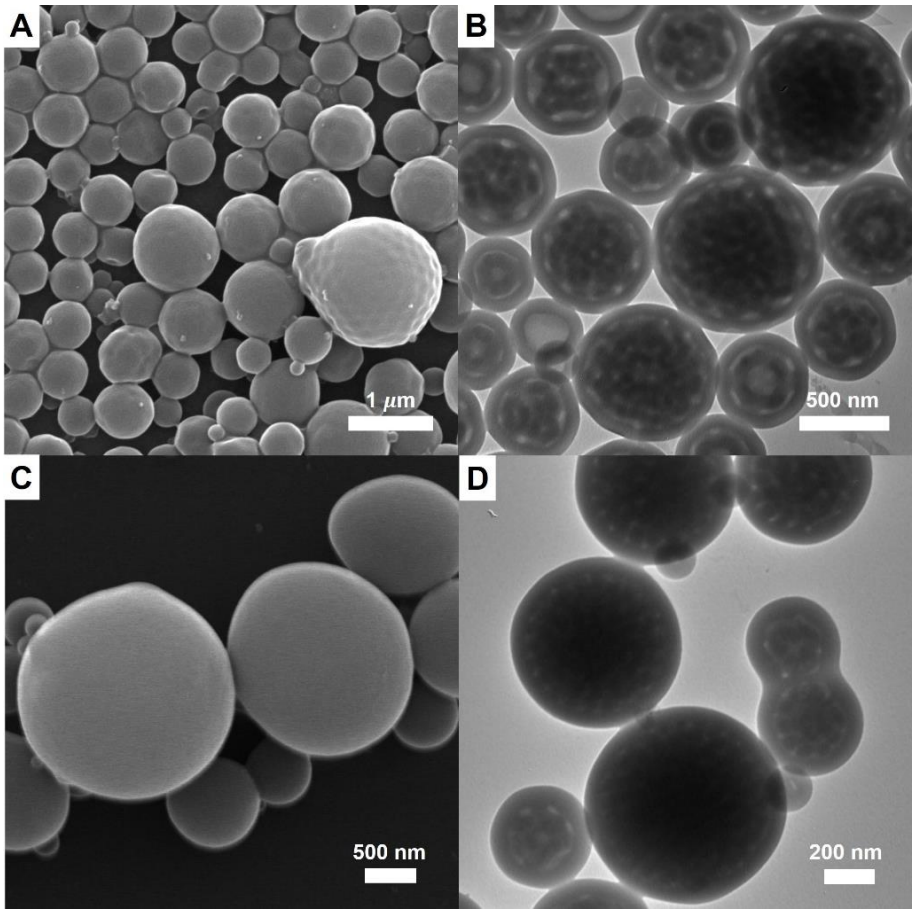

Figure 4-11. (A) SEM and (B) TEM images of self-assembled structures of **3** by the co-solvent method. (C) SEM and (D) TEM images of self-assembled structures of **4** by the co-solvent method.

The co-solvent method for the self-assembly of higher molecular weight BCPs (**3** and **4**) only produced colloidal nanoparticles having ill-defined internal structures, even with a slower rate of water

addition (0.2 mL/h) (Figure 4-11). We suspected that the formation of ill-defined structures might be originated from the difficulty of BCPs with high molecular weight PS blocks (DP_n > 2000) to reach equilibrium during the self-assembly. Therefore, we used the solvent diffusion-evaporation self-assembly (SDEMS) method to introduce a poor solvent (water) into the dioxane solution of a BCP at a much reduced rate[40]. The dioxane solution of $PEG2000_3$-PS_{2012} **3** (0.5 wt%, 1 mL) in a shallow glass container was placed in a saturated humidity chamber for 24 h. In this environment, dioxane slowly evaporated from the container while water vapor diffused into the BCP solution. The solution became turbid after 24 h, and was quenched by diluting the suspension with water (2 mL). The residual organic solvents were removed by dialysis against water for 24 h. This method allowed the high molecular weight BCPs, $PEG2000_3$-PS_{2012} (**3**) (f_{PEG} = 3.0%) and $PEG2000_3$-PS_{2476} (**4**) (f_{PEG} = 2.4%), to self-assemble into polymer cubosomes and hexosomes, respectively. SEM images of the polymer hexosomes of **4** only showed spherical particles without any surface structure (Figure 4-8C), but TEM images of the polymer hexosomes of BCP **4** clearly showed the presence of the internal mesophases composed of hexagonally arranged water channels (Figure 4-8D).

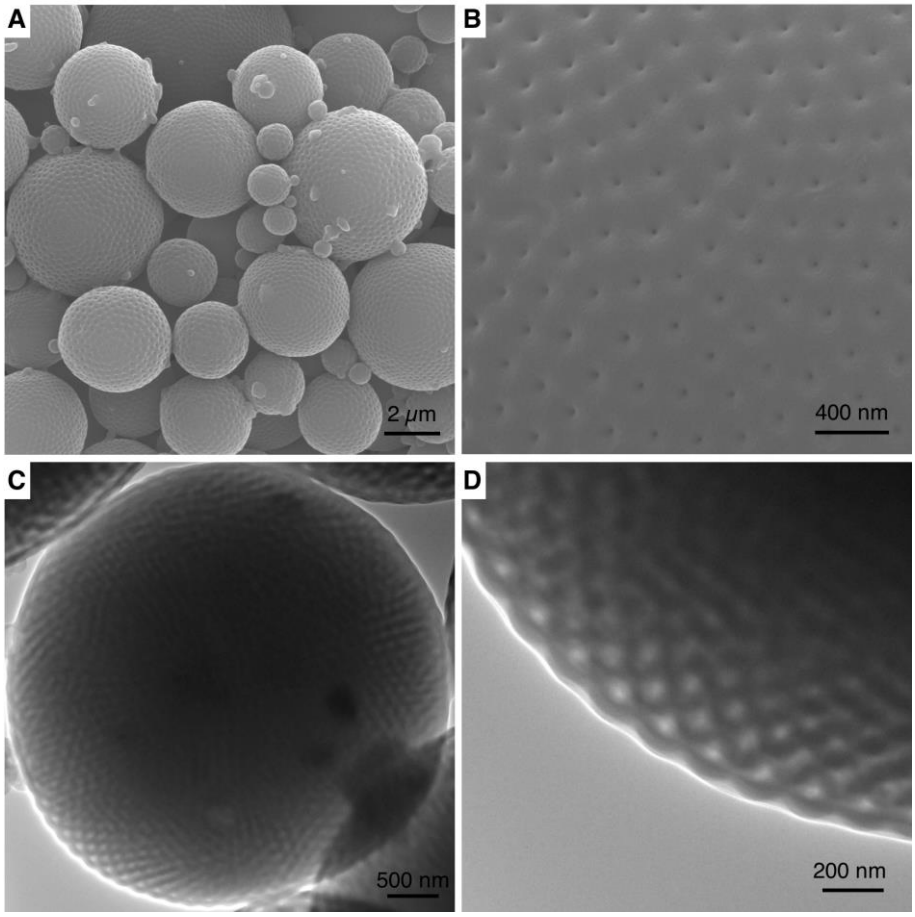

Figure 4-12. (A, B) SEM and (C, D) TEM images of polymer cubosomes of **3** self-assembled by solvent diffusion-evaporation self-assembly method.

The SEM images of the polymer cubosomes of BCP **3** (Figure 4-12A, B) showed the presence of surface pores, and suggested that the internal mesophases have double diamond lattices (*Pn3m* symmetry). The distance between the surface pores of the polymer cubosome was determined to be ~200 nm from the SEM images. TEM images of the polymer cubosomes of **3** (Figure 4-12C, D) suggested the presence of internal P surface (*Im3m* symmetry) by revealing the (100) projection of the lattices. From the TEM images, the lattice parameter of the internal P surface was estimated to ~200 nm (Figure 4-13). Small angle X-ray scattering (SAXS) results for the polymer cubosomes of **3** feature only broad peaks due to the distortion of the lattices and the background scattering from the polymer cubosomes of small diameters (Figure 4-14A). From the SAXS results, the lattice parameters of the internal P surface and D surface were estimated to be 190 nm and 149 nm, respectively; this value is in agreement with the lattice parameter estimated from the analyses of the SEM and TEM images.

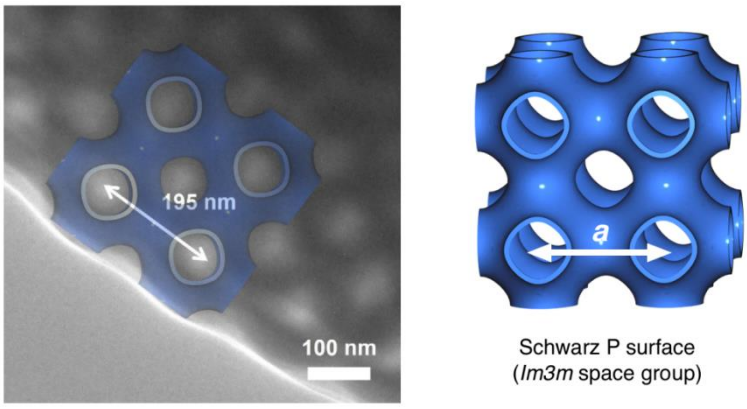

Figure 4-13. TEM image of the polymer cubosome of **3** by SDEMS method and the representative lattice of Schwarz P surface of BCP bilayers. The computer-generated (100) plane of Schwarz P surface was superimposed on TEM image to indicates the lattice parameter.

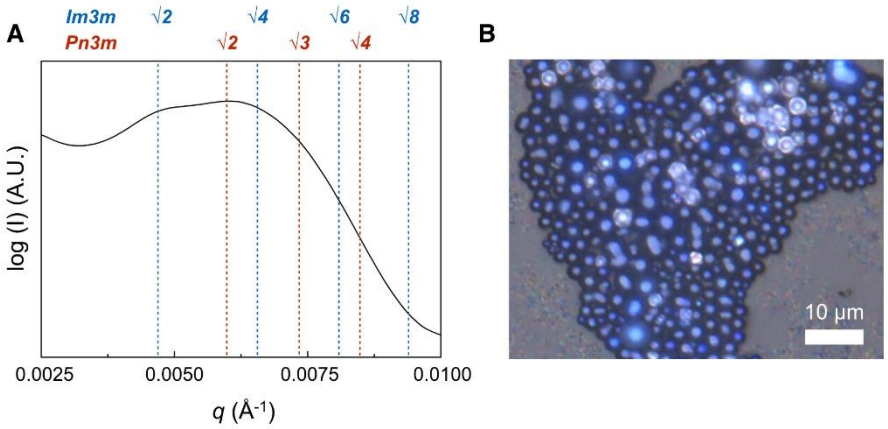

Figure 4-14. (A) Small-angle x-ray scattering result obtained from the dried polymer cubosomes of **3** (*Im3m* symmetry, a = 190 nm and *Pn3m* symmetry, *a* = 149 nm). (B) Optical microscopy image of the polymer cubosomes of **3**.

The observed lattice parameter of the polymer cubosomes of **3** was remarkably larger than the observed lattice parameter for the polymer cubosomes of $PEG550_3$-PS_{168} (~ 45 nm, Figure 4-15). To the best of our knowledge, the polymer cubosomes reported here is the first example of Schwarz D surface with the lattice parameter close to the length scale of biological cubic membranes. The latter cubosomes of $PEG550_3$-PS_{168} (M_n = 17,800 g/mol, $Đ$ = 1.06) had a bilayer thickness of 15 nm, as measured by TEM, whereas the polymer cubosomes of **3** possessed the bilayer membrane of thickness ca. 48 nm thickness (Figure 4-16). This result indicated that the increase of the DP_n of the PS block translated to an increase of the thickness of the bilayer membrane of the BCP, and the chain dimension of the high molecular weight BCP dictates the lattice parameter of the cubic mesophases.

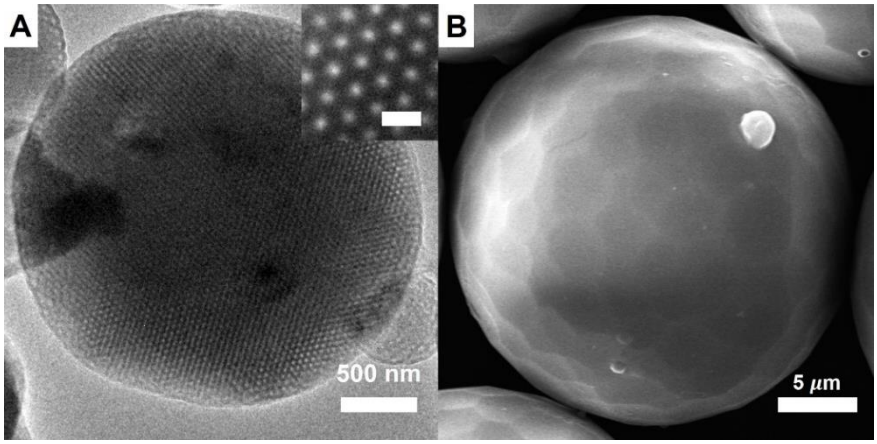

Figure 4-15. (A) TEM and (B) SEM images of polymer cubosomes of $PEG550_3$-PS_{168} (Scale bar in the inset: 50 nm)

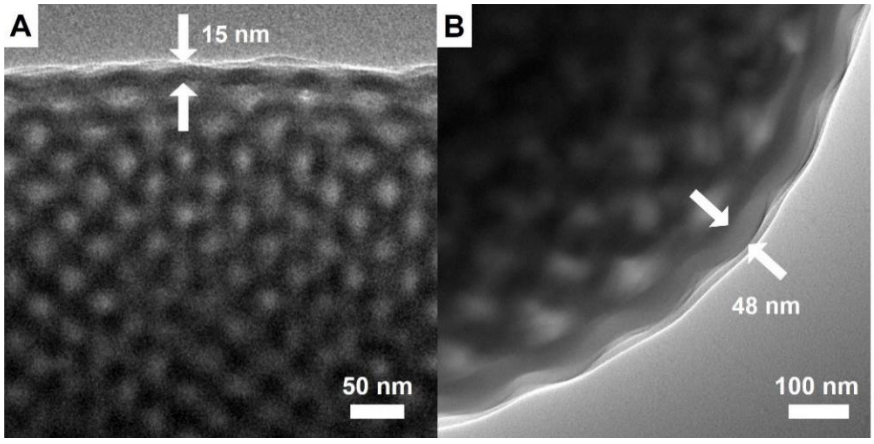

Figure 4-16. TEM images of polymer cubosomes of (A) $PEG550_3$-PS_{168} and (B) **3**

Polymer cubosomes composed of a TPMS of the BCP bilayer may exhibit a partial optical band gap depending on the lattice symmetry and parameter. Martin-moreno and Thomas predicted that a partial band gap would be available from a TPMS with a large lattice parameter.[41,42] Therefore, we inspected

the optical reflection exhibited by the polymer cubosomes of BCP **3** by optical microscopy, which revealed a pale blue hue reflected from the polymer cubosomes. UV-Visible reflectance spectroscopy confirmed the presence of a weak reflection centered at 425 nm (Figure 4-14B). In contrast, polymer hexosomes of **4** or polymer cubosomes of $PEG550_3$-PS_{168}, having smaller lattice parameters, did not show any reflection under the same experimental conditions (Figure 4-17). Our results confirm that the increased molecular weight of the BCP correlates with the increased lattice dimension of the self-assembled TPMS formed by solution self-assembly. The lattice dimension is close to the length scale of nature exhibited in the highly swollen biological cubic membranes that are found in, for example, the ordered smooth endoplasmic reticulum, which serves as templates for the synthesis of biophotonic crystals.

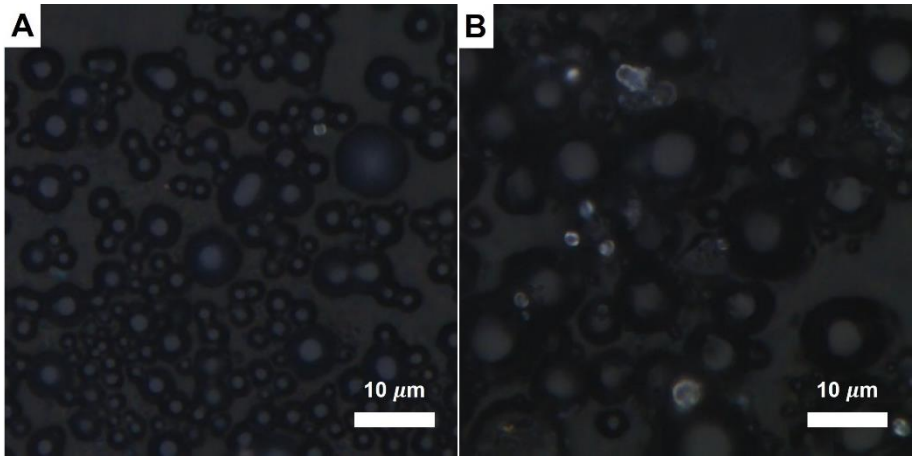

Figure 4-17. Optical microscope images of (A) polymer hexosomes of **4** (B) polymer cubosomes of $PEG550_3$-PS_{168} showing no reflectance.

4.4 Summary

In summary, we synthesized branched-linear BCPs with a high molecular weight polystyrene (PS) block by the atom-transfer radical polymerization (ATRP) of styrene in the bulk, with a branched poly(ethylene glycol) (PEG) macroinitiator. A series of branched-linear BCPs with the hydrophobic PS blocks of 1600–2400 repeating units with a narrow molecular weight distribution ($Đ$ < 1.26) were successfully synthesized and isolated from the reaction mixture containing homo-PS as the major product. Solution self-assembly of these high molecular weight BCPs demonstrated that the inverse mesophases with large lattice parameters can be formed by the slow introduction of non-solvent (water) into the BCP solution because this method of self-assembly avoids the premature trapping of self-assembled structures in a metastable state. The resulting polymer cubosomes exhibit the periodic order on nature's length scale as exhibited by biophotonic structures. Our preliminary results showed that the polymer cubosomes reported here could serve as templates for synthesizing 3-D cubic photonic crystals that possess structural symmetry resembling the biophotonic structures found in insects.

4.5 Experimental

Materials. All reagents and chemicals were used as received unless otherwise noted. Styrene was purified by passing through a basic alumina column before polymerization. All reactions were performed in an inert atmosphere unless otherwise noted.

Methods. ^{1}H NMR spectra was recorded by Agilent 400-MR DD2 Magnetic Resonance System and Varian/Oxford As-500 using CD_2Cl_2 and $CDCl_3$ as solvents and internal standards. Molecular weights and polydispersity index of polymers and block copolymers were measured by two Agilent 1260 Infinity gel permeation chromatography (GPC) system. The first GPC was equipped with a PL gel 5 μm Mixed-D column (Agilent Technologies) and tetrahydrofuran (THF) was used as an eluent with a flow rate of 1.0 mL min^{-1} at 35°C. The second GPC was equipped with a Phenogel 5 μm Linear LC Column 300 x 7.8 mm (Phenomenex) and dimethylformamide (DMF) was used as an eluent with a flow rate of 1.0 mL min^{-1} at 50°C. A PS standard kit (Agilent Technologies) was used for the calibration. Matrix-assisted laser desorption ionization time-of-flight (MALDI-TOF-MS) was performed on a Bruker Ultraflex III TOF-TOF mass spectrometer equipped with a nitrogen laser (335 nm). The analytical sample was prepared by mixing a THF solution of polymers with a THF solution of the matrix (sinapic acid). Dynamic light scattering (DLS) was performed at a Malvern Zetasizer Nano-S. A partial column chromatography was conducted by Isolera™ Specktra System with ACI™ and Assist (Biotage) with Biotage SNAP 100 g column (Figure 4-4).

Optical micrographs of polymer cubosomes were measured on an OLYMPUS BX35M microscope using HAWK-30MU CCD camera. The reflectance spectrum of the polymer cubosomes (PCs) was measured on a CRAIC 20/20 PV microspectrophotometer in 200-800 nm spectral region (5.5 × 5.5 μm^2 aperture size). A drop of sample solution was cast on a Quartz substrate and then dried overnight. A white standard aluminum mirror served as the reference.

Scanning electron microscopy (SEM) was performed on a Hitachi S-4300 at an acceleration voltage of 15 kV. The dried sample was placed on a conductive carbon tape or silver paste and then coated with Pt with a thickness of 3 nm by using Hitachi E-1030 ion sputter. Transmission electron microscopy (TEM) was performed on a Hitachi 7600 operating at 100 kV and JEOL JEM-2100 microscope at 200 kV. Sample specimens were prepared by placing a drop of the sample solution on a carbon-coated Cu grid (200 mesh, EM science). The grid was air-dried overnight. Synchrotron small angle X-ray scattering (SAXS) data were obtained on the 9A SAXS beam line at Pohang acceleration laboratory in Korea (PLS-II, 3.0 GeV). The sample-to-detector distance (SDD) was 3.5 m. The concentrated suspension of the PCs was dried for 24 h in a freeze-dryer.

Synthesis of macroinitiator. A detailed synthetic procedure to macroinitiator **1** was reported previously.[22] Macroinitiator PEG2000$_3$-Br (**1**). ^{1}H NMR (δ = ppm, 400 MHz, $CDCl_3$) 6.60 (s, 2H), 5.10

(s, 2H), 4.14 (m, 6H), 3.85-3.46 (m, 540H), 3.38 (s, 9H), 1.95 (s, 6H)

Polymerization for block copolymers PEG2000$_3$-PS$_n$. CuBr (46 mg, 0.32 mmol) and *N,N,N',N'',N''*-pentamethyldiethylenetriamine (55 mg, 0.32 mmol) were mixed in anisole (5 mL) in a 20 mL Schlenk tube and degassed by bubbling N_2 for 15 min. A solution of styrene (100 mL) and macroinitiator **1** (100 mg, 16 μmol) were charged to a 250 mL Schlenk round bottom flask and degassed by bubbling N_2 for 30 min. The degassed solution of Cu complex was transferred to the styrene solution. The mixed solution flask was immersed in a preheated oil bath (100°C) and the polymerization proceeded at this temperature. The polymerization progress was monitored using GPC. When the molecular weight of the BCP reached the desired value, the reaction was quenched by exposing the solution to air in an ice bath. The quenched solution was directly precipitated into methanol (2 L). The white powder was collected by a vacuum filtration and dried.

Control homo-polymerization without macroinitiator 1. All procedures were same as above without macroinitiator **1**.

Purification of PEG2000$_3$-PS$_n$ block copolymer mixtures by column chromatography. The precipitated BCPs (1 g) was dissolved in 7 mL of dichloromethane (MC). The polymer solution was charged onto silica column (200 mL) and the column was flashed by MC as an eluent (1 L) to collect homopolystyrene (Homo-PS). And then, the column was flashed by gradient Methanol/MC eluent (0% to 4%) to collect our desired BCPs. Collected solution was evaporated under the rotary evaporator and precipitated in methanol (80 mL). The white powder was finally collected for both homo-PS and target block copolymers.

Self-assemblies of PEG2000$_3$-PS$_n$ block copolymers as the co-solvent method. The polymer (10 mg) was dissolved in 1,4-dioxane (2 mL) in a 20 mL capped vial with a magnetic bar. The solution was stirred for 4 h at room temperature (600 rpm). A syringe pump was calibrated to deliver water at a speed of 0.5 mL h^{-1}. The vial cap was replaced by a rubber septum and water was added to the polymer solution for 4 h using a syringe pump with a 6-mL syringe equipped with a steel needle. The resulting suspension was subjected to dialysis (molecular weight cutoff ~12 to 14 kDA (SpectraPor)) against water for 48 h (with frequent changes).

Self-assemblies of PEG2000$_3$-PS$_n$ block copolymers as the solvent diffusion-evaporation self-assembly (SDEMS) method. The polymer (10 mg) was dissolved in 1,4-dioxane (990 mg) in a 4 mL vial and stirred for 4 h at room temperature. A humidity chamber was prepared by mixing 20 mL of 1,4-dioxane and 20 mL of water in a 100 mL vial including a cylindrical column to put a glass substrate. 1

mL of the polymer solution was poured into a shallow glass container on the column in the humidity chamber. The humidity chamber was then sealed. After 24 h, the glass container was immersed into excess water. The polymer cubosomes were collected after removing 1,4-dioxane by dialysis (molecular weight cutoff ~12 to 14 kDA (SpectraPor)) against water for 48 h (with frequent changes).

4.6 References

1. Bates, C. M.; Maher, M. J.; Janes, D. W.; Ellison, C. J.; Willson, C. G. Block Copolymer Lithography. *Macromolecules* **2014**, *47*, 2−12.
2. Cheng, X. Q.; Wang, Z. X.; Jiang, X.; Li, T.; Lau, C. H.; Guo, Z.; Ma, J.; Shao, L. Towards Sustainable Ultrafast Molecular-Separation Membranes: From Conventional Polymers to Emerging Materials. *Prog. Mater. Sci.* **2018**, *92*, 258−283.
3. Jackson, E. A.; Hillmyer, M. A. Nanoporous Membranes Derived from Block Copolymers: From Drug Delivery to Water Filtration. *ACS Nano* **2010**, *4*, 3548−3553.
4. Segalman, R. A.; McCulloch, B.; Kirmayer, S.; Urban J. J. Block Copolymers for Organic Optoelectronics. *Macromolecules* **2009**, *42*, 9205−9216.
5. Fink, Y.; Urbas, A. M.; Bawendi, M. G.; Joannopoulos, J. D.; Thomas, E. L. Block Copolymers as Photonic Bandgap Materials. *J. Lightwave Technol.* **1999**, *17*, 1963−1969.
6. Urbas, A. M.; Maldovan, M.; DeRege, P.; Thomas, E. L. Bicontinuous Cubic Block Copolymer Photonic Crystals. *Adv. Mater.* **2002**, *14*, 1850−1853.
7. Xia, Y.; Gates, B.; Li, Z.-Y. Self-Assembly Approaches to Three-Dimensional Photonic Crystals, *Adv. Mater.* **2001**, *13*, 409−413.
8. Hamley, I. W. Nanostructure Fabrication Using Block Copolymers. *Nanotechnology* **2003**, *14*, 39−54.
9. Kim, J. K.; Yang, S. Y.; Lee, Y.; Kim, Y. Functional Nanomaterials Based on Block Copolymer Self-Assembly. *Prog. Polym. Sci.* **2010**, *35*, 1325−1349.
10. Schacher, F. H.; Rupar, P. A.; Manners, I. Functional Block Copolymers: Nanostructured Materials with Emerging Applications. *Angew. Chem. Int. Ed.* **2012**, *51*, 7898−7921.
11. Hsueh, H.-Y.; Yao, C.-T.; Ho, R.-M. Well-Ordered Nanohybrids and Nanoporous Materials from Gyroid Block Copolymer Templates. *Chem. Soc. Rev.* **2015**, *44*, 1974-2018
12. Hu, H.; Gopinadhan, M.; Osuji, C. O. Directed Self-Assembly of Block Copolymers: A Tutorial Review of Strategies for Enabling Nanotechnology with Soft Matter. *Soft Matter* **2014**, *10*, 3867-3889.
13. Darling, S. B. Directing the Self-Assembly of Block Copolymers. *Prog. Polym. Sci.* **2007**, *32*, 1152-1204.
14. Valkama, S.; Kosonen, H.; Ruokolainen, J.; Haatainen, T.; Torkkeli, M.; Serimaa, R.; Brinke, G. T.; Ikkala, O. Self-Assembled Polymeric Solid Films with Temperature-Induced Large and Reversible

Photonic-Bandgap Switching. *Nat. Mater.* **2004**, *3*, 872−876.

15. Kang, Y.; Walish, J. J.; Gorshnyy, T.; Thomas, E. L. Broad-Wavelength-Range Chemically Tunable Block-Copolymer Photonic Gels. *Nat. Mater.* **2007**, *6*, 957−960.
16. Osuji, C.; Chao, C.-Y.; Bita, I.; Ober, C. K.; Thomas, E. L. Temperature-Dependent Photonic Bandgap in a Self-Assembled Hydrogen-Bonded Liquid-Crystalline Diblock Copolymer. *Adv. Funct. Mater.* **2002**, *6*, 957−960.
17. Miyake, G. M.; Piunova, V. A.; Weitekamp, R. A.; Grubbs, R. H. Precisely Tunable Photonic Crystals from Rapidly Self-Assembling Brush Block Copolymer Blends. *Angew. Chem. Int. Ed.* **2012**, *51*, 11246−11248.
18. Sveinbjornsson, B. R.; Weitekamp, R. A.; Miyake, G. M.; Xia, Y.; Atwater, H. A.; Grubbs, R. H. Rapid Self-Assembly of Brush Block Copolymers to Photonic Crystals. *P. Nat. Acad. Sci. USA* **2012**, *109*, 14332−14336.
19. Runge, M. B.; Bowden, N. B. Synthesis of High Molecular Weight Comb Block Copolymers and Their Assembly into Ordered Morphologies in the Solid State, *J. Am .Chem. Soc.* **2007**, *129*, 10551−10560
20. Rzayev, J. Synthesis of Polystyrene-Polylactide Bottlebrush Block Copolymers and Their Melt Self−Assembly into Large Domain Nanostructures. *Macromolecules* **2009**, *42*, 2135−2141.
21. Gröschel, A. H.; Walther, A. Block Copolymer Micelles with Inverted Morphologies. *Angew. Chem. Int. Ed.* **2017**, *56*, 10992-10994
22. La, Y.; Park, C.; Shin, T. J.; Joo, S. H.; Kang, S.; Kim, K. T. Colloidal Inverse Bicontinuous Cubic Membranes of Block Copolymers with Tunable Surface Functional Groups. *Nat. Chem.* **2014**, *6*, 534−541.
23. An, T. H.; La, Y.; Cho, A.; Jeong, M. G.; Shin, T. J.; Park, C.; Kim, K. T. Solution Self-Assembly of Block Copolymers Containing a Branched Hydrophilic Block into Inverse Bicontinuous Cubic Mesophases. *ACS Nano* **2015**, *9*, 3084−3096.
24. Bobbala, S.; Allen, S. D.; Scott, E. A. Flash Nanoprecipitation Permits Versatile Assembly and Loading of Polymeric Bicontinuous Cubic Nanospheres. *Nanoscale* **2018**, *10*, 5078-5088.
25. Almsherqi, Z. A.; Landh, T.; Kohlwein, S. D.; Deng, Y. Cubic membranes: the missing dimension of cell membrane organization. *Int. Rev. Cell Mol. Biol.* **2009**, *274*, 275–342.
26. Han, L.; Che, S. An overview of materials with triply periodic minimal surfaces and related geometry: from biological structures to self-assembled systems. *Adv. Mater.* **2018**, *30*, 1705708.
27. Gustafsson, J.; Ljusberg-Wahren, H.; Almgren, M.; Larsson, K. Cubic Lipid-Water Phase Dispersed into Submicron Particles. *Langmuir* **1996**, *12*, 4611−4613.
28. Larsson, K. Cubic Lipid-Water Phases: Structures and Biomembrane Aspects. *J. Phys. Chem.* **1989**, *93*, 7304−7314.
29. Negrini, R.; Mezzenga, R. Diffusion, Molecular Separation, and Drug Delivery from Lipid

Mesophases with Tunable Water Channels. *Langmuir* **2012**, *28*, 16455-16462

30. Chong, J. Y. T.; Mulet, X.; Waddington, L. J.; Boyd, B. J.; Drummond, C. J. Steric Stabilisation of Self-Assembled Cubic Lyotropic Liquid Crystalline Nanoparticles: High Throughput Evaluation of Triblock Polyethylene Oxide-Polypropylene Oxide-Polyethylene Oxide Copolymers. *Soft Matter* **2011**, *7*, 4768-4777.
31. Vukusic, P.; Sambles J. R. Photonic Structures in Biology. *Nature* **2003**, *424*, 852−855.
32. Barrows, F. P.; Bartl, M. H. Photonic Structures in Biology: A Possible Blueprint for Nanotechnology. *Nanomater. Nanotechnol.* **2014**, *4*, 1 (doi:10.5772/58289).
33. Ghiradella, H. Light and Color on the Wing: Structural Colors in Butterflies and Moths. *Appl. Opt.* **1991**, *30*, 3492–3500.
34. Borgese, N.; Francolini, M.; Snapp, E. Endoplasmic reticulum architecture: structures in flux. *Curr. Opin. Cell Biol.* **2006**, *18*, 358–364.
35. Wang, J.-S.; Matyjaszewski, K. Controlled/"Living" Radical Polymerization. Atom Transfer Radical Polymerization in the Presence of Transition−Metal Complexes. *J. Am. Chem. Soc.* **1995**, *117*, 5614−5615.
36. Matyjaszewski, K.; Davis, K.; Patten, T. E.; Wei, M. Observation and Analysis of a Slow Termination Process in the Atom Transfer Radical Polymerization of Styrene. *Tetrahedron* **1997**, *53*, 15321−15329.
37. Brede, O.; David, F.; Steenken, S. Photo- and Radiation-Induced Chemical Generation and Reactions of Styrene Radical Cations in Polar and Non-Polar Solvents. *J. Chem. Soc. Perkin Trans. 2*. **1995**, 0, 23−32.
38. Oh, J.; Kuk, J.; Lee, T.; Ye, J.; Paik, H.-J.; Lee, H. W.; Chang, T. Molecular Weight Distribution of Living Chains in Polystyrene Prepared by Atom Transfer Radical Polymerization. *ACS Macro Lett.* **2017**, *6*, 758−761.
39. Azzam, T.; Eisenberg, A. Control of Vesicular Morphologies through Hydrophobic Block Length. *Angew. Chem. Int. Ed.* **2006**, *54*, 7443−7447.
40. Park, C.; La, Y.; An, T. H.; Jeong, H. Y.; Kang, S.; Joo, S. H.; Ahn, H.; Shin, T. J.; Kim, K. T. Mesoporous Monoliths of Inverse Bicontinuous Cubic Phases of Block Copolymer Bilayers. *Nat. Commun.* **2015**, *6*, 6392.
41. Martín-Moreno, L.; García-Vidal, F. J.; Somoza, A. M. Self-Assembled Triply Periodic Minimal Surfaces as Molds for Photonic Band Gap Materials. *Phys. Rev. Lett.* **1999**, *83*, 73-75.
42. Maldovan, M.; Urbas, A. M.; Yufa, N.; Carter, W. C.; Thomas, E. L. Photonic Properties of Bicontinuous Cubic Microphases. *Phys. Rev. B* **2002**, *65*, 165123.

Chapter 5. Morphological Transitions of Multi-Stimuli Responsive Branched-Linear Block Copolymers

5.1 Abstract

Morphologies of block copolymers (BCPs) can be controlled by addition of external stimuli while molecular architectures are unchaining. Branched-linear poly(ethylene glycol)-block-polystyrene (PEG-*b*-PS) BCP with three pyridine groups at junctions of peripheral PEG chains was synthesized by the controlled radical polymerization. The morphologies self-assembled without any stimulus and with external stimuli such as low pH and metal precursors were significantly different.

5.2 Introduction

Self-assembly of amphiphilic block copolymers in aqueous solution has been intensely researched over two decades.[1,2] Because self-assembled structures showed substantially enhanced mechanical properties rather than lipids, they have received attentions for their potential applications such as nano reactors[3,4] and drug delivery system[5-7]. To utilize them, polymer chemists have researched how to achieve desired morphologies of self-assembled structures.[8] In the field of self-assembly of small amphiphilic molecules like lipids, theory to predict morphologies by molecular architectures was already studied, which called packing parameter (*p*).[9] However, self-assembly of block copolymers (BCPs) couldn't be expected by calculation because of their structural complexity.[10] Therefore, various and complicated morphologies have been investigated by a case study. Eisenberg et al. reported novel morphologies of "crew-cut" polystyrene-block-poly(acrylic acid) BCPs and their design rules.[2,11,12] Morphologies of aggregates of linear diblock copolymers were directly related with a block ratio of two blocks and it was modulated by controlling the molecular weight of BCPs. However, our group reported, at 2012, that morphologies could also be controlled by introducing dendritic-linear BCPs with fixed block ratio.[13] From the study, the number of branched hydrophilic chains directly affect morphologies of self-assembled structures because the molecular area of BCPs was increased by branching the hydrophilic block.[14,15]

To achieve the desired morphologies, stimuli-responsive BCPs have also been utilized, which stimuli consisted of pH[16,17] and temperature[18]. In this time, we demonstrate that the molecular area and even morphologies of the branched-linear BCPs can be controlled by addition of external stimulus even though the molecular architectures are unchaining.

5.3 Results and Discussion

Herein, we reported a new branched-linear poly(ethylene glycol)-*b*-polystyrene (PEG-*b*-PS) block copolymer (BCP) system having three pyridine groups in junction points of each PEG chains. We chose

the PEG-*b*-PS system because our groups had intensely studied diverse morphologies of self-assembled structures from micelles to inverse structures along block ratios of branched-linear PEG-*b*-PS. Three pyridine groups located in the hydrophilic block made the molecular area of BCPs broaden by accepting external stimuli such as a low pH and metal complexation. To study control experiments of stimuli-responsive properties, we also designed similar BCPs having benzene groups instead of pyridine groups. BCPs with the desired degree of polymerization (DP_n) of styrene were synthesized by a reversible addition fragmentation chain transfer (RAFT) polymerization technique. The atom transfer radical polymerization (ATRP) method was not acceptable because three pyridine groups acted as ligand molecules and interrupted the propagation of styrene monomers. Therefore, new chain transfer agents (CTAs) containing three PEG chains (M_n = 550 g mol^{-1}) with pyridine (**P-CTA**) or benzene groups (**B-CTA**) were synthesized by multi-step procedures (Scheme 5-1) and characterized by ^{1}H NMR (Figure 5-1 and 5-2) and gel permeation chromatography (GPC) (Figure 5-3). With two CTAs, target BCPs, **P1**–**P4** and **B1**–**B2**, were finally synthesized by RAFT polymerization (Scheme 5-2) and showed well-defined molecular weights with various DP_n and narrow distributions (Table 5-1), as determined by ^{1}H NMR and GPC (Figure 5-4 and 5-5).

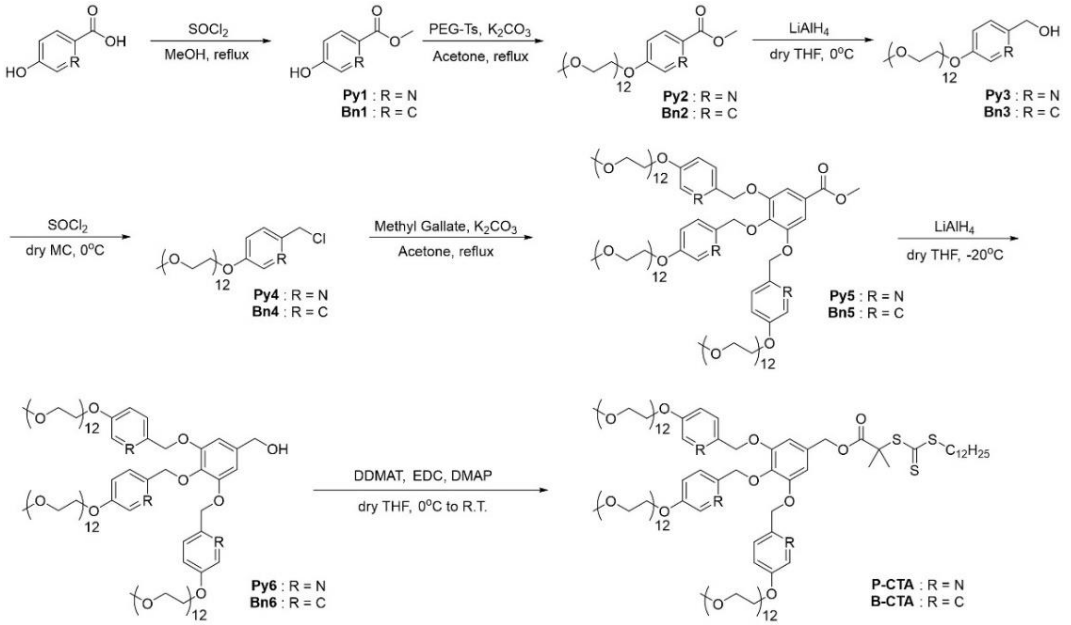

Scheme 5-1. Synthesis of macro-chain transfer agents (macro-CTAs); **P-CTA** and **B-CTA**

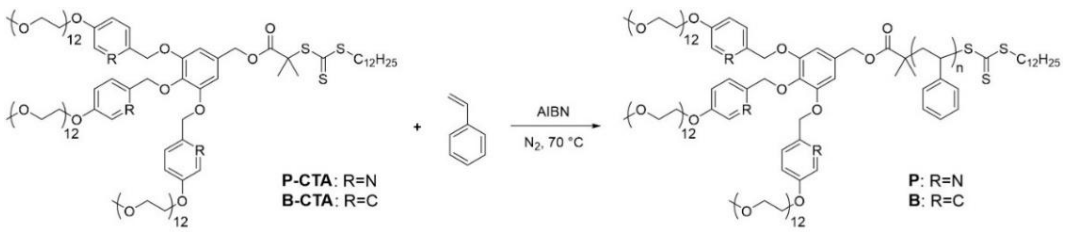

Scheme 5-2. Synthesis of block copolymers with macro-chain transfer agents (macro-CTAs)

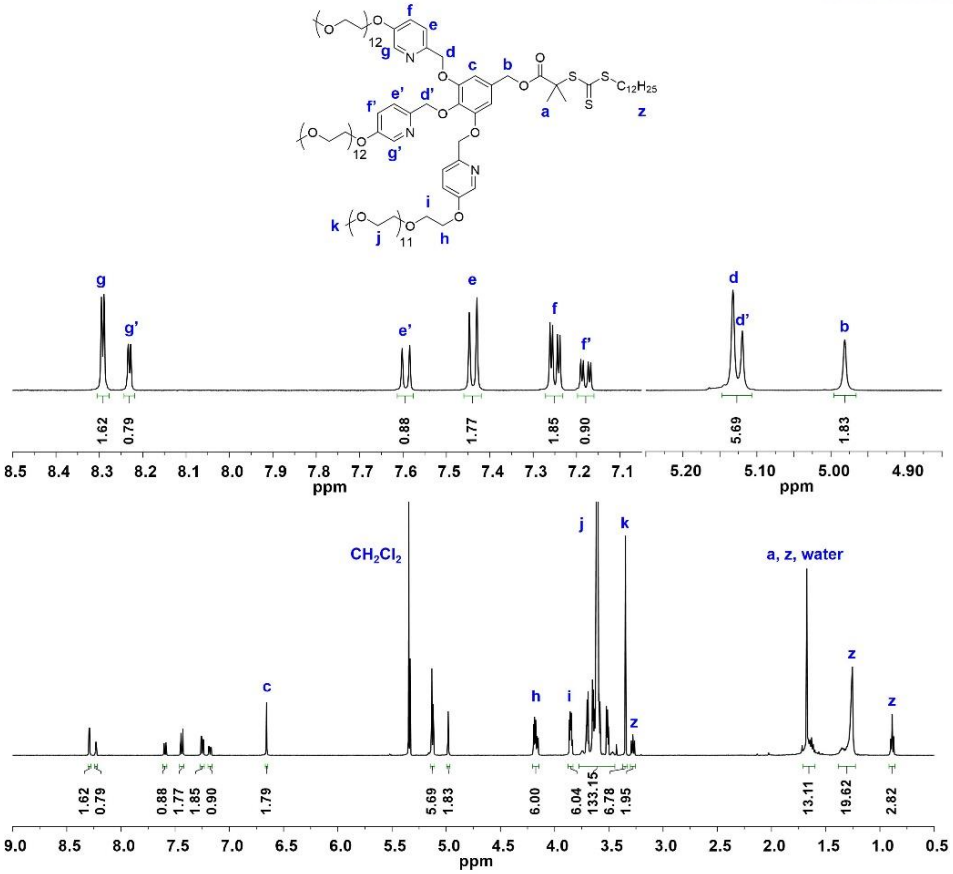

Figure 5-1. ^{1}H NMR spectrum of **P-CTA** in CD_2Cl_2.

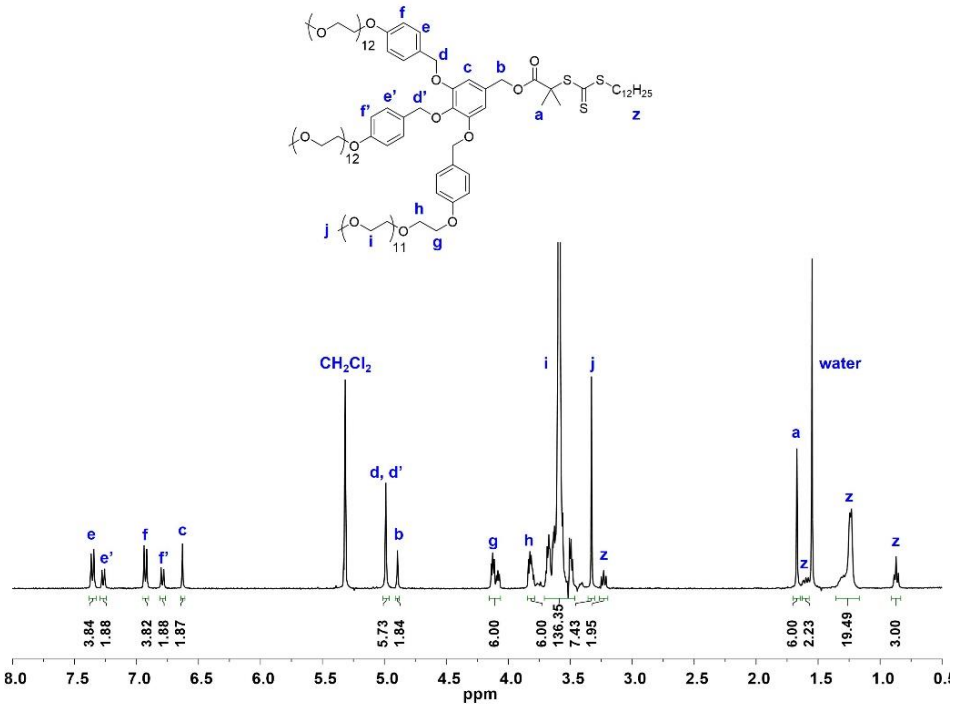

Figure 5-2. ^{1}H NMR spectrum of **B-CTA** in CD_2Cl_2.

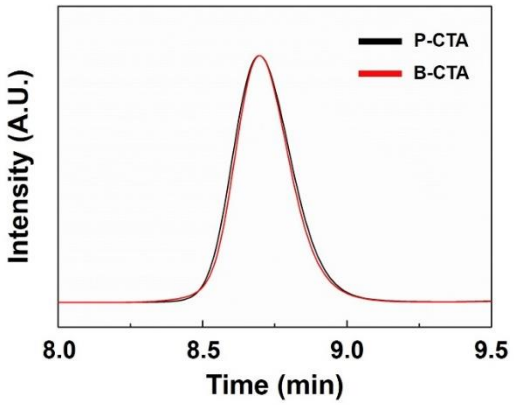

Figure 5-3. GPC plots of **P-CTA** and **B-CTA**

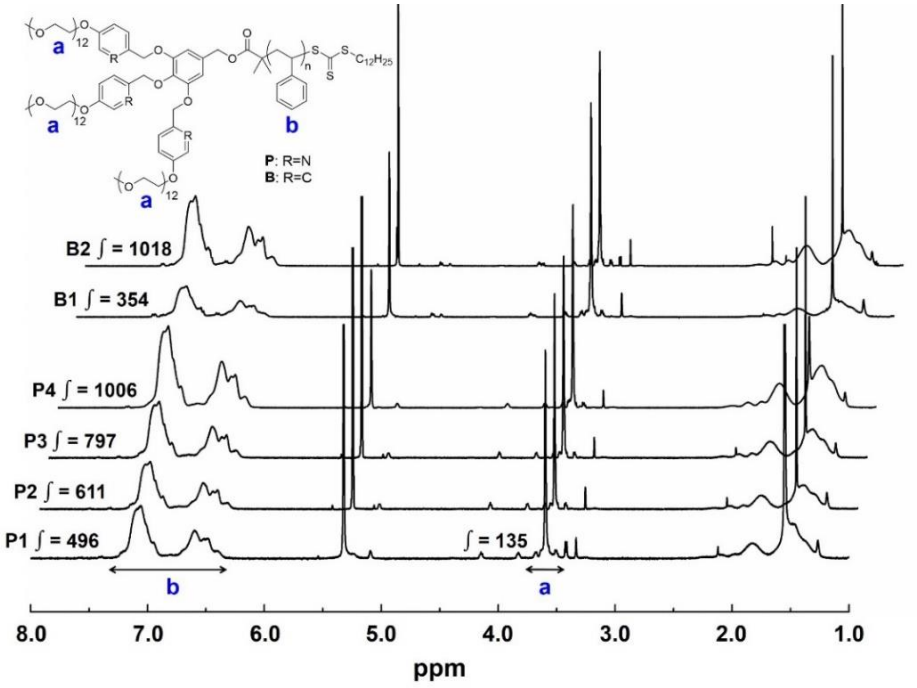

Figure 5-4. ^{1}H NMR spectra of block copolymers (**P1**-**P4** and **B1**-**B2**).

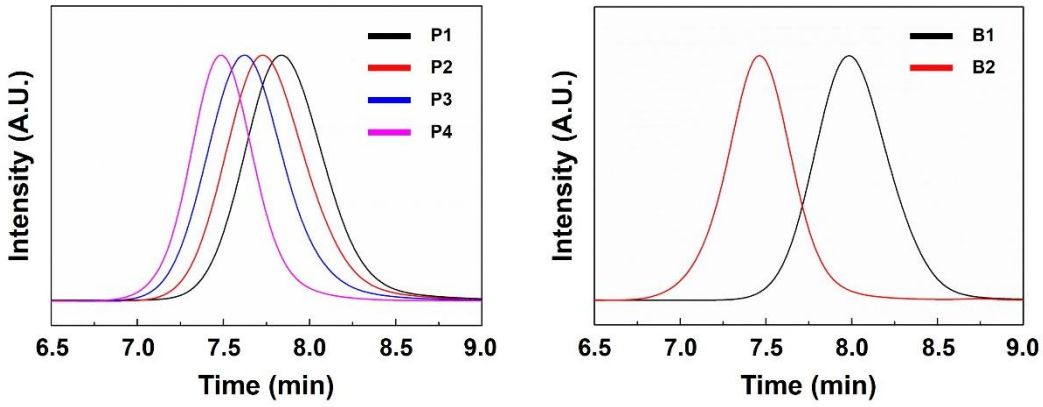

Figure 5-5. GPC plots of block copolymers (**P1**-**P4** and **B1**-**B2**).

Table 5-1. Characterization of BCPs

Sample	CTA	M_n (kg/mol)[a]	$Đ$[a]	DP_n[b]	M_n (kg/mol)[b]	f_{PEG} (%)[c]
P1	P-CTA	11.6	1.19	98	12.6	16.2
P2	P-CTA	13.7	1.21	121	15.0	13.1
P3	P-CTA	16.9	1.20	152	18.3	10.4
P4	P-CTA	22.5	1.14	200	23.2	7.9
B1	B-CTA	9.3	1.15	70	9.7	22.7
B2	B-CTA	24.3	1.14	202	23.5	7.9

[a]Determined by gel permeation chromatography using THF as an eluent. [b]Degree of polymerization (DP_n) and M_n were calculated from the ^{1}H NMR integration of the block copolymers. [c]The molecular weight ratio of the PEG domain (f_{PEG}) was calculated by M_n of PEG (1,650 g/mol)/M_n of a PS.

Table 5-2. Self-assembly of BCPs

BCPs	Code	Good solvent[a]	Poor solvent[a]	Phase[b]
P1	**P1-1**	1,4-Dioxane	Water	Cy, V
	P1-2	1,4-Dioxane	0.05 M HCl	M
P2	**P2-1**	1,4-Dioxane	Water	V
	P2-2	1,4-Dioxane	0.05 M HCl	Cy
P3	**P3-1**	1,4-Dioxane	Water	Large V
	P3-2	1,4-Dioxane	0.05 M HCl	Small V
P4	**P4-1**	Acetone	Water	C
	P4-2	Acetone	0.05 M HCl	L, Small V
	P4-3	1,4-Dioxane	Acetonitrile	Small V
	P4-4	Zn/1,4-Dioxane[c]	Acetonitrile	M
B1	**B1-1**	Acetone	Water	Cy
	B1-2	Acetone	0.05 M HCl	Cy
B2	**B2-1**	Acetone	Water	C
	B2-2	Acetone	0.05 M HCl	C
	B2-3	1,4-Dioxane	Acetonitrile	Small V
	B2-4	Zn/1,4-Dioxane[c]	Acetonitrile	Small V

[a]Self-assembly was done by following procedure. Target BCPs were dissolved in a good solvent (0.5 wt%) and the poor solvent was into the polymer solution via a syringe pump with constant rate (0.5 mL h^{-1}) [b]Morphologies of self-assembled structures; M: micelles, Cy: cylindrical micelles, V: vesicles, L: lamellae, C: polymer cubosomes. [c]2 equivalent of $Zn(OTf)_2$ to BCPs was added into 1,4-dioxane.

All BCPs were self-assembled by co-solvent methods. The BCPs were dissolved in an organic solvent, which is a good solvent to both blocks, and an aqueous solution, which is a poor solvent to the hydrophobic block, was added into the solution of BCPs for several hours with a constant rate. And then the organic solvent was removed by dialysis against distilled water for 24 h. The resulting aqueous suspension showed specific morphologies with various block ratios. We chose 1,4-dioxane for **P1**, **P2** and **P3** and acetone for **P4**, **B1** and **B2** as the organic solvent because we could control morphologies

toward desired structures precisely by selecting a different organic solvent. The solvent condition of the self-assembly and final morphologies of each BCPs were organized as a table (Table 5-2). The self-assembled structures by above co-solvent methods with neutral water were labeled as **Pn-1** (n = 1 to 4) and **Bn-1** (n = 1 and 2) and with an acidic solution were labeled as **Pn-2** (n = 1 to 4) and **Bn-2** (n = 1 and 2).

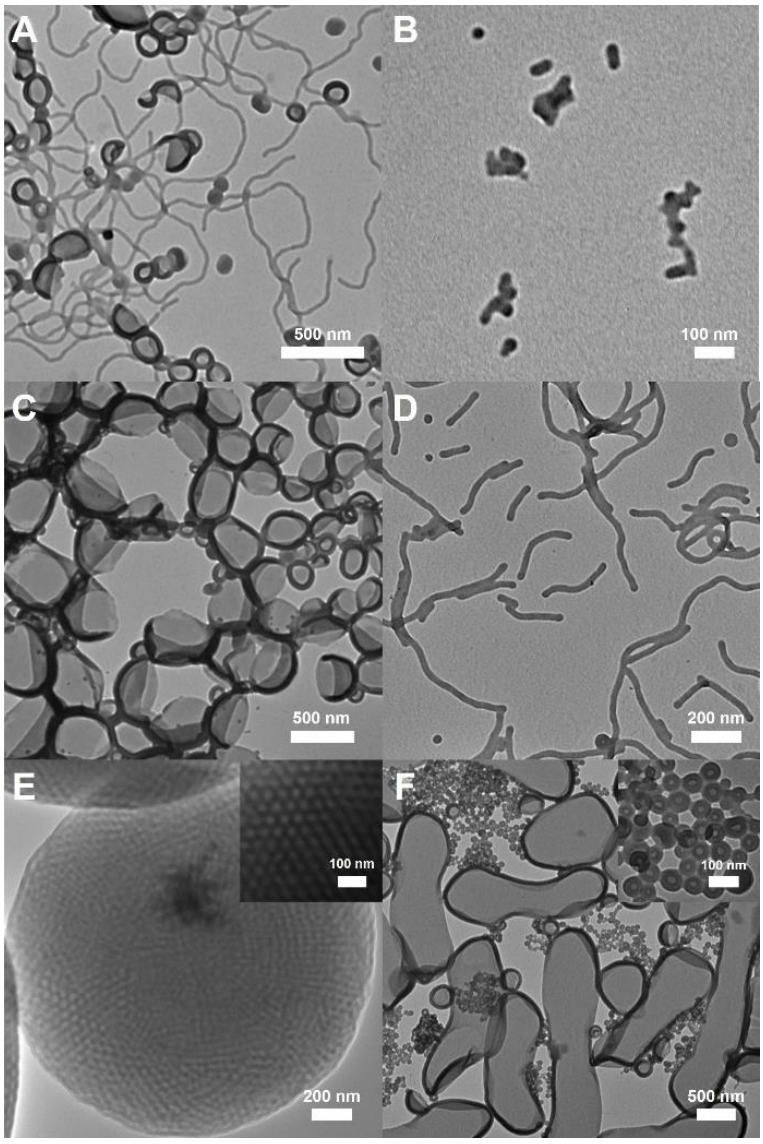

Figure 5-6. TEM images of self-assembled structures of block copolymers having pyridine groups in a neutral condition **P1-1** (A), **P2-1** (C) and **P4-1** (E) and an acidic condition **P1-2** (B), **P2-2** (D) and **P4-2** (F)

The morphologies of self-assembled structures could be estimated by the block ratio, which was directly correlated with a fraction of PEG, f_{PEG}. f_{PEG} could be calculated by the number of molecular weight (M_n) of PEG chains over M_n of the PS chain. And four BCPs polymerized by **P-CTA**, **P1**–**P4**,

had diverse f_{PEG} values so that they showed all different morphologies from self-assemblies. The detailed morphologies of each BCPs were studied by using transmission electron microscopy (TEM) initially and both scanning electron microscopy (SEM) and dynamic light scattering (DLS) measurement were used as necessary. **P1** (f_{PEG} = 16.2%) was self-assembled into mixtures of small vesicles and cylindrical micelles in the 1,4-dioxane/water condition (**P1-1**, Figure 5-6A). Both **P2** (f_{PEG} = 13.1%) and **P3** (f_{PEG} = 10.4%) were self-assembled into vesicles in the same condition. (**P2-1** and **P3-1**, Figure 5-6C, 5-7A). **P4** (f_{PEG} = 7.9%) was self-assembled into polymer cubosomes in the acetone/water condition (**P4-1**, Figure 5-6E). Polymer cubosomes of **P4-1** were further investigated by SEM and small angle X-ray scattering (SAXS) (*Pn3m* symmetry, lattice parameter a = 44.1 nm) (Figure 5-8). Along the decrease of f_{PEG} value from **P1** to **P4**, the morphologies of self-assembled structures became more complex from cylinders to polymeric cubosomes. Those phenomena have already been studied by our previous studies.[19] Therefore, it could be summarized that the morphologies were generally transformed from spherical micelles to cylindrical micelles, vesicular structures, lamellar and inverse structures like polymer cubosomes with decreasing of f_{PEG}.

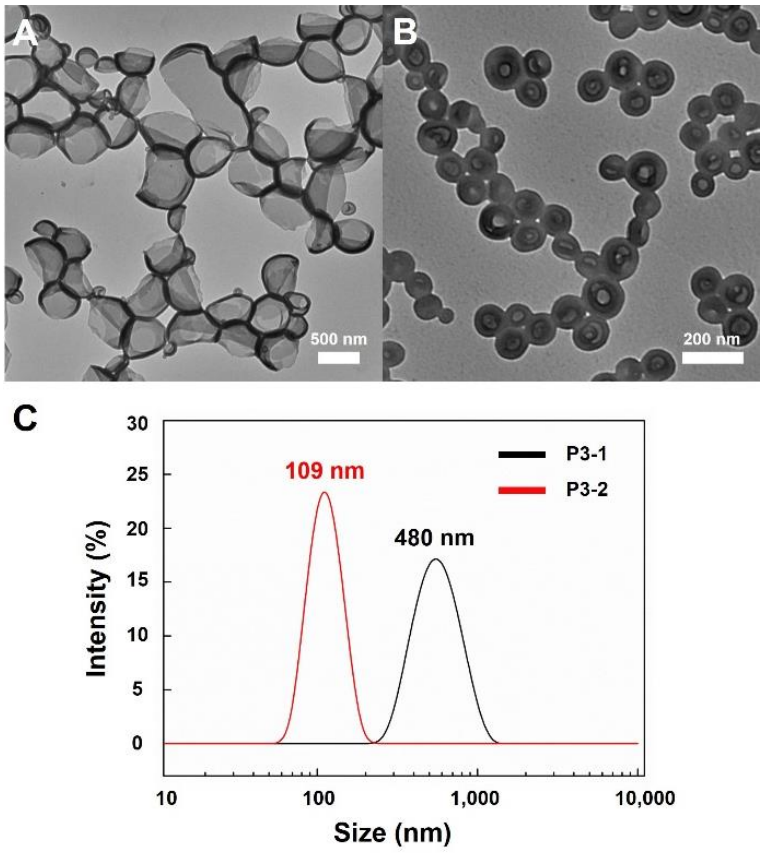

Figure 5-7. (A, B) TEM images of self-assembled structures of **P3** in a neutral condition **P3-1** (A) and an acidic condition **P3-2** (B). (C) Dynamic light scattering (DLS) size plots of **P3-1** (black) and **P3-2** (red).

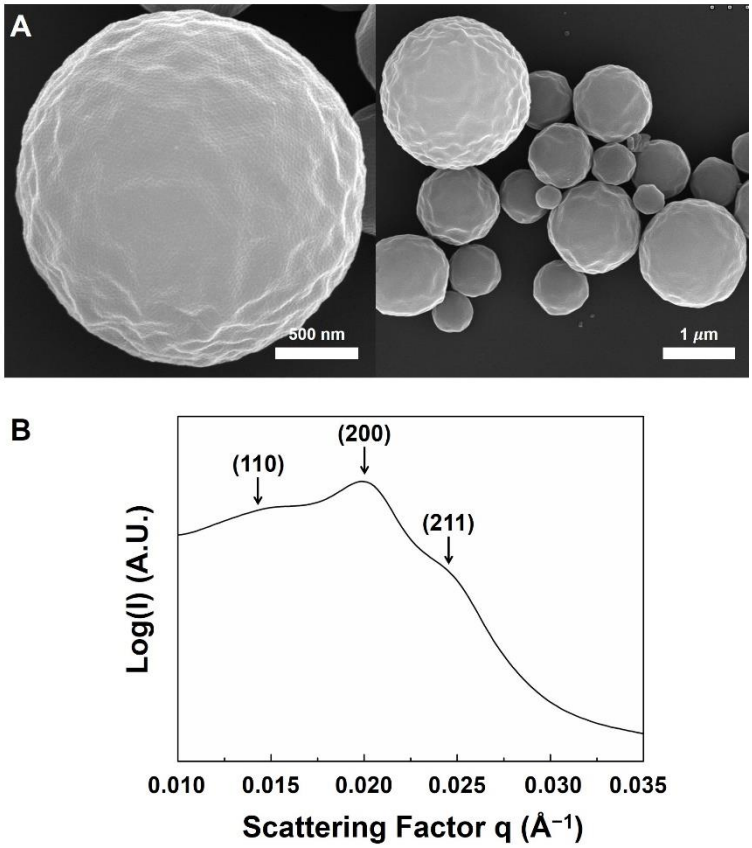

Figure 5-8. (A) SEM images of **P4-1**. (B) Small-angle X-ray scattering result of **P4-1** (*pn3m* symmetry, lattice parameter a = 44.1 nm).

When an acidic solution (0.05 M HCl) was added to the organic solution of BCPs instead of neutral water, different morphologies were observed. **P1** was self-assembled into the aggregation of spherical micelles in 1,4-dioxane/acidic solution condition (**P1-2**, Figure 5-6B). **P2** was self-assembled into cylindrical micelles in the same condition (**P2-2**, Figure 5-6D). And **P3** was self-assembled into smaller vesicles in the same condition (**P3-2**, Figure 5-7B). Both **P3-1** and **P3-2** showed vesicular structures but their sizes were significantly different. From DLS measurements, the average diameter of **P3-1** was 480 nm with polydispersity of 0.165 and the average diameter of **P3-2** was 109 nm with polydispersity of 0.038 (Figure 5-7C). **P4** was self-assembled into mixtures of large lamellae and small vesicles (**P4-2**, Figure 5-6E). In a series of self-assemblies in the acidic condition, the same tendency was observed. From **P1** to **P4**, the morphologies of self-assembled structures became more complex from micelles to lamellae structures. And all morphologies from the acidic self-assembly showed less developed structures than from the neutral self-assembly. In the case of **P1**, mixtures of vesicles and cylindrical micelles of **P1-1** was changed to spherical micelles of **P1-2**. And vesicles of **P2-1** was transformed to cylindrical micelles of **P2-2**. Furthermore, the size of the vesicles decreased from **P3-1** to **P3-2**. Finally, the polymer cubosomes of **P4-1** were changed to the mixtures of lamellae and vesicles of **P4-2**. Acidified pyridine groups in the hydrophilic block became protonated pyridinium groups with positive

charges. And charge-charge repulsions between PEG chains made the molecular area of BCPs increase, which actually decreased packing factors and made less-developed morphologies during the self-assembly.

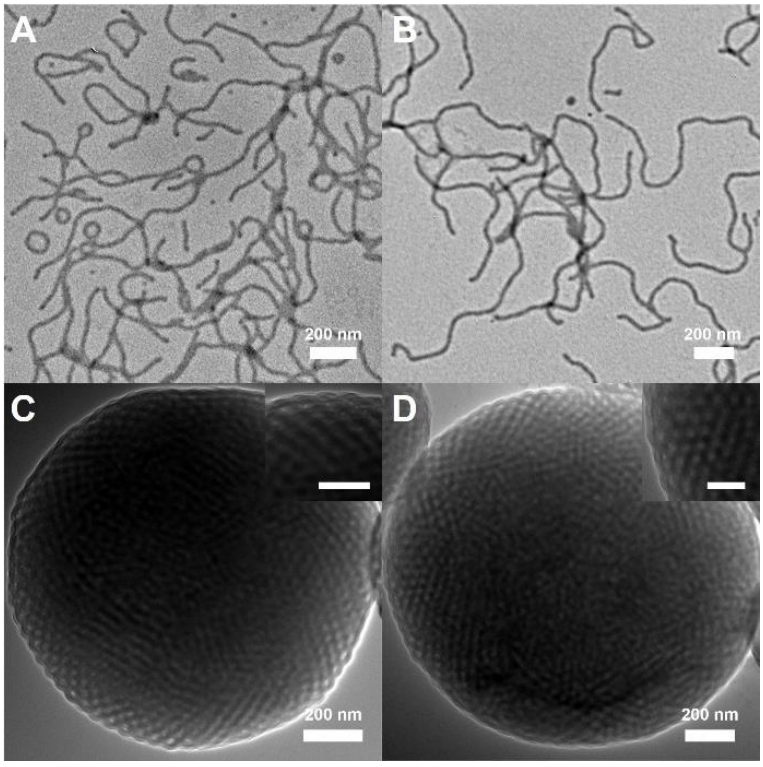

Figure 5-9. TEM images of self-assembled structures of block copolymers that didn't have pyridine groups in a neutral condition **B1-1** (A) and **B2-1** (C) and an acidic condition **B1-2** (B) and **B2-2** (D). Scale bars in insets of (C) and (D) indicated 100 nm.

To prove that the origin of this phenomena came from pyridine groups, we synthesized two BCPs having benzene groups in junction points of PEG chains instead of pyridine groups. Both BCPs, **B1** and **B2**, were self-assembled in same conditions with previous studies. Finally, we could achieve **B1-1** and **B2-1** from the self-assembly in acetone/neutral water (Figure 5-9A, C) and **B1-2** and **B2-2** in acetone/acidic solution (0.05 M HCl) (Figure 5-9B, D). As a result, the morphological transitions between the neutral self-assembly and the acidic self-assembly were not observed. Both **B1-1** and **B1-2** showed cylindrical micelles and both **B2-1** and **B2-2** showed polymer cubosomes. From the series of experiments, we confirmed that the self-assembled structures of our BCPs having pyridine groups in junction points of three PEG chains could be transformed by controlling pH of the solution during the self-assembly.

We also studied another stimuli-responsive morphological transition system. We introduced the metal-ligand coordination system between pyridine groups in the hydrophilic block and metal precursors. The pyridine group was well-known as a ligand molecule with donating a pair of electrons

to a metal center. To investigate the coordination properties, the model compound (**345-Py**) having only a framework without PEG chains of the hydrophilic block was newly synthesized (Scheme 5-3). We chose $Zn(OTf)_2$ as a metal salt to make coordination bonds because of its good solubility in various organic solvents.

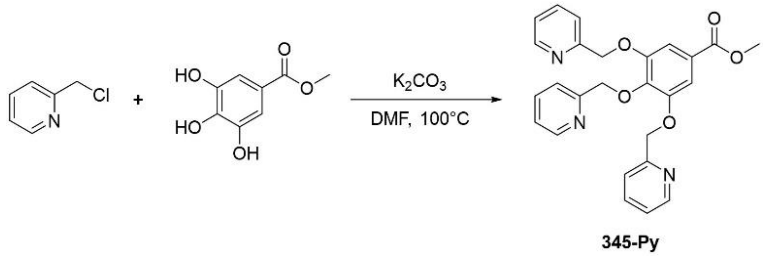

Scheme 5-3. Synthesis of the model compound (**345-Py**)

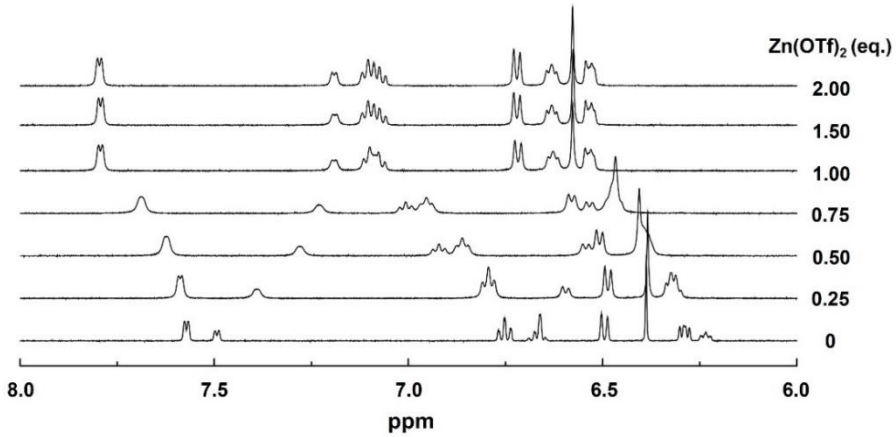

Figure 5-10. Partial ^{1}H NMR plots of model compound (**345-Py**) with various concentrations of $Zn(OTf)_2$.

At first, peak transitions of partial ^{1}H NMR spectra (in acetonitrile-d_3) of **345-Py** with diverse concentrations of $Zn(OTf)_2$ were observed (Figure 5-10). All peaks of neat **345-Py** in the aromatic region shifted with increasing concentrations of $Zn(OTf)_2$. However, after 1 equivalent $Zn(OTf)_2$ was added, the peaks were fixed up to the addition of 2 equivalent $Zn(OTf)_2$. As a result, our three-armed pyridine system could make a coordination with $Zn(OTf)_2$ as a 1:1 ratio. To analyze the complexation further, ^{1}H NMR and ^{1}H-^{1}H COSY NMR of **345-Py** were measured with and without $Zn(OTf)_2$ (Figure 5-11). There were lots of downfield shifts for a- ($\Delta\delta$ = 0.23 ppm), b- ($\Delta\delta$ = 0.34 ppm), b'- ($\Delta\delta$ = 0.30 ppm), c- ($\Delta\delta$ = 0.36 ppm), c'- ($\Delta\delta$ = 0.42 ppm), d- ($\Delta\delta$ = 0.22) protons of the pyridine. And some upfield shifts were also observed for a'- ($\Delta\delta$ = −0.3 ppm) and d'- ($\Delta\delta$ = −0.13 ppm) protons of the pyridine. Because the crystallization of **345-Py/Zn** complex were challenging, X-ray crystallography could not be measured. To study whether **345-Py/Zn** complexation system could adjust to our BCPs or

not, **P-CTA** and **B-CTA** have tried complexation with $Zn(OTf)_2$ and their peak shifts were observed in ^1H NMR in the same way. Only **P-CTA** showed huge peak shifts and any transition of the proton peak was not observed in **B-CTA** (Figure 5-12).

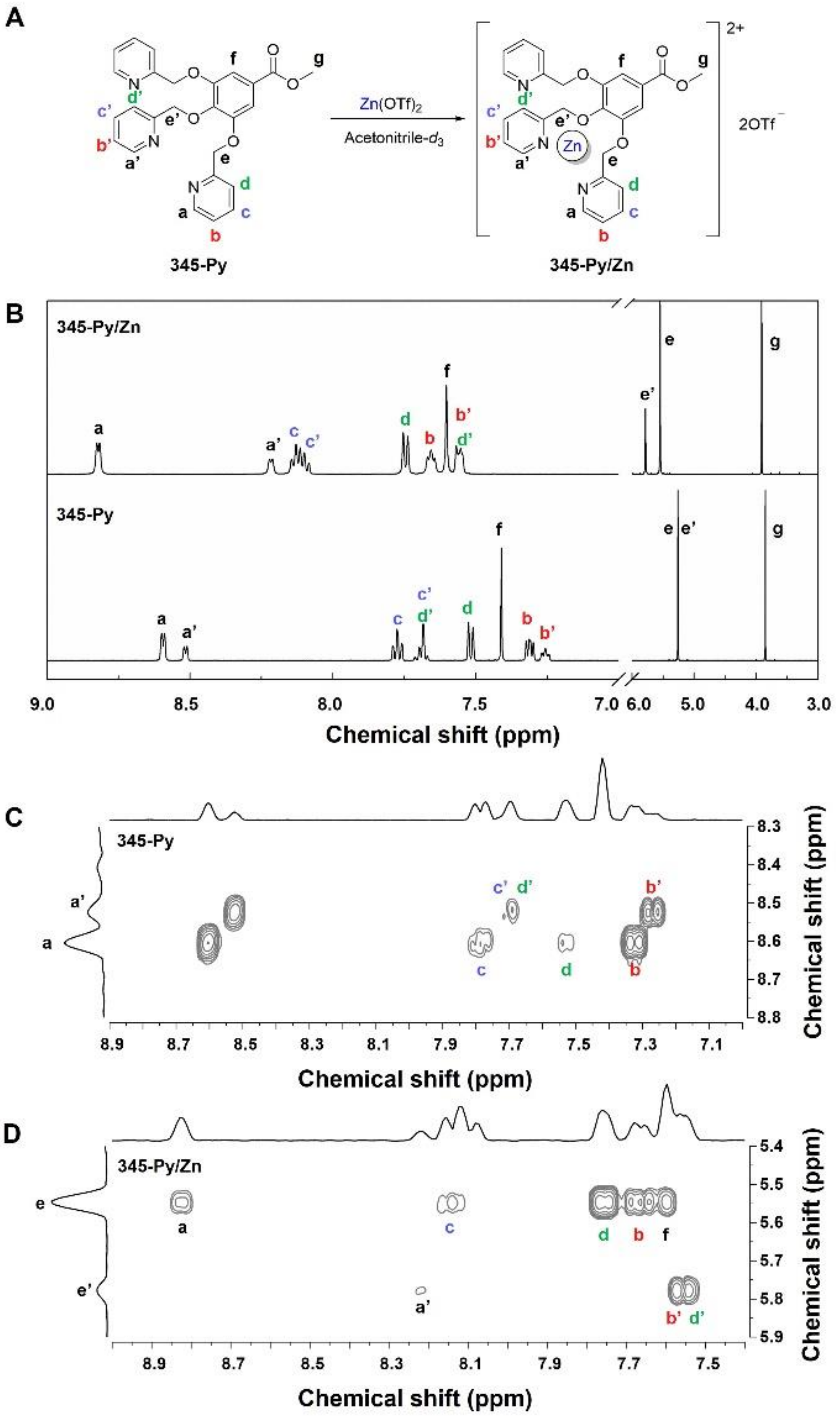

Figure 5-11. (A) Complexation of $Zn(OTf)_2$ with a model compound (**345-Py**). (B) Partial ^1H NMR spectra of **345-Py** and **345-Py/Zn** complex in acetonitrile-d_3. (C, D) ^1H-^1H COSY NMR spectrum of **345-Py** (C) and **345-Py/Zn** complex (D).

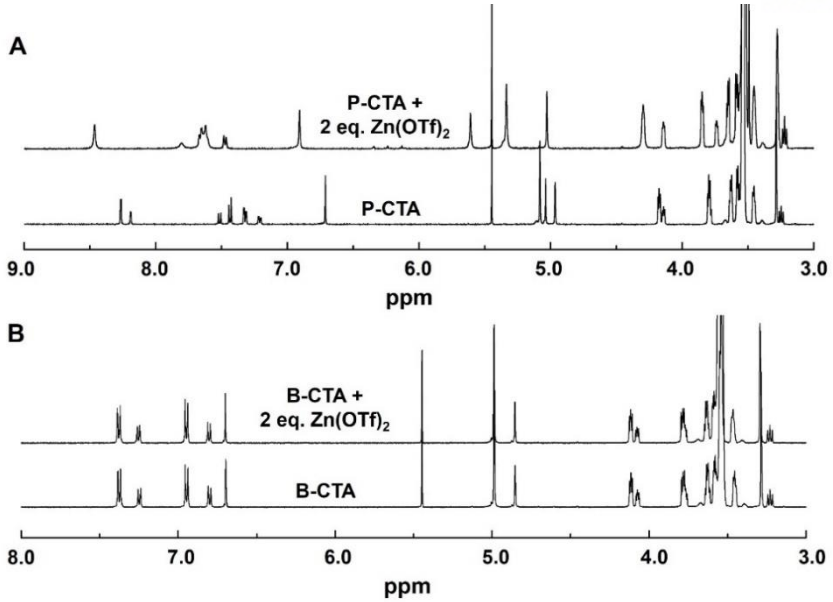

Figure 5-12. (A) ^{1}H NMR plots of **P-CTA** (below) and mixtures of **P-CTA** and $Zn(OTf)_2$ (above) in acetonitrile-d_3. (B) ^{1}H NMR plots of **B-CTA** (below) and mixtures of **B-CTA** and $Zn(OTf)_2$ (above) in acetonitrile-d_3.

Unlike the previous self-assembly in the acidic condition, a self-assembly of BCPs with the metal complexation couldn't be performed by water/organic co-solvent method because water disturbed the coordination bonds between Zn metal center and pyridine groups in the hydrophilic block. Previously, the coordination bonds between **345-Py** and $Zn(OTf)_2$ were identified by ^{1}H NMR in acetonitrile-d_3, but the water addition (25 vol%) broke their bonds and proton peaks in pyridine groups returned back to the original state (Figure 5-13). Furthermore, the proton peak shifts of **P-CTA** were observed by ^{1}H NMR in D_2O with and without $Zn(OTf)_2$, but no peak shift appeared even after 5 times $Zn(OTf)_2$ was added in the solution (Figure 5-14). So acetonitrile was used for the poor solvent to the hydrophobic PS block instead of water.

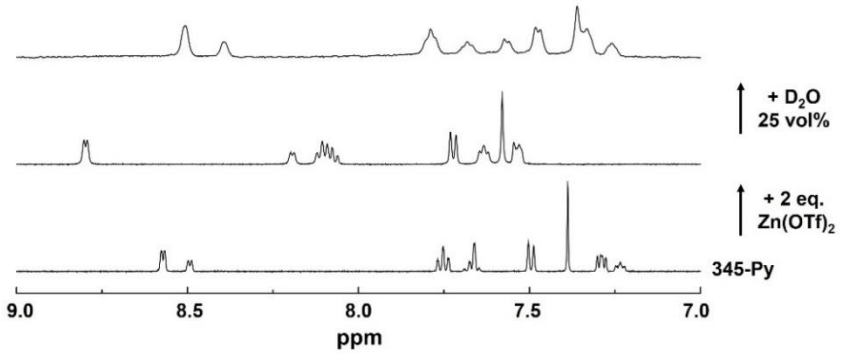

Figure 5-13. Partial ^{1}H NMR spectra of **345-Py** (bottom), addition of 2 equivalent $Zn(OTf)_2$ (middle), and further addition of D_2O (25 vol%) (top) in acetonitrile-d_3.

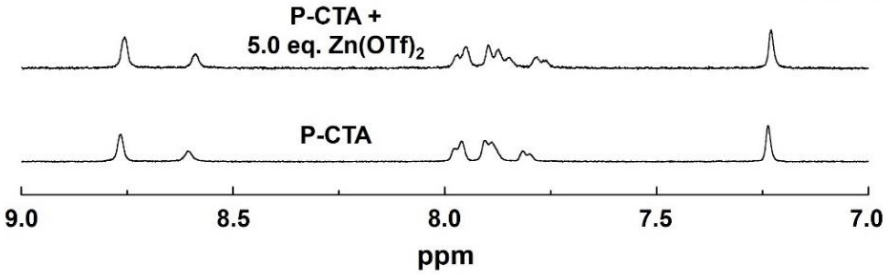

Figure 5-14. Partial ^{1}H NMR spectra of **P-CTA** (bottom) and the addition of 5 equivalent $Zn(OTf)_2$ (top) in D_2O.

P4 and **B2** were dissolved in 1,4-dioxane (0.5 wt%) respectively and acetonitrile was added to the solution at a constant rate. The solution was poured into the excess acetonitrile to quench the morphologies of self-assembled structures (**P4-3** and **B2-3**; Figure 5-15A, D). To investigate the effects of metal complexation to morphologies, another self-assembly was also conducted. At first, 2 equivalence of $Zn(OTf)_2$ was dissolved in 1,4-dioxane and **P4** and **B2** were dissolved in this solution. After 1 h stirring, acetonitrile was injected with a constant rate and the final solution was poured into the excess acetonitrile in the same way (**P4-4** and **B2-4**; Figure 5-15B, E). The morphologies of structures were studied by TEM images and DLS measurements.

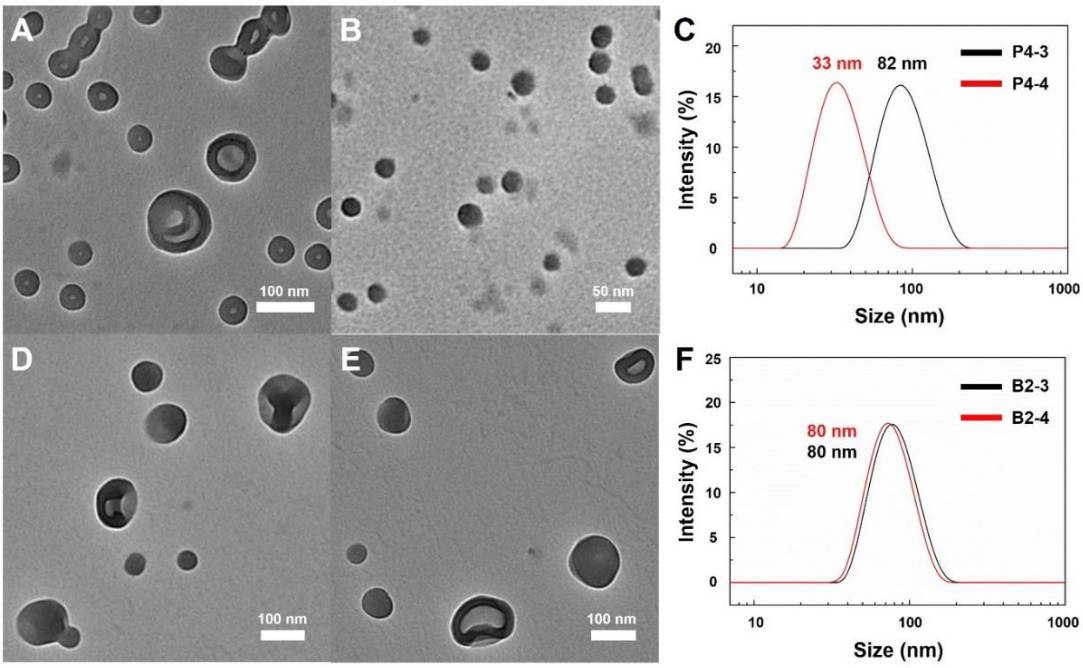

Figure 5-15. (A, B) TEM images of self-assembled structures of **P4** in 1,4-Dioxane/acetonitrile solution **P4-3** (A) and with $Zn(OTf)_2$ **P4-4** (B). (C) Dynamic light scattering (DLS) size plots of **P4-3** (black) and **P4-4** (red). (D, E) TEM images of self-assembled structures of **B2** in 1,4-Dioxane/acetonitrile solution **B2-3** (A) and with $Zn(OTf)_2$ **B2-4** (B). (C) DLS size plots of **B2-3** (black) and **B2-4** (red).

In the case of **P4** containing three pyridine groups in the hydrophilic groups, **P4-3** showed small vesicular structures with 82 nm size in DLS (polydispersity = 0.118) but no vesicular structure was detected from **P4-4**. **P4-4** showed only small spherical micelles with 33 nm size in DLS (polydispersity = 0.204) (Figure 5-15C). For the control experiment, same BCP having benzene groups instead of pyridine groups, **B2**, was self-assembled in the same way. Both **B2-3** and **B2-4** showed the same structures with 80 nm size in DLS (polydispersity = 0.183 and 0.257 respectively) (Figure 5-15F). From the results, the molecular area of the hydrophilic blocks of BCPs was increased by the complexation between Zn^{2+} and three pyridine groups in the hydrophilic blocks. Thus, the increased molecular area of BCPs made morphologies small and less developed similar to acid-triggered morphological transitions.

5.4 Summary

In summary, we synthesized branched-linear PEG-*b*-PS BCPs with stimuli-responsive three pyridine groups at junctions of peripheral PEG chains. We proved that three pyridine groups responded to low pH and $Zn(OTf)_2$ solutions and made charge-charge repulsions and the complexation respectively. Because of those responses, the molecular area of BCPs were expanded during self-assembly processes and significant transitions of morphologies were observed along various molecular weights. Self-assembly of BCPs formed cylindrical micelles, vesicles, and polymer cubosomes without any external stimulus, but less complicated morphologies were achieved with external stimuli. These results suggested that the morphologies of BCPs could be controlled by not only modifying block ratios of the blocks but also adjusting stimuli-responsive groups in hydrophilic blocks.

5.5 Experimental

Materials. All reagents and chemicals were used as received unless otherwise noted. Styrene was purified by passing through a basic alumina column before polymerization. CH_2Cl_2 (MC) was dried (using CaH_2 under a N_2 atmosphere) and distilled. Tetrahydrofuran (THF) was refluxed with Na and benzophenone under a N_2 atmosphere and distilled before used. All reactions were performed in an inert atmosphere unless otherwise noted.

Method. ^{1}H NMR spectra were recorded by an Agilent 400-MR DD2 Magnetic Resonance System and Varian/Oxford As-500 using CD_2Cl_2, DMSO-d_6, and acetonitrile-d_3 as solvents and internal standards. Molecular weights and polydispersity index of block copolymers were measured by an Agilent 1260 Infinity gel permeation chromatography (GPC) system equipped with a PL gel 5 μm Mixed-D column (Agilent Technologies) and tetrahydrofuran (THF) was used as an eluent with a flow rate of 1.0 mL min^{-1} at 35°C. A PS standard kit (Agilent Technologies) was used for calibration. Dynamic light scattering (DLS) was performed at a Malvern Zetasizer Nano-S. Transmission electron

microscopy (TEM) was performed on a Hitachi 7600 operating at 100 kV and a JEOL JEM-2100 operating at 200 kV. Specimens were prepared by placing a drop of the solution on a carbon-coated Cu grid (200 mesh, EM Science). The grid was air-dried overnight. Scanning electron microscopy (SEM) was performed on a Hitach S-4300 operating at 15 kV. The suspension was cast and dried on a slide glass and coated with Pt by using a Hitachi E-1030 ion sputter. Synchrotron small-angle X-ray scattering (SAXS) data were obtained on the SAXS beamline (PLS-II 6D, 11.18 keV, 6.5 m) at the Pohang Accelerator Laboratory. The concentrated suspension of the polymer cubosome was dried for a day in a freeze-dryer.

Synthesis of Py1. A suspension of 5-hydroxypyridine-2-carboxylic acid (15.0 g, 108 mmol) in methanol (200 mL) was charged in a two neck round bottom flask (500 mL). Thionyl chloride (34.2 g, 20.8 mL, 324 mmol) was added to the flask dropwise at 0°C. During the addition, suspension became the clear solution. After the addition was finished, the mixture was heated to reflux (80°C) and stirred for 20 h. Excess reagent and solvent were evaporated under a rotary evaporator and the white solid was collected as the desired product. ^{1}H NMR (δ = ppm, 400 MHz, DMSO-d_6) 8.2 (d, 1H, J = 2.8 Hz), 7.93 (d, 1H, J = 8.8 Hz), 7.25 (dd, 1H, J = 8.8, 2.8 Hz), 3.81 (s, 3H)

Synthesis of Py2. Py1 (3.38 g, 22.1 mmol), PEG550-Ts (17.9 g, 25.4 mmol) and potassium carbonate (6.09 g, 44.1 mmol) were dissolved in acetone (100 mL) in a two neck round bottom flask (250 mL). The mixture was refluxed for 24 h. After the reaction was completed, acetone was removed by a rotary evaporator and the crude mixture was dissolved in chloroform (200 mL). The solution was extracted by water (200 mL; 3 times) and brine (200 mL). The organic phases were collected and dried over $MgSO_4$. The solution was removed under reduced pressure and a crude oil was achieved. Without further purifications, it was progressed to the next steps. **Synthesis of Bn2.** Same procedure with **Bn1** (3.5 g, 23.0 mmol), PEG550-Ts (19.5 g, 27.6 mmol) and potassium carbonate (6.4 g, 46.0 mmol).

Synthesis of Py3. Lithium aluminum hydride (LAH, 1.02 g, 27.0 mmol) was charged in a Schlenk flask (500 mL) and dissolved in dry THF (100 mL). Crude **Py2** (12.4 g, 18.0 mmol) was charged in another Schlenk flask (250 mL) and dissolved in dry THF (100 mL) and the solution was transferred to LAH solution surrounded a NaCl/ice bath (< 0°C) dropwise. A completion of the reaction was traced by ^{1}H NMR (a removal of ester group) and quenched by sequential additions of water and same amounts of 1M NaOH solution. After 15 min further stirring added water was removed by $MgSO_4$ and solvent was removed by a rotary evaporator. The product mixture was purified by column chromatography (eluent MeOH/MC 6%). ^{1}H NMR (δ = ppm, 400 MHz, CD_2Cl_2) 8.25 (d, 1H, J = 2.8 Hz), 7.27 (dd, 1H, J = 8.8, 2.8 Hz), 7.19 (d, 1H, J = 8.6 Hz), 4.64 (s, 2H), 4.17 (t, 2H, J = 4.8 Hz), 3.83 (t, 2H, J = 4.8 Hz), 3.70-3.45 (m, 50H), 3.33 (s, 3H). **Synthesis of Bn3.** Same procedure with **Bn2** (16.5 g, 24.0 mmol) and

LAH (1.36 g, 36.0 mmol). ^{1}H NMR (δ = ppm, 400 MHz, CD_2Cl_2) 7.27 (d, 2H, *J* = 8.8 Hz), 6.90 (d, 2H, *J* = 8.8 Hz) 4.58 (d, 2H, *J* = 5.6 Hz), 4.11 (t, 2H, *J* = 4.8 Hz), 3.80 (t, 2H, *J* = 4.8 Hz), 3.70-3.45 (m, 50H), 3.33 (s, 3H)

Synthesis of Py4. Py3 (5.76 g, 8.70 mmol) was dissolved in dry MC (100 mL) in a Schlenk flask (250 mL). Thionyl chloride (2.07 g, 1.26 mL, 17.4 mmol) was added at ice bath (0°C) dropwise. After overnight stirring, the crude mixture was directly evaporated under a rotary evaporator to remove excess thionyl chloride roughly. A residual oil was dissolved in MC (100 mL) again and extracted by saturated $NaHCO_3$ (100 mL; 3 times) and brine (100 mL) to neutralize the desired product. ^{1}H NMR (δ = ppm, 400 MHz, CD_2Cl_2) 8.26 (d, 1H, *J* = 2.8 Hz), 7.37 (d, 1H, *J* = 8.8 Hz), 7.25 (dd, 1H, *J* = 8.8, 2.8 Hz), 4.63 (s, 2H), 4.18 (t, 2H, *J* = 4.8 Hz), 3.84 (t, 2H, *J* = 4.8 Hz), 3.70-3.45 (m, 50H), 3.33 (s, 3H) **Synthesis of Bn4**. Same procedure with **Bn3** (16.0 g, 24.2 mmol) and thionyl chloride (5.76 g, 3.5 mL, 48.4 mmol). ^{1}H NMR (δ = ppm, 400 MHz, CD_2Cl_2) 7.31 (d, 2H, *J* = 8.8 Hz), 6.90 (d, 2H, *J* = 8.8 Hz), 4.58 (s, 2H), 4.12 (t, 2H, *J* = 4.8 Hz), 3.82 (t, 2H, *J* = 4.8 Hz), 3.70-3.45 (m, 50H), 3.33 (s, 3H)

Synthesis of Py5. Py4 (5.39 g, 7.92 mmol), methyl gallate (405 mg, 2.20 mmol), potassium carbonate (3.65 g, 26.4 mmol) and 18-crown-6 (698 mg, 2.64 mmol) were dissolved in acetone (100 mL) in a two neck round bottom flask (250 mL). The mixture was refluxed for 3 days and reaction progress was monitored by MALDI-TOF until double-armed structures were completely removed. After the reaction was completed, acetone was removed by a rotary evaporator and the crude mixture was dissolved in chloroform (100 mL). The solution was extracted by water (600 mL; 3 times) and brine (60 mL). The organic phases were collected and dried over $MgSO_4$. The solution was removed under reduced pressure and a crude oil was achieved. Without further purifications, it was progressed to the next steps. **Synthesis of Bn5.** Same procedure with **Bn4** (13.7g, 20.1 mmol), methyl gallate (924 mg, 5.02 mmol), potassium carbonate (8.32 g, 60.2 mmol) and 18-crown-6 (1.59 g, 6.02 mmol).

Synthesis of Py6. Lithium aluminum hydride (LAH, 167 mg, 4.42 mmol) was charged in a Schlenk flask (250 mL) and dissolved in dry THF (50 mL). Crude **Py5** (6.19 g, 2.95 mmol) was charged in another Schlenk flask (50 mL) and dissolved in dry THF (50 mL) and the solution was transferred to LAH solution surrounded a NaCl/ice bath (< 0°C) dropwise. A completion of the reaction was traced by ^{1}H NMR (a removal of ester group) and quenched by sequential additions of water and same amounts of 1M NaOH solution. After 15 min further stirring, added water was removed by $MgSO_4$ and solvent was removed by a rotary evaporator. The product mixture was purified by column chromatography (eluent MeOH/MC 6%). ^{1}H NMR (δ = ppm, 400 MHz, CD_2Cl_2) 8.28 (d, 2H, *J* = 2.8 Hz), 8.22 (d, 2H, *J* = 2.8 Hz), 7.59 (d, 1H, *J* = 8.8 Hz), 7.43 (d, 2H, *J* = 8.8 Hz), 7.24 (dd, 2H, *J* = 8.8, 2.8 Hz), 7.17 (dd, 1H, *J* = 8.8, 2.8 Hz), 6.67 (s, 1H), 5.15 (s, 4H), 5.11 (s, 2H), 4.52 (d, 2H, *J* = 5.6 Hz), 4.21-4.12 (m,

6H), 3.87-3.80 (m, 6H), 3.70-3.45 (m, 150H), 3.33 (s, 9H) **Synthesis of Bn6.** Same procedure with **Bn5** (11.0 g, 5.24 mmol) and LAH (238 mg, 6.29 mmol). ^{1}H NMR (δ = ppm, 400 MHz, CD_2Cl_2) 7.36 (d, 4H, *J* = 8.8 Hz), 7.28 (d, 2H, *J* = 8.8 Hz), 6.94 (d, 4H, *J* = 8.8 Hz), 6.80 (d, 2H, *J* = 8.8 Hz), 6.66 (s, 2H), 5.02 (s, 4H), 4.91 (s, 2H), 4.55 (d, 2H, *J* = 5.6 Hz), 4.13 (t, 4H, *J* = 4.8 Hz), 4.09 (t, 2H, *J* = 4.8 Hz), 3.87-3.79 (m, 6H), 3.7-3.45 (m, 150H), 3.33 (s, 3H)

Synthesis of P-CTA. Py6 (0.85 g, 0.40 mmol), 2-(dodecylthiocarbonothioylthio)-2-methylpropionic acid (DDMAT, 179 mg, 0.49 mmol) and 4-dimethylaminopyridine (DMAP, 20 mg, 0.16 mmol) was dissolved in dry MC (5 mL) in a Schlenk tube. 1-Ethyl-3-(3-dimethylaminopropyl)carbodiimide (EDC, 188 mg, 1.00 mmol) was dissolved in dry MC (5 mL) in another Schlenk tube. EDC solution was transferred to the reagent mixture surrounded an ice bath (0°C) dropwise. The reaction was monitored by ^{1}H NMR. After the reaction was completed, the product mixture was extracted by brine (10 mL; 3 times). Organic phases were collected and dried over $MgSO_4$ anhydrous. The crude product was purified by column chromatography (gradient eluent MeOH/MC 6 to 8%). ^{1}H NMR (δ = ppm, 400 MHz, CD_2Cl_2) 8.28 (d, 2H, *J* = 2.8 Hz), 8.22 (d, 1H, *J* = 2.8 Hz), 7.58 (d, 1H, *J* = 8.8 Hz), 7.43 (d, 2H, *J* = 8.8 Hz), 7.24 (dd, 2H, *J* = 8.8, 2.8 Hz), 7.17 (dd, 1H, *J* = 8.8, 2.8 Hz), 6.64 (s, 2H), 5.12 (s, 4H), 5.11 (s, 2H), 4.97 (s, 2H), 4.17 (t, 4H, *J* = 4.8 Hz), 4.15 (t, 2H, *J* = 4.8 Hz), 3.87-3.81 (m, 6H), 3.70-3.45 (m, 140H), 3.33 (s, 9H), 3.26 (t, 2H, *J* = 6 Hz), 1.75-1.60 (m, 14H), 1.37-1.20 (m, 20H), 0.87 (t, 3H, *J* = 6.8 Hz) **Synthesis of B-CTA.** Same procedure with **Bn6** (0.80 g, 0.38 mmol), DDMAT (168 mg, 0.46 mmol), DMAP (18 mg, 0.15 mmol) and EDC (174 mg, 0.91 mmol). ^{1}H NMR (δ = ppm, 400 MHz, CD_2Cl_2) 7.36 (d, 4H, *J* = 8.8 Hz), 7.27 (d, 2H, *J* = 8.8 Hz), 6.93 (d, 4H, *J* = 8.8 Hz), 6.79 (d, 2H, *J* = 8.8 Hz), 6.63 (s, 2H), 4.99 (s, 6H), 4.90 (s, 2H), 4.13 (t, 4H, *J* = 4.8 Hz), 4.09 (t, 2H, *J* = 4.8 Hz), 3.86-3.79 (m, 6H), 3.70-3.45 (m, 140H), 3.33 (s, 9H), 3.23 (t, 2H, *J* = 7.4 Hz), 1.65-1.52 (m, 14H), 1.35-1.18 (m, 20H), 0.87 (t, 3H, *J* = 6.8 Hz)

Synthesis of 345-Py (model compound). 2-(chloromethyl)pyridine hydrochloride (1 g, 6.10 mmol), methyl gallate (280 mg, 1.52 mmol) and potassium carbonate (4.2 g, 30.4 mmol) were dissolved in dimethylformamide (DMF, 50 mL) in a two neck round bottom flask (250 mL). The mixture was immersed into oil bath (100°C) and stirred for 3 days. After the reaction was finished, the solvent was evaporated under reduced pressure. And the crude mixture was dissolved in 1M HCl solution and neutralized by adding NaOH powder. Target model compound was collected as the white powder above neutral pH (0.585 g, 84.2%). ^{1}H NMR (δ = ppm, 400 MHz, acetonitrile-d_3) 8.57 (d, 2H, *J* = 4.5 Hz), 8.49 (d, 1H, *J* = 4.5 Hz), 7.75 (td, 2H, *J* = 8.0 Hz, 1.5 Hz), 7.67 (m, 2H), 7.49 (d, 2H, *J* = 8.0 Hz), 7.39 (s, 2H), 7.29 (dd, 2H, *J* = 7.0 Hz, 5.0 Hz), 7.24 (m, 1H), 5.24 (s, 4H), 5.23 (s, 2H), 3.83 (s, 3H)

Polymerization for P series and B series. P-CTA or **B-CTA** (20 μ mol, 49 mg),

azobisisobutyronitrile (AIBN, 4 μmol, 0.7 mg) were dissolved in styrene (24 mmol, 2.5 g) in 5 mL Schlenk tube with magnetic bar. The solution was degassed by purging N_2 for 15 min and then immersed in a preheated oil bath (70°C). The polymerization progress was monitored using GPC at 1 h intervals. When the molecular weight reached to the desired value, the reaction was quenched by exposing the solution to air and ice bath. The quenched solution was precipitated in methanol (80 mL) and the powder was collected by vacuum filtration. Block copolymers were characterized by ^{1}H NMR and GPC.

Self-assembly of block copolymers (co-solvent method) in 4 types.

Series 1 (Neutral condition). A target BCP (10 mg) in dissolved in 1,4-dioxane or acetone (2 mL) in a 20 mL capped vial with a magnetic bar. The solution was stirred for 1 h at room temperature (600 rpm). A syringe pump was calibrated to inject water at a speed of 0.5 mL h^{-1}. The vial cap was replaced by a rubber septum, and neutral water was added to the polymer solution for 4 h using a syringe pump with a 6 mL syringe equipped with a steel needle. The resulting suspension was subjected to dialysis (molecular weight cutoff 12 – 14 kDa (SpectraPor, Rancho Dominguez, CA)) against water for 24 h.

Series 2 (Acidic condition). 0.05 M HCl solution was injected instead of neutral water. Other procedures were the same as **series 1**.

Series 3 (Non-coordination condition). A target BCP (10 mg) in dissolved in 1,4-dioxane (2 mL) in a 20 mL capped vial with a magnetic bar. The solution was stirred for 1 h at room temperature (600 rpm). A syringe pump was calibrated to injected acetonitrile at a speed of 0.5 mL h^{-1}. The vial cap was replaced by a rubber septum, and acetonitrile was added to the polymer solution for 4 h using a syringe pump with a 6 mL syringe equipped with a steel needle. The resulting suspension was poured to 10 mL acetonitrile to quench the morphologies of self-assembled structures.

Series 4 (Coordination condition). A target BCP (10 mg) and $Zn(OTf)_2$ (0.3 mg) were dissolved in 1,4-dioxane (2 mL) in a 20 mL capped vial with a magnetic bar. Following procedure was same as **series 3**.

5.6 References

1. van Hest, J. C. M.; Delnoye, D. A. P.; Baars, M. H. P.; van Genderen, M. H. P.; Meijer, E. W. Polystyrene-Dendrimer Amphiphilic Block Copolymers with a Generation-Dependent Aggragtion. *Science* **1995**, *268*, 1592.
2. Zhang, L.; Eisenberg, A. Multiple Morphologies of "Crew-Cut" Aggregates of Polystyrene-*b*-Poly(acrylic acid) Block Copolymers. *Science* **1995**, *268*, 1728.
3. Kim, K. T.; Meeuwissen, S. A.; Nolte, R. J. M.; van Hest, J. C. M. Smart Nanocontainers and Nanoreactors. *Nanoscale* **2010**, *2*, 844-858.
4. Renggli, K.; Baumann, P.; Langowska, K.; Onaca, O.; Bruns, N.; Meier, W. Selective and Responsive Nanoreactors. *Adv. Funct. Mater.* **2011**, *21*, 1241-1259.

5. Brinkhuis, R. P.; Rutjes, F. P. J. T.; van Hest, J. C. M. Polymeric Vesicles in Biomedical Applications. *Polym. Chem.* **2011**, *2*, 1449-1462.
6. Massignani, M.; Lopresti, C.; Blanazs, A.; Madsen, J.; Armes, S. P.; Lewis, A. L.; Battaglia, G. Controlling Cellular Uptake by Surface Chemistry, Size, and Surface Topology at the Nanoscale. *Small* **2009**, *5*, 2424-2432.
7. Onaca, O.; Enea, R.; Hughes, D. W.; Meier, W. Stimuli-Responsive Polymersomes as Nanocarriers for Drug and Gene Delivery. *Macromol. Biosci.* **2009**, *9*, 129-139.
8. Mai, Y.; Esienberg, A. Self-Assembly of Block Copolymers. *Chem. Soc. Rev.* **2012**, *41*, 5969-5985.
9. Israelachvili, J. N.; Mitchell, D. J.; Ninham, B. W. Theory of Self-Assembly of Hydrocarbon Amphiphiles into Micelles and Bilayers. *J. Chem. Soc., Faraday Trans. 2* **1976**, *72*, 1525-1568.
10. He, X.; Liang, H.; Huang, L.; Pan, C. Complex Microstructures of Amphiphilic Diblock Copolymer in Dilute Solution. *J. Phys. Chem. B* **2004**, *108*, 1731-1735.
11. Zhang, L.; Yu, K.; Eisenberg, A. Ion-Induced Morphological Changes in "Crew-Cut" Aggregates of Amphiphilic Block Copolymers. *Science* **1996**, *272*, 1777-1779
12. Zhang, L.; Eisenberg, A. Multiple Morphologies and Characteristics of "Crew-Cut" Micelle-like Aggregates of Polystyrene-*b*-poly(acrylic acid) Diblock Copolymers in Aqueous Solutions. *J. Am. Chem. Soc.* **1996**, *118*, 3168-3181
13. Jeong, M. G.; van Hest, J. C. M.; Kim, K. T. Self-Assembly of Dendritic-Linear Block Copolymers with the Fixed Molecular Weight and Block Ratio. *Chem. Commun.* **2012**, *48*, 3590-3592.
14. La, Y.; Park, C.; Shin, T. J.; Joo, S. H.; Kang, S.; Kim, K. T. Colloidal Inverse Bicontinuous Cubic Membranes of Block Copolymers with Tunable Surface Functional Groups. *Nat. Chem.* **2014**, *6*, 534-541.
15. An, T. H.; La, Y.; Cho, A.; Jeong, M. G.; Shin, T. J.; Park, C.; Kim, K. T. Solution Self-Assembly of Block Copolymers Containing a Branched Hydrophilic Block into Inverse Biocntinuous Cubic Mesophases. *ACS Nano* **2015**, *9*, 3084-3096.
16. Rodríguez-Hernández, J.; Lecommandoux, S. Reversible Inside−Out Micellization of pH-responsive and Water-Soluble Vesicles Based on Polypeptide Diblock Copolymers. *J. Am. Chem. Soc.* **2005**, *127*, 2026.
17. Lovett, J. R.; Warren, J. W.; Ratcliffe, L. P. D.; Kocik, M. K.; Armes, S. P. pH-Responsive Non-Ionic Diblock Copolymers: Ionization of Carboxylic Acid End-Groups Induces an Order-Order Morphological Transition. *Angew. Chem. Int. Ed.* **2015**, *54*, 1279-1283.
18. Moughton, A. O.; O'Reilly, R. K. Thermally Induced Micelle to Vesicle Morphology Transition for a Charged Chain End Diblock Copolymer. *Chem. Commun.* **2010**, *46*, 1091-1093.
19. Jeong, M. G.; Kim, K. T. Covalent Stabilization of Inverse Bicontinuous Cubic Structures of Block Copolymer Bilayers by Photodimerization of Indene Pendant Groups of Polystyrene Hydrophobic Blocks. *Macromolecules* **2017**, *50*, 223-234.